# Relationships Between Wintertime Modes of Atmospheric Variability on Intermediate and Long Timescales.

Kevin J. Rennert

A dissertation submitted in partial fulfillment of
the requirements for the degree of

Doctor of Philosophy

University of Washington

2007

Program Authorized to Offer Degree: Atmospheric Sciences

University of Washington
Graduate School

This is to certify that I have examined this copy of a doctoral dissertation by

Kevin J. Rennert

and have found that it is complete and satisfactory in all respects,
and that any and all revisions required by the final
examining committee have been made.

Chair of the Supervisory Committee:

John M. Wallace
John M. Wallace

Reading Committee:

David Battisti
David Battisti

Gerard Roe
Gerard Roe

John M. Wallace
John M. Wallace

Date: Dec. 10, 2007

In presenting this dissertation in partial fulfillment of the requirements for the doctoral degree at the University of Washington, I agree that the Library shall make its copies freely available for inspection. I further agree that extensive copying of this dissertation is allowable only for scholarly purposes, consistent with "fair use" as prescribed in the U.S. Copyright Law. Requests for copying or reproduction of this dissertation may be referred to Proquest Information and Learning, 300 North Zeeb Road, Ann Arbor, MI 48106-1346, 1-800-521-0600, to whom the author has granted "the right to reproduce and sell (a) copies of the manuscript in microform and/or (b) printed copies of the manuscript made from microform."

Signature 

Date December 10, 2007

University of Washington

**Abstract**

Relationships Between Wintertime Modes
of Atmospheric Variability on Intermediate and Long Timescales.

Kevin J. Rennert

Chair of the Supervisory Committee:
Professor John M. Wallace
Atmospheric Sciences

Variability in daily wintertime (DJF) 500 hPa geopotential heights on short ($< 6$ days), intermediate (6-30 days), and long ($> 30$ days) timescales is examined. Sectoral EOF analysis shows the leading patterns of variability on short timescales to correspond to the climatological storm tracks, and on long timescales to resemble the North Atlantic Oscillation (NAO) and the Pacific-North America (PNA) pattern. The intermediate timescale variability is best described by large-scale, zonally-oriented patterns: In the Atlantic sector the leading pattern is a dipole with centers of action over Greenland and Scandinavia; The leading Pacific pattern is dominated by a center of action over the Gulf of Alaska flanked by a pair of lower amplitude centers of opposing sign.

Non-linear relationships between fluctuations on long timescales and shorter timescale variance are determined using maximum covariance analysis (MCA). In the Atlantic sector, the negative polarity of a pattern resembling the NAO is associated with enhanced intermediate-timescale variability in a region extending from Baffin Bay to Scandinavia. In the Pacific sector, the negative polarity of a PNA-like pattern is associated with an enhancement of intermediate-timescale variance for a region centered over Alaska and extending over the North Pacific. Similar relationships are demonstrated by regression of the variance fields onto monthly indices of the NAO and PNA, and by the compositing of intermediate timescale variance by polarity of these modes. Hence, the leading patterns of

intermediate timescale variability are shown to be enhanced during low-index months of the NAO and PNA.

The skewness of the 500 hPa height field, an indicator of blocking activity polewards of the midlatitude jet, is attributable to contributions from intermediate and monthly timescale skewness, as well as a cross-frequency term involving monthly anomalies and intermediate timescale variance. This cross-frequency term is shown to be the dominant source of skewness in the total field, and a simple conceptual model for how large-scale modes of variability generate skewness is discussed.

Composites of extreme positive and negative intermediate timescale events over Baffin Bay and Anchorage demonstrate a high degree of symmetry, aside from a reversal of sign. This symmetry is shown to extend throughout the lifetimes of these events over these locations, and they are shown to exhibit the westward phase propagation and downstream development characteristics of Rossby waves. The spatial patterns of these events resemble the two polarities of the leading sectoral EOFs on this timescale, and their symmetry is consistent with the normal distribution of their principal component timeseries. Therefore, it is suggested that the intermediate timescale is governed primarily by linear, Rossby wave dynamics. Rossby wave generation is favored for these regions during periods of low-index NAO and PNA, and the non-linear appearance of the positive skewness at these locations may be explained as a superposition of the intermediate timescale Rossby waves on a background state set by the NAO or PNA.

# TABLE OF CONTENTS

## LIST OF FIGURES

## ACKNOWLEDGMENTS

Throughout the long process of earning my doctorate, I've had the great fortune to be surrounded by wonderful, supportive friends, family, and colleagues. Without them, my education here would have been much less complete, and the experience not nearly as rich.

Lisa Reynolds has been my partner throughout my education here. She's been a constant source of support, and her laughter, infinite kindness, boundless creativity, and ability to see beauty in all its forms, have been a constant source of inspiration to me. I am tremendously grateful for all of the love, and perspective, she's given me all of these years.

My mother Cathy, brother Jeff, and Grandmother Hilda, have all helped me in their own special ways. Each of them at different times have come through with just the right words of encouragement, and it's been wonderful to be able to share my experiences here with them. Thoughts of my father, as he wrote his dissertation long ago, were ever-present as I wrote mine, and I felt a new closeness to him through our shared experience.

Ben Stenberg has been a close friend since we transferred into the same high school in Rockford, IL, and whose time earning a doctorate in Philosophy (a "proper" Ph. D., as he's sure to remind you) here at the University of Washington has overlapped with mine. Though our interests have diverged since high school, the core of our friendship has only grown stronger over the years. I consider myself extremely lucky to have had such a close friend, one who has known me in so many different phases of my life, to share this time with.

My classmates in the class of '00 have been some of the best friends and peers one could ever ask for. In particular, Justin Wettstein, Rob Elleman, Mike Town, and Will Roberts have all been continuous sources of fun, support, and even scientific feedback. I can't imagine having gone through this program without them, and consider their life-long friendship to be one of the most important results of this education. I'm grateful to the

"elder students" of JISAO (it's all relative to when you arrive...) , especially Ioana Dima, Roberta Quadrelli, Michela Biasutti, Dan Vimont, and Craig Brown, all of whom were tremendously helpful and kind to this fledgling scientist. Todd Mitchell also deserves a special thank you for his help and advice over the years. Joe Casola and Jimmy Booth arrived at the climate palace just as it was losing many students to graduation, and their mix of brilliance and irreverence served to reinvigorate JISAO at a critical time.

My studies here have been conducted under the supervision of Mike Wallace. I've greatly appreciated his guidance and support, his time, and his seemingly inexhaustable supply of ideas throughout our time together. It's been a circuitous path to the subject of this thesis; before we settled on this topic, we had already conducted detailed investigations of topics ranging from the signature of climate change in the Arctic to the expansion of the tropics. It is tempting to view studies that weren't carried through to publication as failures, but each of these projects has taught me a great deal about a different aspect of the climate system. As a result, my education here has had considerable breadth, and that breadth has informed all of my more recent research. Few advisors have the wide range of experience, and the patience, required to support such an education. I'm grateful that Mike Wallace is such a scientist.

I owe a great deal of thanks to my other committee members as well. Gerard Roe and Cecilia Bitz involved me in one of their projects midway through my time here, broadening my experience and exposing me to even greater community of scientists. David Battisti has been a continued source of interesting and helpful discussions since I arrived as a prospective. Peter Rhines, in addition to contributing useful insight relative to this work, also gave me an excellent introduction to geophysical fluid dynamics through a pair of courses he instructed during my first year. I'm also thankful to Jim Riley for serving as my graduate school representative. All of these professors have taught me that to be a truly great scientist requires talent and hard work, but also requires integrity, respect for others, warmth, and kindness. I hope that I am able to emulate them in my career.

Thanks, to everyone who has been a part of my life here. It's been an incredible time.

# Chapter 1

# INTRODUCTION

Atmospheric variability may be usefully decomposed into contributions from phenomena operating on three different timescales: Short timescale phenomena associated with baroclinic waves yield variations at a fixed point with a period of less than ~6 days. Weather events with high amplitude features, such as blocking anticyclones or cutoff lows, contribute to variability on timescales of one to two weeks. Variability on monthly or seasonal timescales is largely due to fluctuations of planetary scale modes.

Variability on each of these timescales is interesting and worthy of study in its own right. Besides being responsible for our day to day weather, storms play a critical role in the general circulation, transporting heat and zonal momentum polewards from the tropics to the high latitudes. Blocking anticyclones exert considerable influence over regional climate (Rex, 1950b), and depending on their timing and positioning can have tragic societal consequences. Planetary scale modes like the North Atlantic Oscillation (NAO, van Loon and Rogers, 1978; Hurrell, 1995) and the Pacific-North America (PNA) pattern (Wallace and Gutzler, 1981) are associated with large-scale seasonal surface temperature and precipitation anomalies throughout the northern hemisphere (Hurrell et al., 2003). Nearly all of the trends in sea level pressure and surface air temperature from 1958 to 2003 may be accounted for by trends in these patterns (Quadrelli and Wallace, 2004a).

The phenomena encompassed within the high, intermediate, and low frequency bands may be considered separately, but it is clear that there is a rich and complex set of interactions between them. In this dissertation, we explore these associations through the analysis of a consistent, three-frequency band framework based on filtered versions of the wintertime 500 hPa geopotential height field. The specifics of the filtering scheme employed will be discussed in Chapter 2, but here we introduce the nomenclature: $z_{HP}$ will be used to indicate

heights which have been high-pass filtered to retain fluctuations shorter than 6 days, $z_{int}$ refers to heights that have been band-passed to retain intermediate-scale variability between 6-30 days, and $Z_{30}$ has been low-pass filtered to retain variability on timescales of 30 days and longer. The distinction between the use of capital $Z$ and lower-case $z$ in our nomenclature is that fields with capital $Z$ may be thought of as full fields, whereas the lower-case $z$ fields are always either anomalies from climatology or else have been treated with either a high- or band-pass filter. In this study, particular attention is paid to understanding the dominant sources of variability in $z_{int}$, and to the role of fluctuations in the $z_{30}$ band in generating nonlinearity on shorter timescales. This chapter introduces and motivates this topic by providing a brief dynamical background for each of the three timescales.

## *1.1 Background*

### *1.1.1 Dynamics of long and short timescale variability*

Quadrelli and Wallace (2004a) have shown that almost half of the low-frequency variability in the northern hemisphere winter can be ascribed either to fluctuations in the so-called "Northern Hemisphere Annular Mode" (NAM, Thompson and Wallace, 1988) and a pattern they refer to as "PNA-like", or a functionally equivalent set of basis patterns comprised of the North Atlantic Oscillation and the PNA. These latter patterns, whose expression in the 500 hPa geopotential height field is shown in Fig. 1.1, play a central role throughout the present study. The signature of the NAO, as shown here in its positive polarity, is a dipole with anomalously low heights over the polar cap and relatively high heights over the midlatitude Atlantic. In accordance with geostrophic balance, the related wind field features a relatively intense, zonally-oriented jet that is shifted polewards from its climatological mean position. The alternating centers of action of the PNA pattern resemble a Rossby wave-train emanating from the tropical Pacific and following a great-circle route over North America.

The prominence of the NAM and PNA are thought to be achieved through different dynamical mechanisms. Lorenz and Hartmann (2001, 2003) attributed the selection of the the annular modes as the dominant modes of variability in both northern and southern

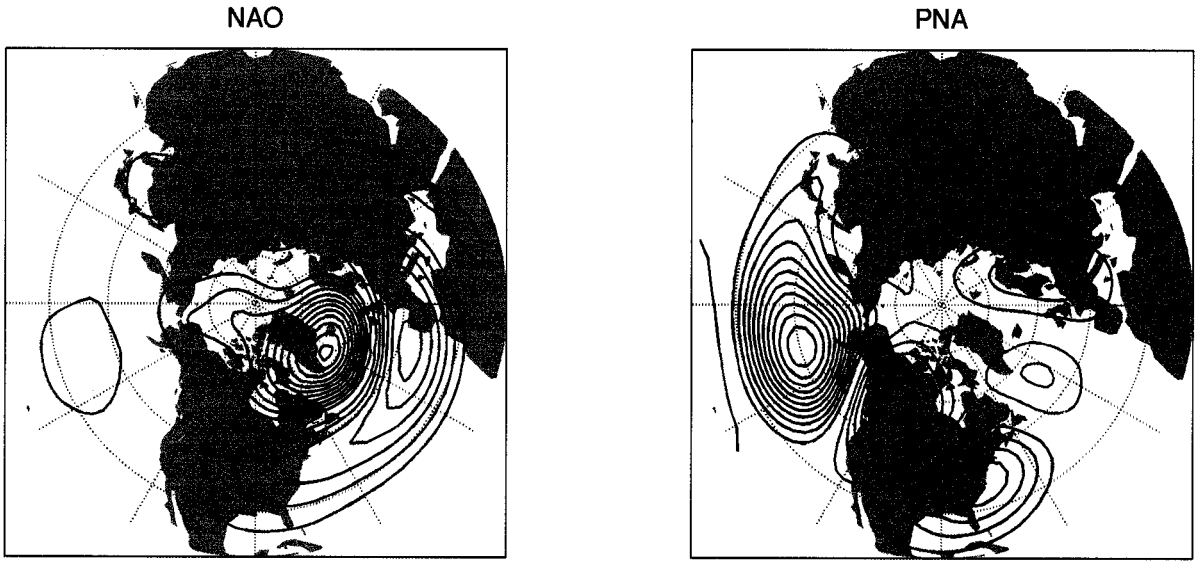


Figure 1.1: The signature of the NAO (left) and PNA (right) in the 500 hPa geopotential height field. Contour interval is 10 m.

hemispheres to a feedback process involving the high-frequency transients. In essence, perturbations to the zonal wind field associated with fluctuations in the annular modes shift the region of strongest baroclinicity, thereby shifting the region of cyclogenesis of subsequent storms. The anomalies from the shifted storm then serve to reinforce the original zonal perturbation, thereby increasing the lifetime of a typical excursion the mode and reddening its spectrum. The prominence of the PNA was explained by Simmons et al. (1983), who found a pattern resembling the PNA to be the fastest growing eigenmode in a barotropic model linearized about a wintertime basic state. Their results indicated that the PNA derives its energy from the mean state primarily through barotropic conversion in the Pacific jet exit region.

The high-frequency part of the spectrum is dominated by traveling synoptic disturbances. The development and decay of these storms is well explained by linear theories of cyclogenesis, and their climatological organization into storm tracks (Fig. 1.2) with greatest intensity just downstream and poleward of the jet exit in each ocean basin has been

well-documented (Blackmon et. al 1977, Chang and Orlanski 1993). As discussed above, storms both act to maintain, and are influenced by, fluctuations in the low-frequency planetary scale modes. Fluctuations in both modes have been shown to shift meridionally and influence the intensity of the storm tracks (Lau, 1988; Chang et al., 2002).

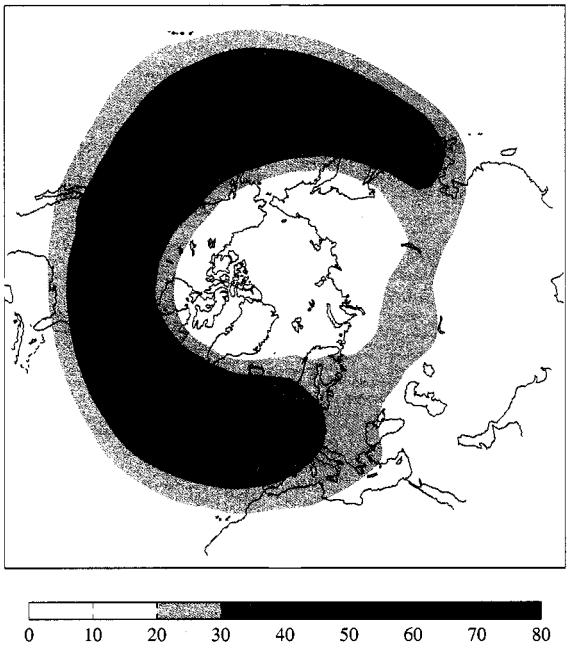


Figure 1.2: Climatological storm tracks, as evidenced in a 6 day high-pass filtered $v'v'$ at 200 mb. Units are $m^2s^{-2}$. *Figure courtesy of J. Wettstein.*

### *1.1.2 Dynamics of intermediate timescale variability*

The evolution of our current understanding of blocking began in the late 1940's and early 50's with a series of papers describing specific blocking events (Namias, 1947; Elliott and Smith, 1949; Rex, 1950a). As more data became available, attention increasingly turned towards determining regions favorable to blocking episodes by creating climatologies of their occurrence. To create such a climatology requires a formal definition of what qualifies as a block, and the differences between the climatologies largely results from slight differences in that definition. Generally speaking, all of the definitions focus on the signature of a strong, fairly stationary, equivalent barotropic anticyclone along a central blocking latitude.

Lejenäs and Økland (1983) used a zonal index, requiring that a 20 degree latitude swath centered at 50 N be easterly to be considered blocked. Tibaldi and Molteni (1990) added the additional constraint that latitudes north of the blocked region must also have westerly flow, and allowed a flexibility of $\pm 4$ degrees about the 50N central blocking latitude. More recently, Pelly and Hoskins (2003) used a reversal of the potential temperature gradient on the tropopause as their indicator of blocking, and allowed the central blocking latitude to vary with longitude to follow the storm tracks in each basin. The consensus among these climatologies is that there are two main types of blocking activity: One is a dipole with the anticyclone centered over the eastern North Atlantic / Western Europe and a cyclone to the southeast, and the other is the so-called "omega block" with an anticyclone centered over the north Pacific and deep companion troughs digging into its flanks. The comprehensive, 55-year blocking climatology generated by Barriopedro et al. (2006) (Fig. 1.3) using the high resolution NCEP/NCAR reanalysis product and a slightly modified methodology for identifying blocks from Tibaldi and Molteni (1990) is in general agreement with the prior studies, though they further subdivide the Atlantic and Pacific blocking regions into two regions each to reflect localized, seasonally dependent blocking behavior.

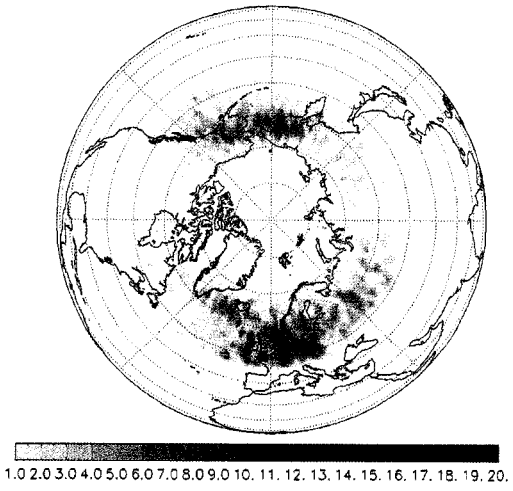


Figure 1.3: Number of wintertime blocks from 1950-2005, reproduced from Fig. 8d of Barriopedro et al. (2006)

While the climatologies of the blocking events have converged, there are still a multitude of theories explaining how the blocking anticyclones occur and are maintained against advection and dissipation by the time-mean flow. The role of upstream, transient eddies in reinforcing the blocks was investigated by Austin (1980) using a simple, quasi-geostrophic model. Her results showed that anticyclonic eddy forcing by transients one quarter wavelength upstream of the blocking ridge was necessary to oppose the advection of the block by the time-mean flow. This configuration of transient eddies was shown by Shutts (1986) to occur naturally in a barotropic channel model as upstream eddies were deformed as they approached the block. Observational evidence for this theory was first provided by Mullen (1987), who examined the eddy vorticity forcing from synoptic timescale transients for a composite of 17 blocking events over the North Atlantic. His composites confirmed the role of the upstream eddy vorticity forcing in maintaining the block, but also pointed out that temperature advection due to the transients acted to weaken the block's thermal perturbation. Trenberth (1986) found a similar result by employing Eliassen-Palm flux diagnostics to analyze a southern hemisphere blocking incident.

To further clarify the role and structure of the synoptic scale eddies, Nakamura and Wallace (1993) allowed for flexibility between the individual baroclinic wave events involved in blocking composites, shifting each one slightly in time and space to minimize cancellation between synoptic eddies during the compositing process. Their examination of amplifying blocks for five different regions found that blocking anticyclones that formed just polewards of the jet could be reinforced by a train of baroclinic eddies that traveled polewards around the block, without undergoing stretching or deformation. Amplifying blocks that formed farther polewards from the jet in regions of weak background PV gradient exhibited different behavior, with upstream anticyclonic eddies becoming substantially deformed as they approached the block, and becoming absorbed into the block.

The tendency for blocks to form anticyclone/cyclone pairs has led a number of investigators to use modon theory as a theoretical framework for understanding blocking. Obtaining stationary, steady numerical solutions to the quasi-geostrophic vorticity equation in physically relevant shear flows proved difficult initially (Swenson, 1986), but were achieved in subsequent work (Haines, 1989; Haupt et al., 1993). In this framework, transient eddies

are still thought to provide the forcing necessary to maintain the modon structure against dissipation (Pierrehumbert and Malguzzi, 1984).

While the role of the high-frequency timescale has been emphasized for amplification and maintenance of the blocks, there is also a large body of literature documenting the statistical linkage between blocking and the low-frequency modes of variability, particularly in the high latitudes. The negative polarity of the NAO pattern has been associated with blocking near Greenland by Vautard (1990), Kimoto and Ghil (1993), Cheng and Wallace (1993), and Quadrelli and Wallace (2004b). Shabbar et al. (2003) found that North Atlantic blocking occurs on 67% more winter days during the negative phase of the NAO than the positive, and that the events during the negative polarity are nearly twice as long lived. The negative phase of the PNA has also been shown to favor blocking in the North Pacific / Alaska region by Palmer (1988). Subsequent work by Renwick and Wallace (1996) documented an even stronger relationship with the cold phase of ENSO.

The associations between blocking and the principal modes of low-frequency variability are statistically robust, but the dynamical underpinnings of those connections are still a subject of debate. One paradigm holds that the more slowly varying modes set a background state favorable for the occurrence of blocking. In support of this framework, Shabbar et al. (2003) proposed a conceptual model based on the theory of Charney and Devore (1979) to explain the relationship. In short, the surface temperature anomalies associated with the negative phase of the NAO warm the Labrador Sea and cool the North American continent to the west, providing surface thermal conditions favorable to the creation of long lived anticyclones in the Greenland region. The positive phase of the NAO has the opposite surface temperature anomalies, and thus serves to oppose the formation of blocking anticyclones.

More recently, a different interpretation of the relationship has been put forward by Woollings et al. (2007). Rather than viewing the large scale modes as pre-conditioning the atmosphere for the occurrence of blocking, he has instead proposed that the negative NAO itself is actually a consequence of an anomalously high frequency of occurrence of these blocks. In his work, he uses the Pelly and Hoskins interpretation of blocking events as the breaking of Rossby waves on the dynamical tropopause, and finds no evidence of an NAO

negative signature before or after these events occur. His proposed paradigm holds that the negative and positive polarities of the NAO should properly be viewed as a pair of states: one that features a high frequency of wave-breaking events, and a contrasting state with a relative absence of such events.

If correct, this interpretation is quite important, as it calls into question the current state of understanding of the dynamics of these large scale modes. It sets a fundamental timescale of the NAO on the order of two weeks or less, and calls into question the body of literature emphasizing the importance of the high-frequency transients of timescales shorter than a week in the maintenance of the annular modes and downplaying the role of events on longer timescales. If blocking events are truly important in this regard, then it would indicate that we should be focusing on the dynamics that modulate the frequency of blocking to understand the dynamics of the longer lived modes.

### *1.2 Overview*

It is the goal of this thesis to generate new insight into the relationships between variability on these three different timescales. We pay particular attention to documenting the relationships between variability on intermediate timescales with that of variability on low and high-frequency timescales, with an intent to further understand how high-latitude NAO/PNA-related blocking differs from blocking in the midlatitudes. Our study methodology is unique in that we do not impose a strict definition of blocking on the data. Instead, we employ linear analysis techniques to determine the dominant structures of variability for each timescale, and allow those structures to act as a proxy for blocking behavior. One consequence of this choice is our emphasis on certain preferred high-latitude regions of blocking, such as Baffin Bay. These regions appear in conventional blocking climatologies, but their distance from the storm tracks and midlatitude jet, and subsequent tendency to divert, rather than "block" the mean midlatitude flow, has caused them to receive less emphasis in the literature.

A brief overview of the organization and results of this dissertation is as follows: In Chapter 2 we formally define the three frequency bands of interest and document the basic statistics and dominant modes of variability for each band using EOF analysis. The EOFs

for the low-frequency band are familiar patterns corresponding to the NAO and PNA, and the patterns obtained for the high-frequency bands correspond to the climatological storm tracks. The dominant structures of variability in the intermediate-scale frequency band are shown to correspond to an $\Omega$ blocking pattern in the Pacific, and a tendency for Greenland blocking events to be associated with deep troughs over Scandinavia, and vice versa.

Chapter 3 provides an investigation into nonlinear relationships between variability in the different frequency bands. This inter-frequency analysis is performed by applying maximum covariance analysis (MCA) to the low-frequency 500 hPa height field, along with the squared geopotential height fields from the intermediate and high-frequency bands. In addition to extracting well-documented associations between fluctuations in the NAO and PNA patterns and shifts in position and intensity of the storm tracks, the MCA also associates extended periods of $NAO^-$ and $PNA^-$ with an enhancement of intermediate-scale scale variability over the northern Atlantic and Pacific regions. In the Atlantic sector, this indicates that $NAO^-$ conditions are associated with an equatorward shifted storm track and enhanced blocking activity polewards of the jet. In the Pacific, $PNA^-$ conditions are associated with an enhanced, poleward-shifted storm track that is largely coincident with the region of increased blocking activity.

In Chapter 4 we discuss the skewness of the 500 hPa height field and its utility as an indicator of regions with a high frequency of occurrence of blocking events. By decomposing the skewness into contributions from variations on low and intermediate frequencies, we show that the dominant source of skewness comes from a cross-frequency term involving low-frequency fluctuations and the intermediate-scale variance. This result leads to a simple conceptual model for understanding blocking events as a superposition of variability on intermediate timescales with low-frequency height fluctuations from the planetary-scale modes. This framework is explored for relevant locations in the northern hemisphere.

Chapter 5 concerns the evolution of the most intense events in the full and intermediate-scale variance fields in the Atlantic and Pacific sectors. Intense positive anomalies over Baffin Bay and the the Gulf of Alaska are shown to exhibit westward propagation, consistent with documented behavior of retrograding blocks in these regions. Compositing analysis in this chapter indicates that baroclinic waves play a relatively small role in the development of

the blocks, and this result is discussed. The dissertation concludes with a discussion and synthesis of our major results in Chapter 6.

# Chapter 2

# STATISTICS OF A 3 FREQUENCY BAND SYSTEM

## *2.1 Introduction*

Throughout this thesis we investigate the relationships between atmospheric phenomena on three different timescales: $Z_{30}$, the 30 day low pass filtered data that encompasses the slowly varying modes of large-scale variability; $z_{int}$, the 6-30 day bandpass filtered data that corresponds to nonlinear weather events such as blocking, and $z_{HP}$ the 6 day high pass filtered data representing mainly baroclinic waves. Relatively few papers have fully decomposed variability into three timescales in this manner. The most relevant are the studies of Blackmon et al. (1984a,b) that documented differences in the horizontal structure of one-point correlation maps of the northern hemisphere 500 hPa height field for a similar set of timescales. In this chapter we formally introduce the data and filtering scheme employed, and establish the basic statistics of the northern hemisphere wintertime 500 hPa geopotential height field for the low, intermediate, and high-frequency bands.

## *2.2 Data*

The data used in this study are based on the ECMWF ERA-40 reanalysis 500 hPa geopotential height field (Uppala and coauthors, 2005). The ERA-40 provides 6-hourly output for the period Sept. 1957 through Aug. 2002 on a 2.5 x 2.5 degree grid. Daily means generated from the 6-hourly output were filtered with a pair of fourth-order Butterworth filters with cutoff frequencies near 1/6 and 1/30 $day^{-1}$ to generate 6 and 30-day low-pass filtered height fields. These fields will be referred to as $Z_6$ and $Z_{30}$ respectively. A 6-day high-pass field ($z_{HP}$) was created by subtracting the $Z_6$ data from the unfiltered daily mean heights, and the band-pass field $z_{int}$ was generated by subsequently subtracting both $z_{HP}$ and $Z_{30}$ from the unfiltered data. After filtering, daily values only from DJF 1958-2001 were retained.

The response functions for these three filters are shown in Fig. 2.1. The frequency

response function confirms that the high-pass filter response is $(1/\sqrt{2})$ for periods of 6 days, indicating that it is passing half the power of fluctuations with that period. The low-pass filter is shown to cut off near 30 days. It is expected that the characteristic timescales of the phenomena of interest in this dissertation are sufficiently different so that the results presented herein are insensitive to changes in filter construction. Analysis is currently in progress to verify this expectation.

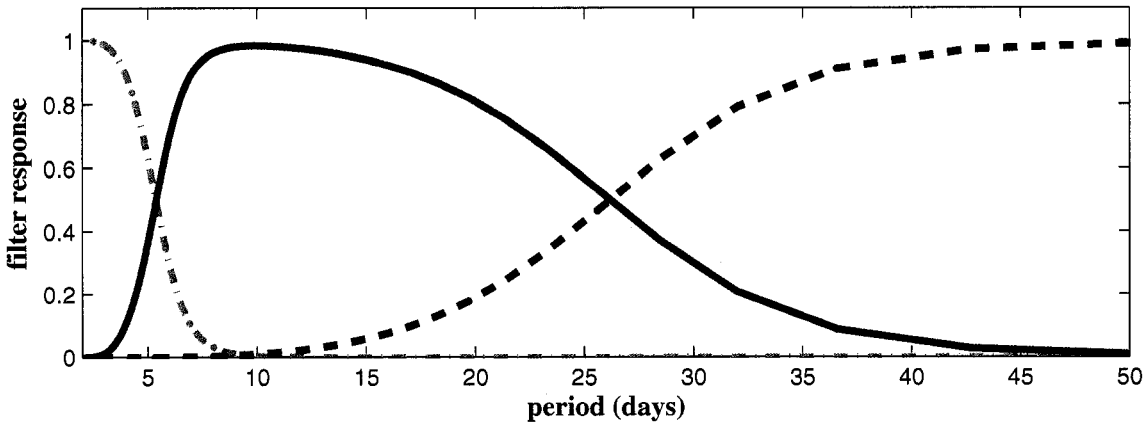


Figure 2.1: Response functions for the three filters: high frequency (green dash-dotted), intermediate frequency (red solid), and low-frequency (blue dashed).

### *2.3 Variance by filter cutoff frequency*

Figure 2.2 shows the variance of the daily winter DJF height fields for the period from 1958-2001 for the low pass, intermediate, and high pass frequency bands. The low pass data exhibit the highest variance of the three, accounting for 45% of the total variance of the unfiltered data. This field has four regional variability maxima, the strongest of which is centered near the southeastern tip of Greenland. In the Pacific sector, there is a strong variance maximum southwest of the Aleutian Islands which Blackmon et al. (1984a) associated with fluctuations in the Pacific-North American pattern on this timescale. In addition to these two centers of variance, there are two others over northern Russia and the Arctic Ocean north of Siberia that are slightly weaker in amplitude.

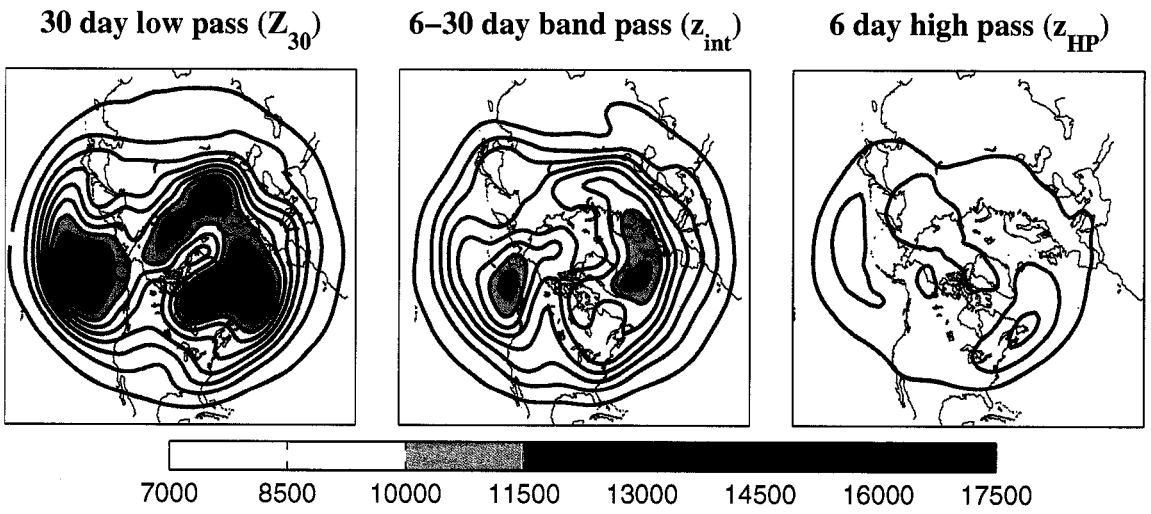


Figure 2.2: Variance of 500 hPa height field by frequency band. Contour interval is 1500 $m^2$.

For the choice of filters used in this study, variance on intermediate timescales as defined in this section is less than that for the low frequencies. More significant is the fact that the centers of maximal variance are slightly different. In the Atlantic sector, the strongest center is shifted eastwards of the center in the $Z_{30}$ variance and it is more zonally elongated. The Pacific center is located over the southwest coast of Alaska, well to the north and east of the maximum in the $Z_{30}$ variance. Variability in this region will be shown to be due to a relatively high occurrence of blocking ridges and deep troughs. Variance in the high pass field accounts for only 10% of the total variance of the unfiltered data, and the maxima in both the Pacific and Atlantic basins are coincident with the climatological storm tracks (Blackmon, 1976; Blackmon et al., 1977; Chang et al., 2002).

### *2.4 Hemispheric EOFs by frequency*

To diagnose the underlying structures of variability responsible for the features in Figure 2.2, EOF analysis was performed for what will be hereafter referred to as the Atlantic (90W - 90E) and Pacific (90E - 90W) sectors. Both sectors extend latitudinally from 20N - 90N. The analysis was performed for sectors, rather than over the full hemisphere because

it yields a slightly simpler set of patterns. All the maps shown in this section are based on modes derived from EOF analysis of sectoral data only. Full hemispheric patterns are derived by regressing the hemispheric fields on the expansion coefficient time series of the sectoral modes.

The leading EOF for each of the frequency bands in the Atlantic sector is shown in Figure 2.3. The leading mode for the low pass data corresponds closely to the NAO pattern shown in Fig. 1.1 aside from a reversal of sign. In the polarity shown here, anomalously high heights centered over southern Greenland occur in association with anomalously low heights over a broad swath of the midlatitudes that stretches from the eastern United States across the Atlantic and over Scandinavia. The axis of this dipole occurs near 50 N. The 16% of the variance explained by this mode in the $Z_{30}$ field is slightly lower than the 18% of the variance of the monthly anomaly field explained by the pattern in Fig. 1.1. The lower explained variance is a consequence of performing the EOF on daily data with a 30 day lowpass filter rather than on monthly averages.

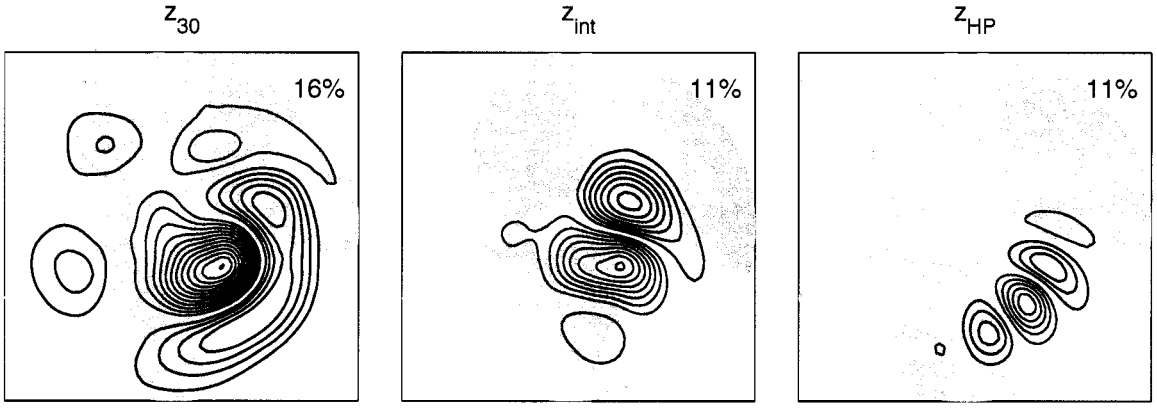


Figure 2.3: The leading EOF of wintertime 500 hPa height anomalies in the Atlantic sector based on time-filtered data for the three frequency bands. Contour interval is 10 m in all panels, percentage of variance explained is located in the upper right hand corner.

The first EOF of the intermediate timescale data is also primarily a dipole, with centers of action over southern Greenland and eastern Scandinavia. The occurrence of anomalies of opposing sign over these two regions suggests that blocking over Greenland might be

associated with high amplitude troughs or cutoff lows over Scandinavia, and vice versa. The Greenland center is collocated with the primary center of action of the NAO pattern, but is more meridionally elongated. The third, much weaker center of action in the pattern is located over the northeastern U.S., and its placement to the west of the primary centers gives the impression of a zonally oriented wave-train. The distinction between the low-frequency "dipole" pattern and the intermediate frequency "wavetrain pattern" is consistent with the idealized model in Fig. 13 of Blackmon et al. (1984a).

The leading EOF of the high pass data set is a wave train along the Atlantic storm track with wavelength $\sim$ 4000 km, corresponding to that of baroclinic waves. The second EOF of this data set yields a similar pattern, but is offset zonally, providing further indication that the leading high pass EOFs reflect baroclinic waves propagating across the Atlantic.

The set of leading EOFs for the Pacific sector (Fig. 2.4) follow a similar pattern. The leading EOF of the low pass data resembles the PNA pattern, the most prominent large-scale mode of variability in the Pacific on monthly timescales. On intermediate timescales, the leading mode of variability is suggestive of a more zonally oriented wavetrain, with a strong center over the southwest coast of Alaska, coincident with the variance maximum shown in the middle panel of Fig. 2.2. In contrast to the North-Atlantic pattern shown in the previous figure, this mode is dominated by a single center of action, rather than a dipole, and is flanked by two much weaker centers of opposing sign. A large amplitude anomaly with the polarity shown in Fig. 2.4 would look like a Pacific $\Omega$ blocking pattern in the full Z field (Rex, 1950a) and a large amplitude anomaly of opposing polarity would be characterized by a deep trough or cutoff low. As in the Atlantic sector, the leading mode of variability in the high pass data is the signature of baroclinic waves propagating along the climatological storm track.

### *2.5 EOFs of the intermediate timescale variance field*

The leading EOFs of the variance of $z_{int}$ (*i.e.* ${z_{int}}^2$) for each sector (Fig. 2.5) show that the primary mode of variability for each basin is a pulsing of the regions of largest intermediate timescale climatological variance. In the Pacific, this pattern takes the form of a single center over the Gulf of Alaska, and in the Atlantic it assumes the form of a high latitude

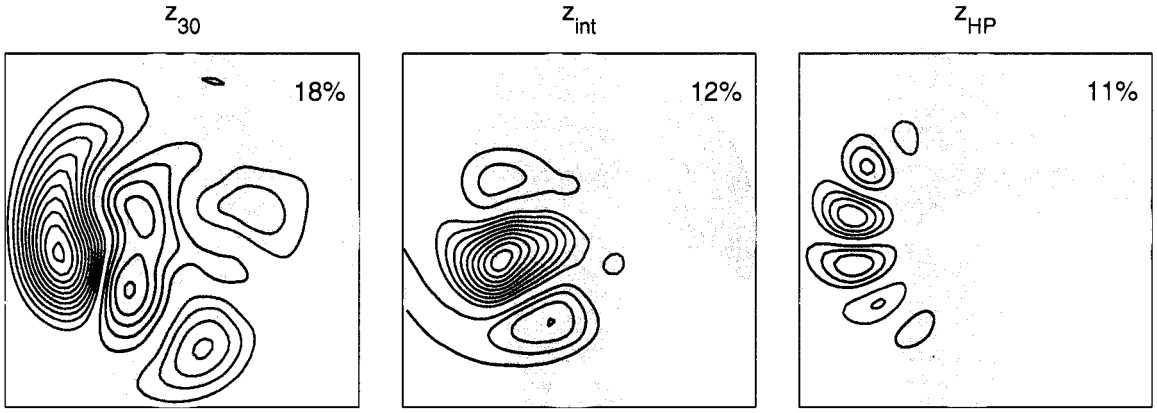


Figure 2.4: As in Fig. 2.3 but for the Pacific sector.

"dumbbell" pattern joining two maxima over Greenland and Scandinavia. In each case there is only one distinct and significant mode.

It should be noted that performing EOF analysis on a nonlinear field such as variance is quite different from analyzing linear fields, because the probability density function resembles the chi-squared distribution rather than the normal distribution. This non-normality carries over to the PDFs and principal component time series (Figs. 2.6 and 2.7) that show how the spatial structures shown in Fig. 2.5 vary with time. The PDFs for both sectors are non-normal and exhibit considerable positive skewness. The PC timeseries are characterized by relatively long periods of near zero values, punctuated by high amplitude, positive spikes. These spikes convey no information about the polarity of the height anomalies; they could be either positive or negative.

The $z_{int}$ anomalies associated with spikes in Atlantic PC1 are shown for the two Atlantic centers of action in Fig. 2.6. There is a strong correspondence between the two sets of anomalies, with spikes in PC1 being associated predominantly with positive intermediate-scale height anomalies over Scandinavia, and simultaneous negative anomalies over Greenland. Some high amplitude events exhibit anomalies of both polarities over both regions, indicative of a single event being associated with blocking over one center of action early in the event and the other center of action later in the event. The relationship between

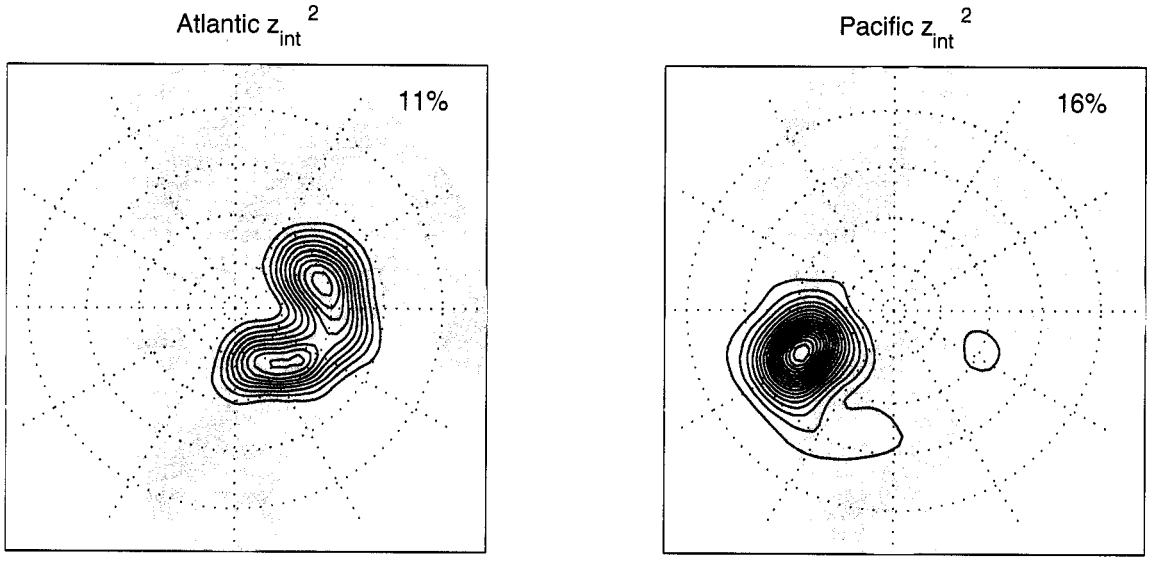


Figure 2.5: Leading EOF of intermediate scale variance $z_{int}{}^2$ for the Atlantic (left) and Pacific (right) sectors. Contour interval is 2000 $m^2$.

height anomalies over these two centers will be further explored in Chapter 4. In Chapter 5, we will show that the association between PC1 spikes and this configuration of height anomalies is consistent with the tendency for blocks over Scandinavia to retrograde across the North Atlantic.

The height anomalies over Anchorage associated with spikes in the Pacific PC1 (Fig. 2.7) appear not to favor one sign of anomaly; spikes associated with individual positive and negative anomalies are found in approximately equal numbers. The largest spikes appear to be associated with an evolution of anomalies over Anchorage, from large positive values to large negative values, which is consistent with the signature of blocks that form near Anchorage and are replaced within a few days, by a high amplitude trough or cutoff low.

The interpretation of these time series and patterns is that, rather than being indicative of a sinusoidally varying, pulsing mode, they are more appropriately viewed as a sequence of irregularly spaced, short duration, high-amplitude events. These rather localized patterns emerge as EOFs because high amplitude events in the intermediate frequency variability tend to be spatially localized, as indicated in the variance maps in Fig. 2.2.

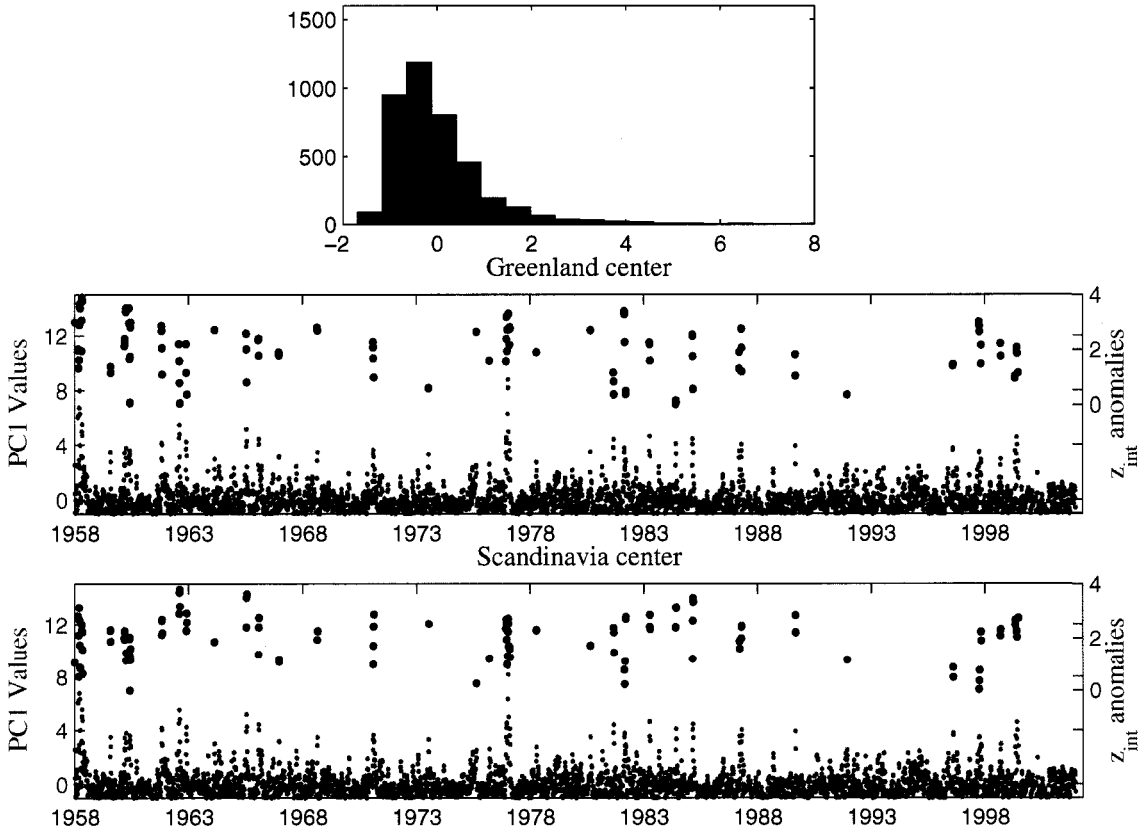


Figure 2.6: The top panel shows the PDF of PC1 of ${z_{int}}^2$ for the Atlantic sector. The corresponding PC1 timeseries is shown in the middle panel in gray, and repeated in the bottom panel. For normalized PC1 values $> 2.5$, standardized anomalies in $z_{int}$ are shown for the two Atlantic centers of action over Greenland (middle) and Scandinavia (bottom). Negative anomalies are represented by blue circles, positive anomalies are shown in red. The abscissa in the bottom panels is time, in days, and labeled tick marks indicate Jan. 1 of the year indicated.

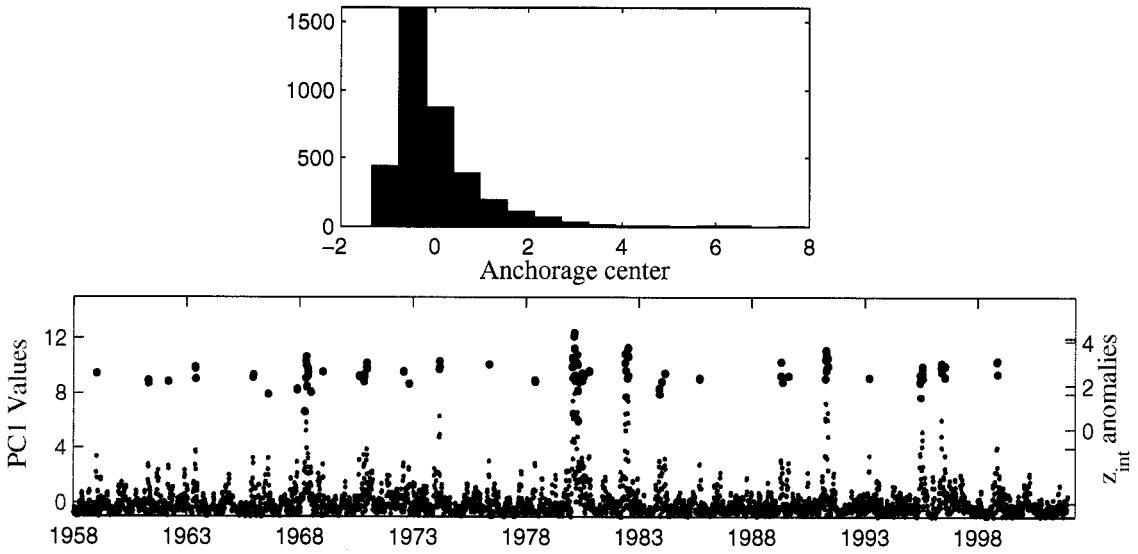


Figure 2.7: As in Fig. 2.6, but for the Pacific sector, and for the single center of action over Anchorage.

### *2.6 Variance by polarity of the NAO and PNA*

As a simple step towards demonstrating the existence of a significant relationship between fluctuations in ${z_{int}}^2$ and the dominant modes of low-frequency variability in each basin, ${z_{int}}^2$ was evaluated for subsets of data that have been sorted in accordance with the value of the PNA or NAO (Fig. 2.8). During periods when the NAO $< -1$ , the high latitude centers of variance over Baffin Bay and Scandinavia are 2-3 times as large as they are during NAO $> 1$. In the Pacific, the $PNA^-$ phase favors enhanced variance over the Gulf of Alaska and most of the northern Pacific when compared with $PNA^+$, consistent with the results of Palmer (1988).

### *2.7 Summary*

The evaluation of the basic statistics and primary modes of variability for the three frequency bands in this chapter has laid the foundation for the analyses that follow. We have shown that each of the three frequency bands considered in this study exhibits its own distinctive patterns of variability. As documented in many previous studies, the low-frequency

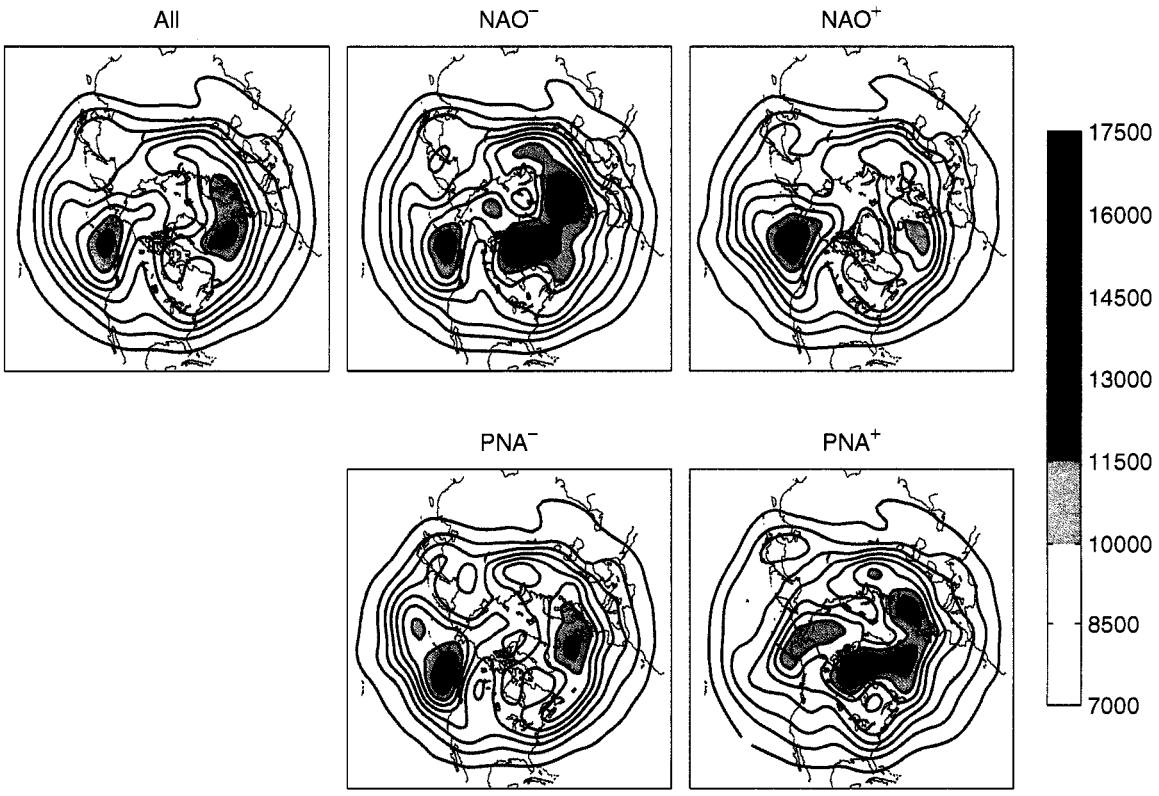


Figure 2.8: The variance of $z_{int}$, composited by polarity of the NAO and PNA. The threshold for positive and negative polarities of the indices are $+1$ and $-1$ standard deviations respectively. Contour interval is 1500 $m^2$.

variability variability is dominated by teleconnection patterns, and the high-frequency variability by baroclinic waves. The intermediate frequency variability exhibits patterns with well-defined centers of action in each basin. In the Pacific, the most prominent feature is centered over southern Alaska, while the Atlantic variability is most explained by a pair of centers over Greenland and Scandinavia.

The most important idea contained in this chapter is that, even for the most basic climatological statistics and EOF analysis of the intermediate frequency variability in the 500 hPa wintertime height field, certain locations appear repeatedly as both centers of climatological-mean variance, and centers of action of the dominant modes of variability of fluctuations in that variance. In the Pacific, this center is primarily over the southwest coast of Alaska. In the Atlantic, a pair of centers is involved: one over Greenland and the other over Scandinavia. It is evident even from crudely stratifying the data by polarity of the NAO and PNA that the variability near these centers is enhanced during the negative polarities of these two modes. In the following chapters we will further investigate these relationships.

# Chapter 3

# NONLINEAR RELATIONSHIPS BETWEEN $Z_{30}$ AND SHORTER TIMESCALE VARIANCE

## *3.1 Introduction*

By construction, fluctuations in the three frequency bands defined in section 2.1 are largely linearly independent of each other and therefore have minimal covariance with one another. In the previous chapter, however, the polarities of the NAO and PNA were shown to influence the level of intermediate scale variance in their respective ocean basins. This suggests the possibility of a nonlinear relationship between fluctuations in low and intermediate frequency bands, in the sense that linear fluctuations on long timescales can modify the frequency of occurrence of extreme events on intermediate timescales. This chapter is devoted to elucidating these relationships.

A set of *a priori* expectations for relationships between the frequency bands may be obtained from the literature. The associations between the low- and high-frequency bands, for the Atlantic sector in particular, have been extensively documented (Rogers, 1990, 1997; Hurrell and van Loon, 2003; Serreze et al., 1997; Alexandersson et al., 1998). This body of work has shown that fluctuations in the NAO are strongly associated with shifts in position and intensity of the wintertime mean storm track. When the NAO is in its positive polarity, the storm track shifts northeastward and intensifies, as evidenced by enhanced storm activity in a region from Newfoundland to northern Europe and Scandinavia, as well as moderate decreases in storminess to the south of these regions. The Pacific storm track has been shown to exhibit similar meridional shifting in association with variations in the PNA (Lau, 1988), though the sign is reversed; $PNA^+$ winters tend to have enhanced storm tracks equatorward of their climatological mean position.

The relationship between the low-frequency and the intermediate-scale frequency has received less study. Kimoto and Ghil (1993) examined flow regimes in the 10-day low

pass filtered 700 hPa geopotential heights, and found the Atlantic and Pacific basins to exhibit states of zonal flow and blocked flow corresponding to opposing polarities of the NAO and PNA respectively. Quadrelli and Wallace (2004b) generated "spaghetti plots" of dectads of specific 500 hPa contours for contrasting polarities for the NAM and their "PNA-like" sea level pressure pattern. They found a strong tendency for a persistent ridge near Greenland to develop during the months of negative polarity of the NAM, as well as a tendency towards large meridional displacements of representative height contours over the North Pacific. Shabbar et al. (2001) found more frequent, and longer-lived North Atlantic blocks during $NAO^-$ months. Renwick and Wallace (1996) found a similar relationship in the North Pacific, but with more blocking during $PNA^-$ months.

In this chapter, we elicit the relationships between our three frequency bands utilizing three methods: The first is to apply maximum covariance analysis (MCA) to the 500 hPa height field from one frequency band and the 500 hPa variance field of another band. The second is through simple regression analysis of the variance fields onto the dominant modes of low-frequency variability (i.e., the NAO and PNA pattern). The third is to contrast the dominant structures of variability of $z_{int}$ and ${z_{int}}^2$ during extended intervals with contrasting polarities of the NAO and PNA patterns.

## *3.2 Inter-frequency Maximum Covariance Analysis*

Maximum covariance analysis in the atmospheric sciences is typically performed between a pair of linear, normally distributed data sets as described in Bretherton et al. (1992) and Wallace et al. (1992). The analysis yields ordered pairs of patterns and associated coefficient time series which, taken together, explain the greatest amount of squared covariance between two data sets. The relatively small overlap in frequency space between our data sets implies that MCA between the fields themselves will have weak structures and amplitudes; they have little covariance to explain. If nonlinear relationships exist between the two bands, however, MCA has the potential to extract relevant spatial structures and time series. If anomalies in one field of a given polarity implied an increased likelihood of an extreme event in the other, for example, MCA between the first field and the square of the second should be capable of extracting that relationship. This example has relevance for the relationship

between low-frequency modes and intermediate-scale blocking episodes. MCA provides an objective means of letting the data determine the relevant structures in each field. MCA has been used widely in the atmospheric science literature, but we are unaware of any other study utilizing it in this manner.

One consequence of utilizing MCA on squared fields is that, as discussed for the EOFs of ${z_{int}}^2$ in Chapter 2, the timeseries associated with the squared fields are non-normally distributed and prone to spikiness. Typically MCA makes use of statistical quantities such as the squared covariance fraction (SCF) and correlation coefficients between expansion coefficient timeseries of the pattern pairs as a means of determining the significance of the patterns. The interpretation of these values for the configurations we use here is less clear. In the present analysis, we use these statistics only as a guide, but also emphasize the consistency of the MCA results with the published literature and other results in this study.

We employ three configurations for the MCA: Low pass height anomalies ($z_{30}$) with intermediate scale variance (${z_{int}}^2$), $z_{30}$ with high pass variance (${z_{HP}}^2$) , and intermediate scale height anomalies ($z_{int}$) with the high pass variance (${z_{HP}}^2$). The set of heterogeneous covariance maps for the first configuration in the Atlantic sector are shown in Fig. 3.1. The structure in ${z_{int}}^2$ that explains the largest amount of covariance between it and $z_{30}$ shows that increased variability, with maxima over Baffin Bay and northern Scandinavia, occurs in association with a structure that strongly resembles the negative polarity of the NAO. The expansion coefficient time series associated with this structure is correlated with the NAO index generated in the previous chapter at a level of $-0.92$. Again we see that the centers of enhanced variance shown in this figure agree well with the highest latitude centers of the "pulsing" EOF of the variance field shown in Fig. 2.5. The maximum over Baffin Bay is consistent with the established relationship between Greenland blocking during $NAO^-$, as discussed in the previous chapter. The relative weakness of the Scandinavian center of action in relation to the Baffin Bay center as compared with the more balanced pattern in Fig. 2.5, as well the tendency for Baffin Bay to have below-normal geopotential heights during excursions in that pattern, indicate that the two analyses may be capturing different blocking behavior in the North Atlantic region. In a future extension of this work, this behavior is to be further diagnosed utilizing a similar methodology to that shown in Fig.

2.6.

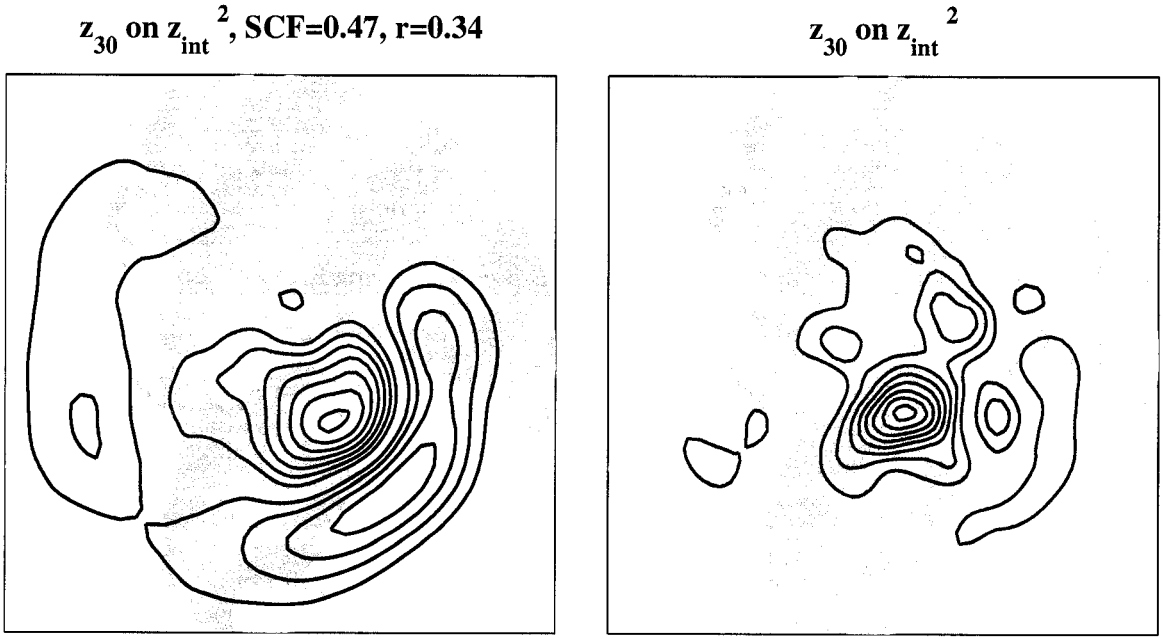


Figure 3.1: Leading heterogeneous maps between $z_{30}$ (left) and ${z_{int}}^2$ (right). Contour intervals are 5 m and 500 $m^2$ respectively.

The first pair of heterogeneous covariance maps of $z_{30}$ with ${z_{HP}}^2$ (Fig. 3.2) shows a different relationship. The pattern in the $z_{30}$ field is again a dipole that bears a resemblance to the NAO pattern, though the axis of the dipole is 5-7 degrees northwards of the axis of the NAO pattern. The associated structure in the ${z_{HP}}^2$ field indicates decreased high pass variance along this axis, indicating a decrease in storm activity there, and an associated increase in storminess equatorwards of the midlatitude center of the $z_{30}$ dipole pattern. This weakening and equatorward shifting of the storm track is consistent with the patterns documented for the $NAO^+$ phase (*e.g.* Fig 15. Hurrell et al., 2003 ), taking into account the reversal of sign.

It is noteworthy that despite the existence of an extensive literature on the relationship between high frequency transients and nonlinear weather events such as blocking (Shutts (1983), Mullen (1986) (Nakamura and Wallace, 1993)), the MCA of $z_{int}$ and ${z_{HP}}^2$ did not show a strong relationship. The expansion coefficients for the first two pairs of patterns

have low correlation ($r = .35$), explain a small amount of covariance ($SCF = .26$), and have weak amplitudes (not shown). One plausible explanation for this could be that there is simply not enough consistency in development or location between individual blocking events, much less in the associated synoptic scale eddies, to allow for a consistent signal to emerge from MCA between the fields.

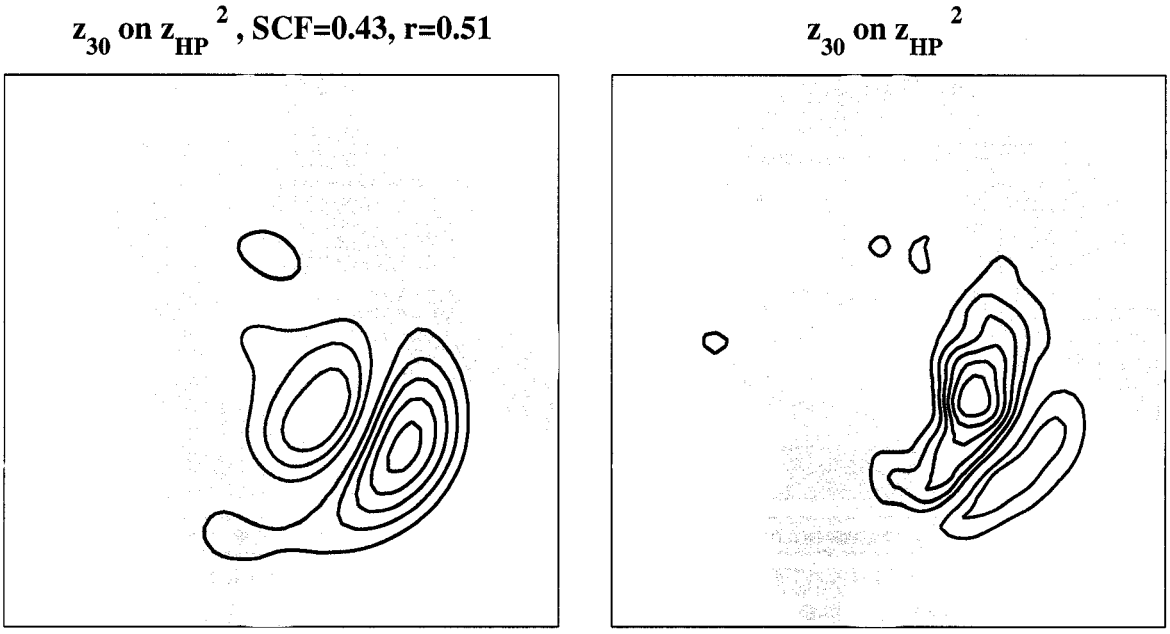


Figure 3.2: As in Fig. 3.1 but for $z_{30}$ (left) and $z_{HP}{}^2$ (right).

The spatial structures for the leading Pacific sector MCA mode between $z_{30}$ and $z_{int}{}^2$ (Fig 3.3) consist of a dipole in $z_{30}$ and an associated, basin-scale center of fluctuating variance in the $z_{int}{}^2$ field centered over southwestern Alaska. Though the dipole is reminiscent of an NAO$^-$ like pattern in the Pacific, it is highly temporally correlated with the PNA ($r = 0.8$), and fairly well spatially ($r = 0.5$). The slight northwestward shifting of the axis of the pattern relative to the PNA wave-train pattern detracts from the spatial correlation but doesn't affect the temporal correlation as much. The MCA patterns have a high squared covariance fraction (0.64) and are relatively well correlated in time, so there is reason to believe they represent viable, physically valid structures. The other configurations for Pacific

MCA perform much more poorly, however, and are difficult to interpret physically. In the remainder of the chapter we will use the PNA pattern, as defined in Wallace and Gutzler (1981), as a proxy for the low-frequency pattern in Fig. 3.3.

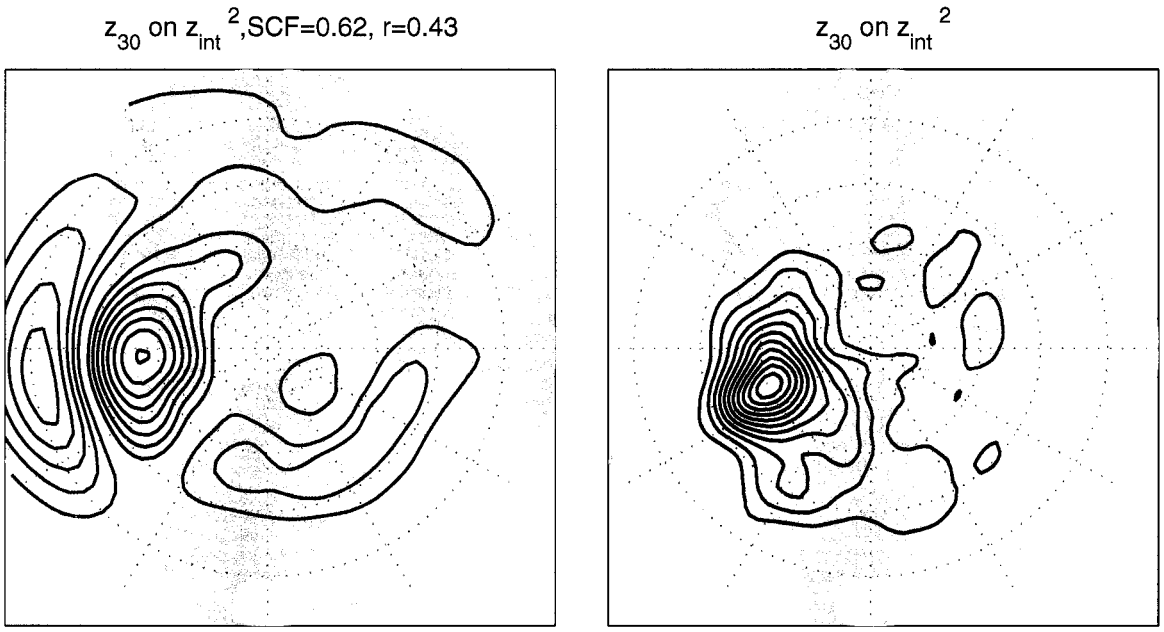


Figure 3.3: As in Fig. 3.1 but for the Pacific sector.

### *3.3 Regression Analysis*

Results from the previous sections lead us to view the NAO and PNA-like patterns as the most important $z_{30}$ modes related in a non-linear way to intermediate timescale perturbations. To further place our results in this framework, we regressed the intermediate frequency variance field upon the time-varying indices of the NAO and the PNA pattern. The extremely high level of correlation between the NAO index and the $z_{30}$ expansion coefficient time series from the MCA implies that the regression of ${z_{int}}^2$ and ${z_{HP}}^2$ onto the NAO index will yield a set of maps similar to those derived from MCA. Indeed, the left panels of Fig. 3.4 show this to be true: the negative polarity of the NAO is associated with an anomalously southward shifted and weakened storm track, and enhanced intermediate

scale variance over Greenland and Scandinavia.

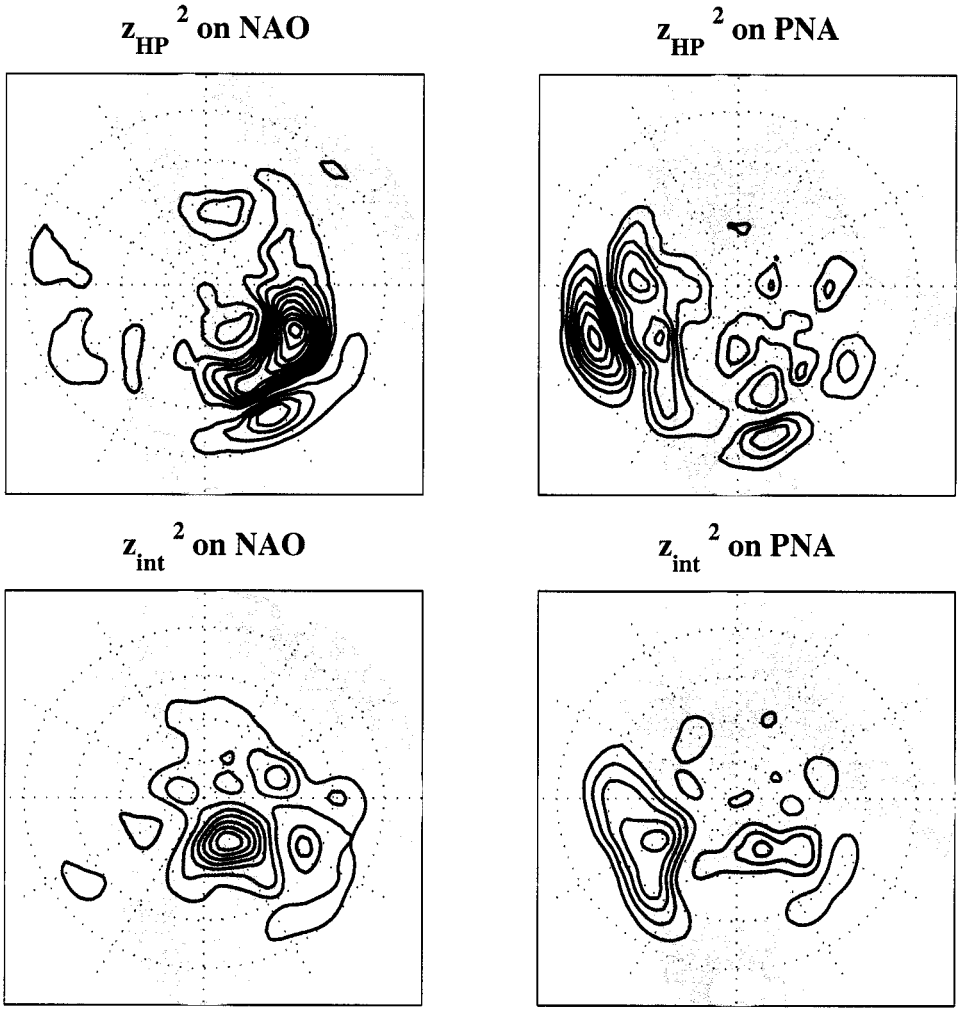


Figure 3.4: Regression maps of (a) $z_{HP}{}^2$ and (c) $z_{int}{}^2$ on the NAO, and (b) $z_{HP}{}^2$ and (d) $z_{int}{}^2$ onto the PNA. Contour interval for panels (a) and (b) is 100 $m^2$ and 500 $m^2$ for panels (c) and (d).

The relationships in the Pacific are slightly different from the corresponding relationships in the Atlantic sector. The negative polarity of the PNA is also associated with a shifting of the Pacific storm track, as shown in Fig, 3.4. In this case the shifting is poleward rather than equatorward as it is for $NAO^-$ in the Atlantic sector, consistent with the results of Lau (1988). $PNA^-$ favors enhanced $z_{int}{}^2$ centered over the Gulf of Alaska and southern

Alaska. In the Pacific sector, then, the negative polarity of the PNA pattern is associated with increased variance on both short and intermediate timescales for a swath that extends across most of the Gulf of Alaska and down the west coast of North America.

### *3.4 Sectoral EOFs for contrasting polarities of the NAO and PNA*

One drawback to the MCA and EOF analysis is that they yield a set of spatially fixed patterns that can only vary in amplitude in accordance with its expansion coefficient or principal component time series. If there were fundamentally different structures in $z_{int}{}^2$ that occurred during the contrasting polarities of the NAO, for example, the variance pattern associated with the NAO structure would be constrained to be some linear combination of the two. One way to circumvent this constraint is to examine the sensitivity of the primary modes of variability in the $z_{int}$ and $z_{int}{}^2$ fields to background state changes corresponding to contrasting polarities of the NAO and PNA.

To carry out this analysis, the data are broken into a series of four subsets in accordance with the normalized values of the NAO and PNA in the Atlantic and Pacific sectors respectively. EOFs were then calculated for these subsets of $z_{int}$ and $z_{int}{}^2$. The threshold for the positive subsets is that the standardized index value be greater than 1, and the negative subsets be less than -1. The high and low subsets both contain approximately 800 daily values.

Results for the Atlantic sector are shown in Fig 3.5. Under the background conditions of anomalously high Arctic heights and a relatively weak jet associated with $NAO^-$, the primary mode of variability of $z_{int}$ is a high latitude dipole with centers over Baffin Bay and northern Scandinavia. The centers are meridionally elongated and tilted in opposite directions. This mode accounts for 18% of the variance of the 500 HPa height field during these intervals, and is the only one that is distinct. The first EOF of $z_{int}{}^2$ for $NAO^-$ is a monotonic field with two centers of action over the same, high-latitude locations.

The leading EOF of $z_{int}$ for $NAO^+$ conditions also resembles a dipole, but in this case the centers are weaker and the pattern explains only 13% of the variance; the stronger of the two features is centered south of Iceland in the North Atlantic, and is paired with a relatively weaker downstream feature centered over Eastern Europe. Both of the centers

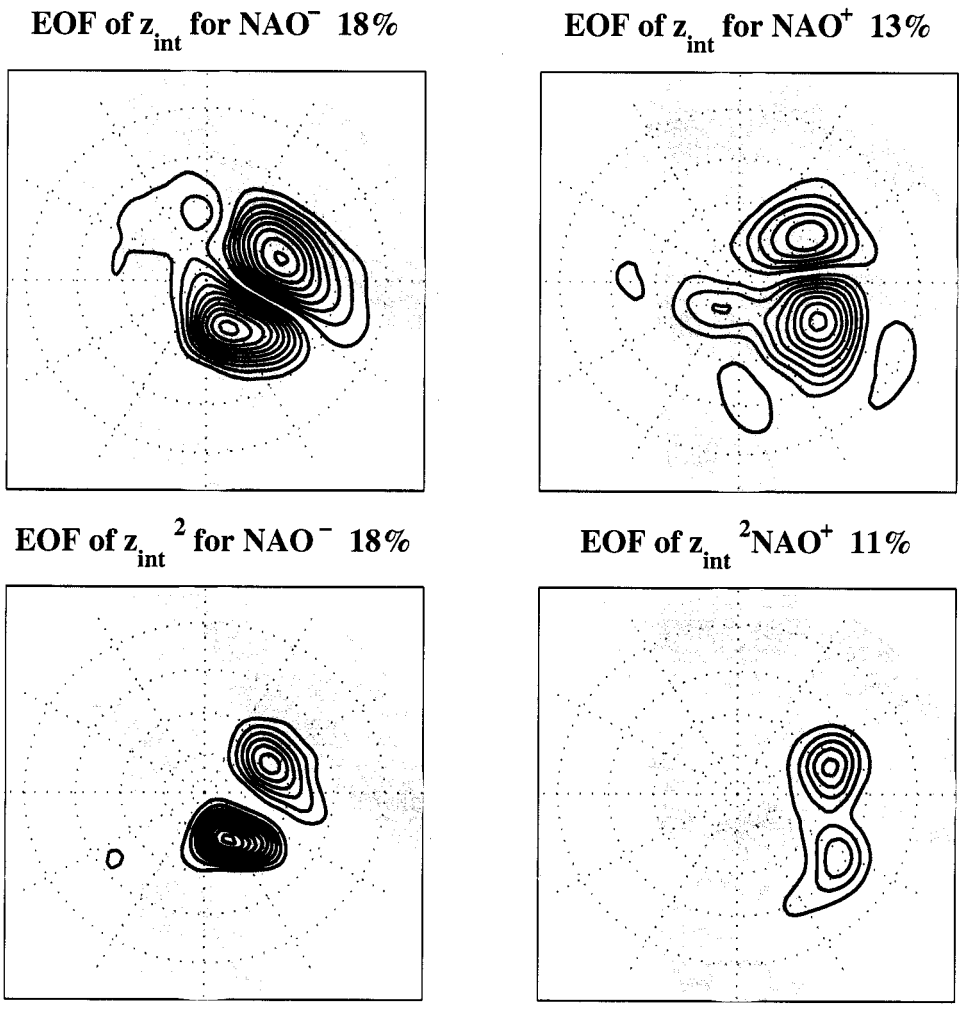


Figure 3.5: Atlantic EOFs of $z_{int}$ and ${z_{int}}^2$ for $NAO^-$ (NAO < -1) and $NAO^+$ (NAO > 1) conditions. The top panels are contoured at an interval of 10 m; the bottom panels at 2000 $m^2$.

are more isotropic than their counterparts from the $NAO^-$ subset. The $NAO^+$ variance EOF is weaker and its centers of action are located farther south than those for its $NAO^-$ counterpart. The differences are especially pronounced over the western Atlantic.

It should be noted that, though the dominant patterns from contrasting polarities of the NAO have distinctly different characters, the leading EOF of the complete data record as shown in the previous chapter is clearly a linear combination of the two. The full EOF thereby obscures what is evident from this analysis, that it is the $NAO^-$ polarity that exhibits the stronger, more distinctive structures, whereas the patterns during $NAO^+$ are weaker and less distinct.

The results from repeating this analysis for the Pacific sector stratified by polarity of the PNA are shown in Fig. 3.6. For the $PNA^-$, the first EOF of $z_{int}$ is the same pattern that appears as the first mode of variability of the unstratified $z_{int}$ field shown in Fig. 2.4. The first mode of ${z_{int}}^2$ variability captures essentially the same behavior, with a strong center of action located over the Gulf of Alaska. The results for $PNA^+$ are much more difficult to interpret, though they explain an equally large amount of variance. EOF 1 contains elements of a wave train in the $z_{int}$ field, tracing a great circle from Korea through eastern Siberia, Alaska, and to the eastern subtropical Pacific. The centers of action are weaker in amplitude than in the $PNA^-$ case, but are considerably greater in spatial extent. The EOF of the variance field indicates a monotonic pulsing of variance over the Northwest Territories of Canada and the Chukchi Sea. In this case there is no obvious relationship between the centers of action in the $z_{int}$ and ${z_{int}}^2$ fields. Though we are unaware of any other references showing evidence associating $PNA^+$ background conditions with an enhancement of intermediate scale variability in the high-latitudes, this relationship is suggested in Fig. 2.8 by a strong enhancement in intermediate-scale variance over precisely these locations for the $PNA^+$ subset.

### *3.5 Summary*

The results from this chapter further develop the relationship between the frequency bands in the Atlantic and Pacific sectors. The ability of the MCA to extract coupled patterns in the low-frequency data and the high-frequency band that are consistent with the literature

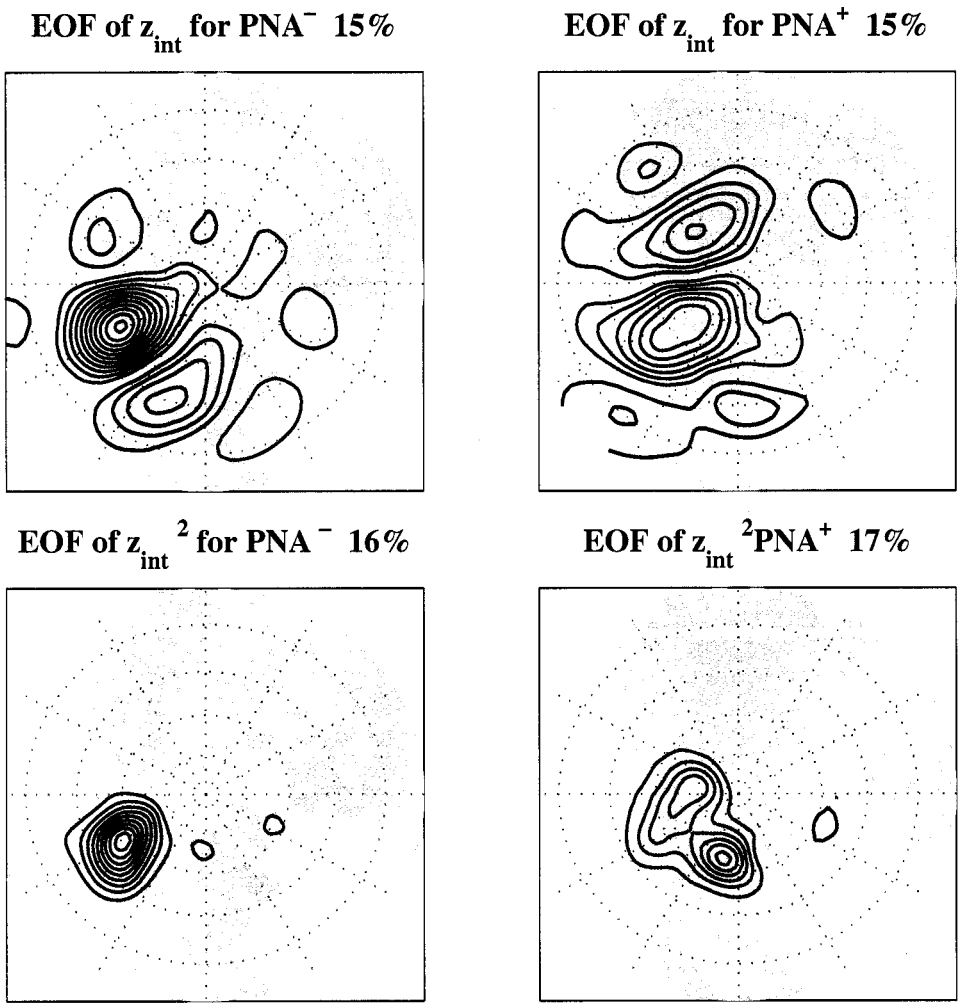


Figure 3.6: As in Fig. 3.5 but for the Pacific sector and using the PNA.

gives us confidence in the structures that it yields for the intermediate-scale variability. The MCA selects the NAO in the Atlantic sector and a PNA-like pattern in the Pacific sector as the dominant low-frequency patterns that covary with the variance in the other frequency bands. In the Atlantic, it yields a clear separation of behaviors between the high and intermediate-scale variance; for $NAO^-$, ${z_{int}}^2$ is enhanced over the North Atlantic, and in particular over Baffin Bay, while ${z_{HP}}^2$ is decreased in the same region as the storm track shifts equatorward. An analogous separation is not observed in the Pacific sector, where $PNA^-$ favors enhanced activity on both timescales for a region stretching across the North Pacific and down the west coast of North America. These relationships are further confirmed by regression analysis of the variance fields onto indices of the NAO and PNA.

That the MCA and regression analysis are constrained to yield fixed patterns that can vary only in amplitude may obscure important differences between the two polarities of the low-frequency modes. The structures of variability for the $NAO^-$ background state are sufficiently strong in relation to those of the $NAO^+$ as to suggest there is something inherently special about the $NAO^-$ polarity that allows for coherent, intermediate-timescale anomalies to develop, while suppressing the high-frequency variability along the northern flank of the storm track. The centers of action over Baffin Bay and Scandinavia present in the EOF pattern have now emerged repeatedly in the present study, having been evident in the variance maps and the EOF patterns of ${z_{int}}^2$ of Chapter 2, as well as in the MCA of $z_{30}$ and ${z_{int}}^2$ in this chapter. These centers are more prominent during the $NAO^-$ polarity, and we believe they are vital to understanding this timescale of variability in the Atlantic sector overall. Diagnosing the relationship between these two centers of action is a central theme of the following chapter.

# Chapter 4

# ON SKEWNESS IN THE Z FIELD

## *4.1 Introduction*

Blocking events have a distinctly nonlinear signature in the geopotential height field. During their onset, blocks develop linearly as a ridge, but if the ridge amplifies beyond a certain threshold, it can persist for as long as about a week as a closed, quasi-stationary anticyclone. A discussion and pictorial description of this process as one of "wave breaking" in the potential temperature field on the tropopause is provided by Pelly and Hoskins (2003).

The nonlinear appearance of these events would seem to require a nonlinear mechanism for their development and maintenance. As discussed in Chapter 1, one paradigm holds that the the pre-existing ridges are both amplified by vorticity perturbations from upstream transient activity, and then further maintained by the high-frequency transients against dissipation and advection by the mean flow (Shutts, 1986; Trenberth, 1986; Mullen, 1987; Haines, 1989; Nakamura and Wallace, 1993). Frederiksen (1989) and Frederiksen and Bell (1990) further confirmed the role of baroclinic waves in the onset stage of blocking using three-dimensional instability theory, but also highlighted the role of large-amplitude, barotropic, fast-growing normal modes in the transition to the mature blocking phase.

Large scale, relatively low-frequency disturbances in the form of Rossby waves have also been shown to play a role in the development of blocks. Takaya and Nakamura (2005) investigated blocking events associated with intraseasonal amplification of the Siberian high, and found them to be regionally dependent on quasi-stationary Rossby waves from different sources. Blocks over western and central Siberia were found to be amplified by Rossby waves emanating from the North Atlantic, while blocks in eastern Siberia were associated with Rossby-wave forcing retrograding through the Bering Strait from the North Pacific. Noting the frequent spatial and temporal coincidence of regional blocking events and the westward-propagating, free Rossby waves documented in Kushnir (1987) and Branstator

(1987), Lejenäs and Madden (1992) studied the role of traveling planetary-scale waves of wavenumbers 1 and 2. They found that, depending on longitude, between 20-40% of blocks were coincident with large-scale traveling waves of wavenumber 1. They did not offer a dynamical interpretation of the relationship between the two, but rather considered their interaction as a simple superposition of anomalies from two sources operating on different timescales.

In the first part of the chapter, we discuss the skewness field of the 500 hPa geopotential height field and its use in distinguishing between linear and nonlinear behavior of the intermediate frequency variability. We diagnose the source of skewness in the 500 hPa geopotential height field, and show that it is largely due to a superposition of the intermediate timescale variance field upon lower frequency anomalies. Results from this section and the previous chapter indicate that, for certain regions, nonlinear blocking events can be viewed as a superposition of variability on these two timescales, both of which appear to behave quite linearly in their own right. This behavior is somewhat similar to that discussed by Lejenäs and Madden (1992), though in this case, it is variations in heights due to slowly-varying fluctuations in the NAO and PNA that serve to augment transient ridges rather than their traveling wavenumber 1. In the latter part of this chapter, we explore this alternate framework by contrasting the appearance of composites of the most extreme high and low-amplitude anomalies in the full geopotential height field, the climatological anomaly field, and as departures from the monthly mean field, for locations of interest.

### *4.2 Insights derived from the skewness distribution*

We begin by documenting the skewness of $Z_6$, the daily DJF 500 HPa height field that has had the same 6 day low pass filter applied to it as was employed in the previous chapters. Fig. 4.1(a) shows the nondimensionalized coefficient of skewness $a_3 = \frac{m_3}{\sigma_x^3}$ for this field, where $m_3 = \frac{1}{N}\sum_{i=1}^{N}(x_i - \bar{x})$ and $\sigma_x$ is the standard deviation of the time series at a given grid point.

In his study of the skewness and kurtosis of this field, White (1980) noted that that fluctuations on this timescale are positively skewed to the north of the climatological storm tracks, and negatively skewed equatorward of them. He attributed this feature, evident

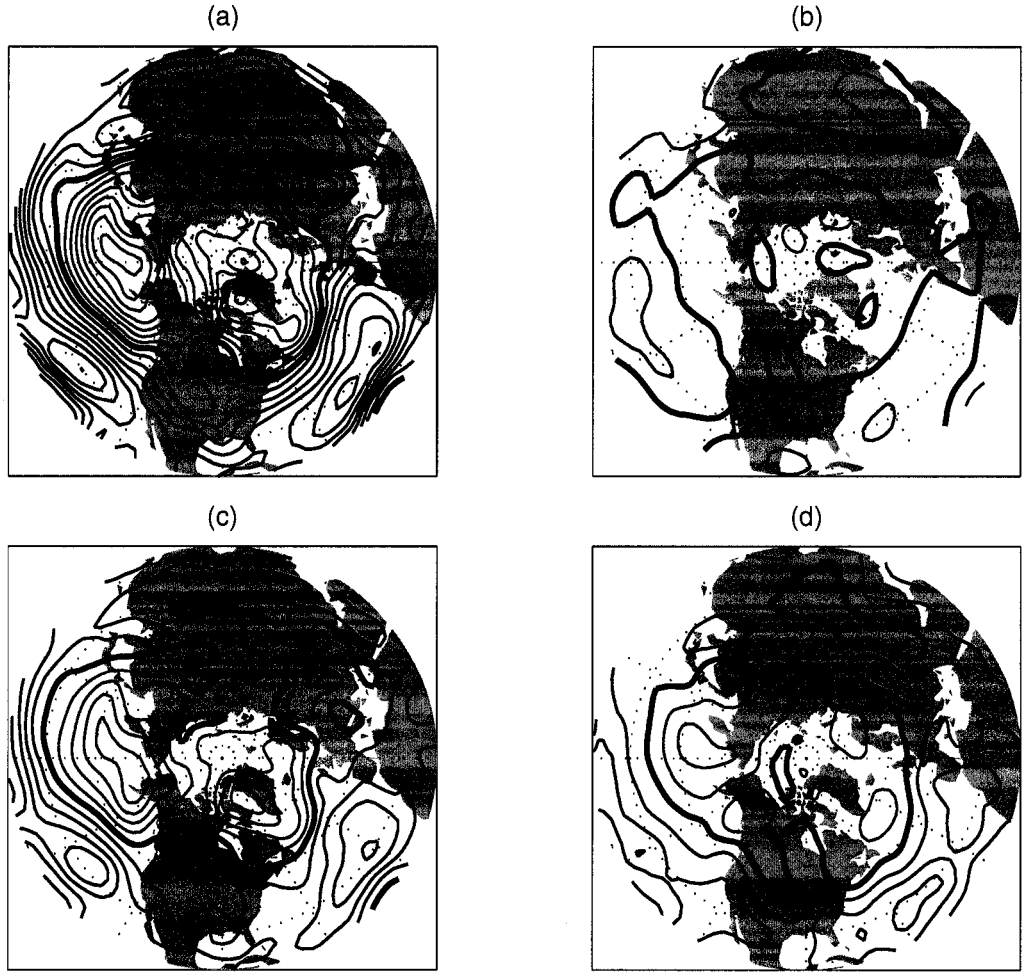


Figure 4.1: (a) Total normalized skewness magnitude of $Z_6$. (b)-(d) Contributions to that skewness from the $(Z_m Z_m Z_m)$ term, the $3\,(Z_m z'^2)$ cross-frequency term, and the $(z'z'z')$ terms respectively. In all panels, the contour interval is 0.1. Red and blue contours indicate positive and negative values respectively, and the thick black line is the zero contour.

in Fig. 4.1(a), to meridional displacements of the upper-level jet, which is the locus of the strongest gradients in geopotential height. The skewness field has been revisited by Nakamura and Wallace (1991), who attributed the positive skewness values to the occurrence of blocking anticyclones to the north of the storm tracks, and cutoff lows south of them. They further found that most of the skewness was due to a relatively small ($< 5\%$ of total) number of extreme events.

Other features of the skewness field that are significant for this study are the broad maximum centered over the Gulf of Alaska, which is largely coincident with the region of enhanced intermediate and high-frequency variability associated with the $PNA^-$ polarity in the previous chapter. In the Atlantic sector, the maximum in skewness is located over Baffin Bay, with additional local maxima over Scandinavia, and just south of the southern tip of Greenland. Of perhaps less direct relevance to the present study, there is also an interesting structure over Eurasia, with a narrow corridor of negative values extending from the Middle East to China north of the Tibetan plateau. Branstator (2002) has shown evidence of a wave guide for planetary wave propagation across this region.

As discussed above, positive skewness values of $Z_6$ are indicative of regions of blocking activity, so it is of interest to determine how fluctuations with different time scales contribute to the skewness field. For this purpose it is useful to decompose the height field into low frequency and intermediate frequency components, making use of the relation:

$$Z_6 = z' + Z_m \tag{4.1}$$

where $Z_m$ is the monthly average of $Z_6$, and $z'$ is the deviation of the daily low pass data ($Z_6$) data from its monthly mean. The $Z_m$ and $z'$ fields correspond closely to our $Z_{30}$ and $z_{int}$ fields from the previous chapters, but are derived more simply. Similar results are obtained decomposing $Z_6$ into $Z_{30}$ and $z_{int}$.

Cubing the above relationship allows us to rewrite the skewness of $Z_6$ as the sum of four terms:

1. $Z_m Z_m Z_m$ : the skewness contribution from the skewness of the monthly mean field.

2. $3\left(Z_m z'^2\right)$ : The cross frequency term resulting from the linear relation between the variance of $z'$ and the monthly anomaly field.

3. $3\left(z' {Z_m}^2\right)$ : identically zero when averaged over a month

4. $z'z'z'$ : The contribution from the skewness of the $z'$ field.

The results of this partitioning for terms 1, 2, and 4, are shown in Fig. 4.1 (b), (c), and (d) respectively. The contribution to the skewness of $Z_6$ from the skewness of monthly mean anomalies, shown in panel 4.1(b), is much smaller than the contributions from the other terms. The smallness of this term reflects the relatively small r.m.s. amplitude of $Z_m$ compared to that of $z'$. The term involving the linear correlation between the monthly mean anomalies and the shorter timescale variance shown in Fig. 4.1(c) is the largest contributor to the overall $Z_6$ skewness field. The distinct skewness maximum centered over Baffin Bay and a broad center over the northern and northeastern Pacific in Fig. 4.1(a) are primarily due to this term. The contribution by the shorter timescale skewness of $z'$, shown in 4.1(d), is much smaller and has a maximum off of the southern tip of Greenland and two distinct maxima in the Pacific sector centered over the north central Pacific and over southeastern Alaska. The strongest relative contribution from $z'^3$ comes in the north central Pacific, where it contributes $\sim 1/3$ of the total skewness of $Z_6$.

The region of strong skewness in the vicinity of Baffin Bay, which comes from the cross-frequency term in Fig. 4.1(c), is a reflection of the greater frequency of occurrence of high amplitude, intermediate timescale events during months of anomalously high values of $Z_m$ at Baffin Bay than during months of low $Z_m$. Fluctuations in $Z_m$ over Baffin Bay primarily reflect fluctuations in the NAO; the timeseries of $Z_m$ over Baffin Bay is correlated with an NAO timeseries generated from $Z_m$ at a level of $-0.86$. Hence Baffin Bay skewness reflects increased numbers of high amplitude blocking events during the negative polarity of the NAO than during the positive polarity. To illustrate how this occurs, we've created histograms of $Z_6$ for contrasting polarities of the NAO. Figure 4.2 shows the distribution of $Z_6$ for standardized monthly NAO index $< -1$, all data, and for the NAO index $> 1$. The increased variance for $\mathrm{NAO}^-$ is reflected in a much broader range ($\sim$900 m) of heights

than for $NAO^+$ ($\sim$500 m). Both distributions are fairly symmetric. The total distribution is positively skewed ($\sim$.53), but neither of the distributions separated by polarity of the NAO are significantly skewed. The skewness of the total field is thus coming from the superposition of two nearly symmetric distributions of different widths and with different means. It is also of note that the $NAO^-$ distribution exhibits 500 hPa heights that are as low as the lowest heights observed during $NAO^+$.

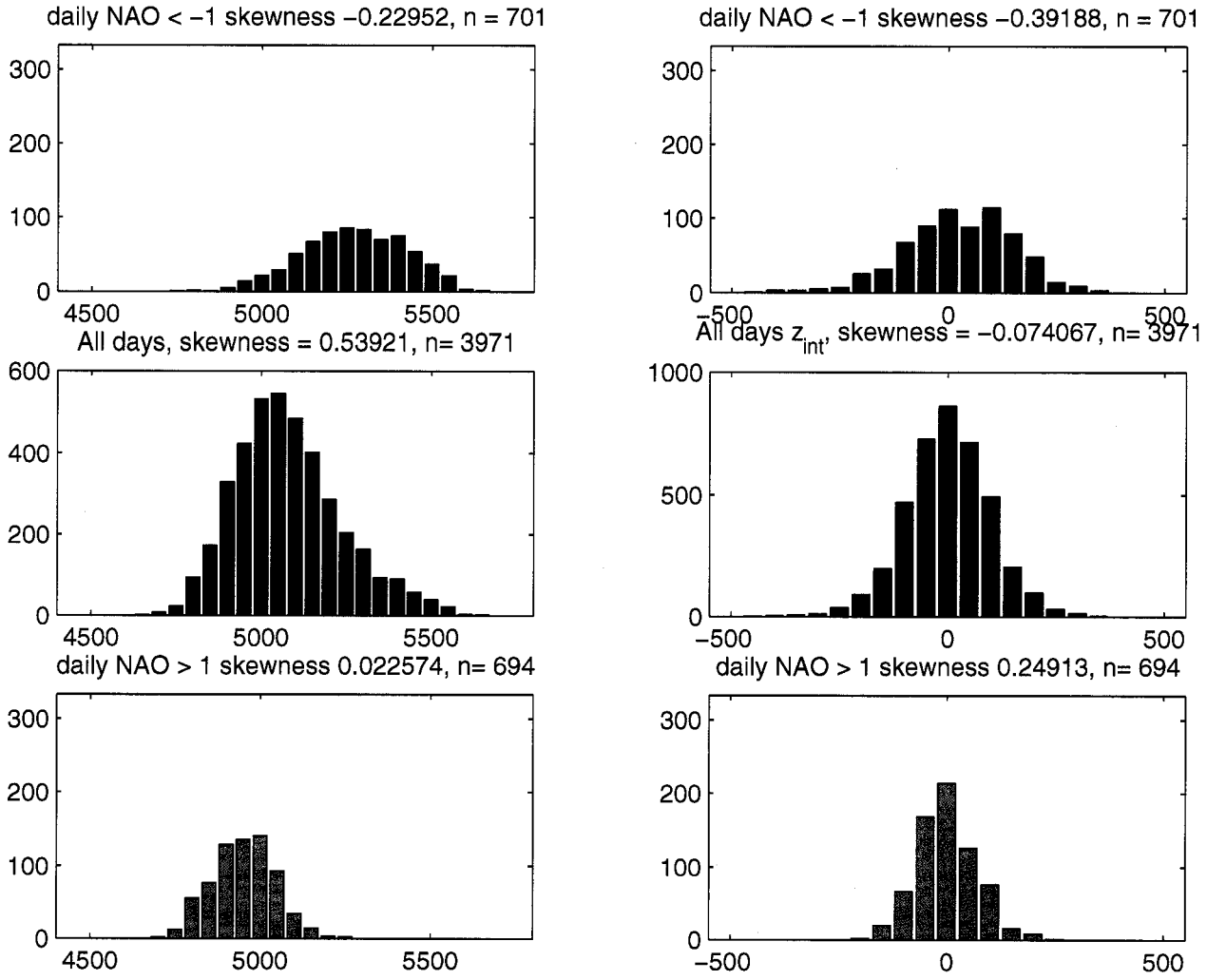


Figure 4.2: Histograms of $Z_6$ and $z'$ for the point $(70N, 60W)$ in Baffin Bay for contrasting polarities of the daily NAO index. The positive and negative groupings include 750 and 691 days out of a total of 3971 total days.

Repeating this exercise for $z'$ at the same Baffin Bay point yields the results shown in panels (b), (d), and (f) of Fig. 4.2. We would expect from Fig. 4.1(d) that the skewness of $z'$ at this point should be nearly zero, and this is reflected in the nearly normal distribution for the set of all days. The range for the $NAO^-$ is still much greater than for the $NAO^+$, but removing the low frequency $Z_m$ variability has brought the means of $z'$ for both $NAO^-$ and $NAO^+$ close to zero. The superposition of the frequency distributions of $z'$ for the positive and negative polarity of the NAO yields a non-skewed total distribution. Hence, the skewness of $Z_6$ at this grid point is due to the linear relation between $Z_{30}$ and the width of the frequency distribution of $z'$.

For the remainder of the chapter, we return to our previously-defined three-frequency framework of high, low, and bandpass filtered data that we've referred to as $z_{HP}$, $Z_{30}$, and $z_{int}$ respectively. In addition, we will also refer to daily data which has had the same 6-day low-pass filter applied to it as $Z_6$, and the departure of that field from its climatological mean as $z_6$.

To more clearly show the relationship between NAO phase and the individual heights comprising the distributions in Fig. 4.2, Fig. 4.3 shows a scatter plot of the individual heights in $z_6$ versus the a daily NAO index generated from the $Z_{30}$ data set. The left panel shows evidence of a linear relationship between the two ($R^2 = 0.45$) as well as an increase in scatter about the linear fit line with decreasing NAO index. This increase in scatter is even more apparent in the right panel that shows $z'$ plotted versus the same daily NAO index.

Baffin Bay is an obvious choice of points for the above analysis, because it is a strong center of skewness and intermediate scale variance, located near the Arctic center of action of the NAO pattern, and has emerged as a center of action repeatedly in the EOF and MCA analysis shown in previous sections. It is clear, however, that not all skewness and blocking is attributable to a similar superposition of effects. To show an example of contrasting behavior, the above analysis was repeated for the grid point at $(60N, 15W)$, just southeast of Iceland, which is located at the col between the two strongest $NAO^-$related centers in the ${z_{int}}^2$ field, as shown in Fig. 3.1, as well as at the minimum of both sets of ${z_{int}}^2$ variability shown in Fig. 3.5. As such, we will refer to it as the "Atlantic col" grid point. Geopotential

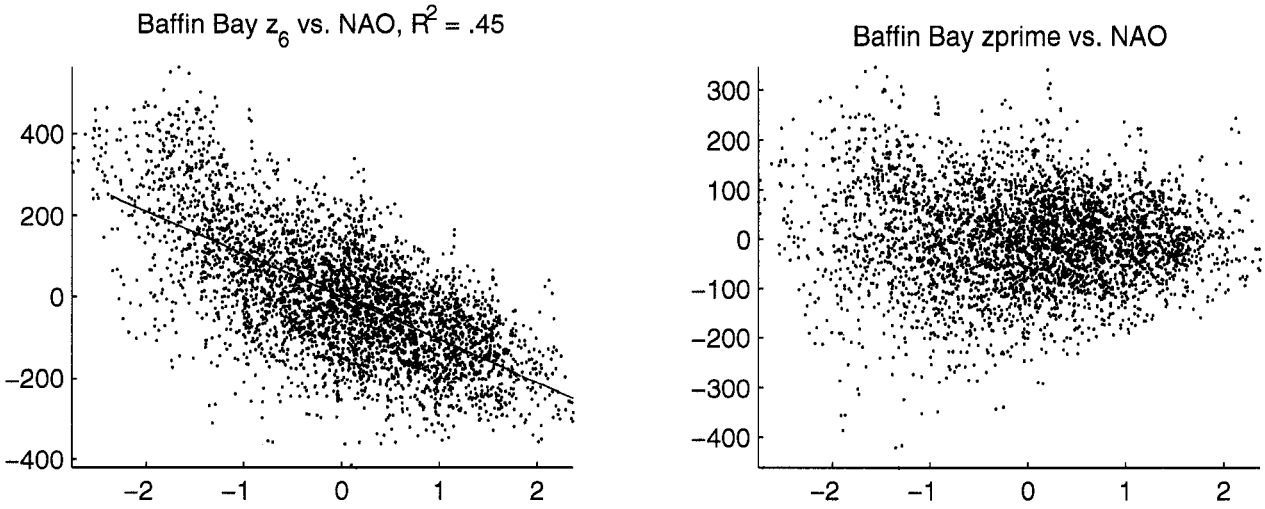


Figure 4.3: Scatter plots of the daily NAO index generated from the $Z_{30}$ data set versus $z_6$ (left) and $z_{int}$ (right). The NAO is on the abscissa.

height at this grid point exhibits relatively little overall skewness ($\sim 0.2$). As can be seen in Fig. 4.4, the effect of the NAO polarity on the width of height distributions is negligible. At this location, much of the weak overall skewness is attributable to the positive skewness (0.45) occurring during $NAO^+$ months.

### *4.3 Composite maps for extreme values of Z over Baffin Bay*

It is evident from the above set of histograms that a wide range of weather patterns are observed during negative index months of the NAO. To explore the extremes of this range in terms of the full hemispheric 500 hPa height fields, a set of four composite maps have been created as follows: Using the monthly NAO index, the months with the 20 highest and 20 lowest values are selected, which represent approximately the top and bottom 15% of all of the monthly values of the index. Then from within each of these two subsets of data, the days on which the 10 highest and 10 lowest values of $Z_6$ occurred for our point over Baffin Bay are selected, and the means of these these two sets of 10 $Z_6$ maps were calculated. The selection of the daily values is restricted so that no two days within 10 days of one another are selected, to ensure that the events sampled are distinct. This protocol yields a total of

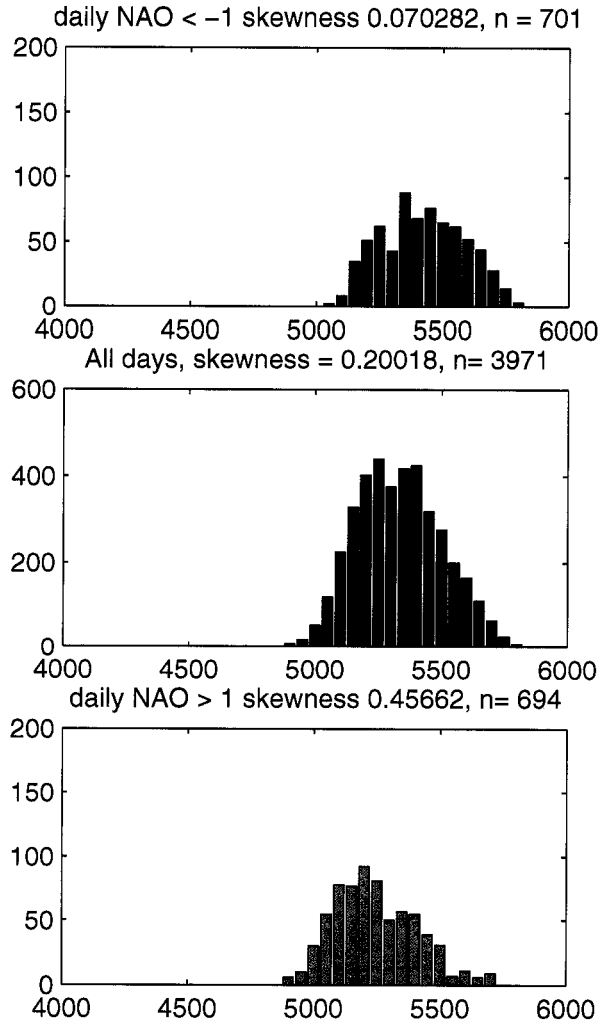


Figure 4.4: As in the left panels of Fig. 4.2, but for the "Atlantic col" point $(60N, 15W)$.

4 sets of composites: the highest and lowest $Z_6$ days over Baffin Bay for the negative phase of the NAO index, and likewise for the positive phase.

The results for the negative months are shown in Fig. 4.5. The highest value composites over Baffin Bay correspond to a state of Greenland blocking. The pattern shown in the full $Z_6$ field (Fig. 4.5(c)) features a strong anticyclone located directly over Baffin Bay and southern Greenland, just east of the core of the climatological-mean polar vortex. The positive anomaly is of sufficient strength that height contours from the midlatitudes bend back on themselves over the Atlantic ocean in forming an anticyclone over Greenland with several closed contours. These events also feature a downstream trough over the U.K. and Scandinavia, a pattern that is observed in association with extreme negative values of the NAO (e.g. Quadrelli and Wallace (2004b), Fig. 6.). Compositing the lowest extremes in $Z_6$ yields a much different anomaly map, showing an enhancement and shifting of the center of the polar vortex eastwards of its climatological mean position, a sharpening of the weak climatological-mean ridge over central and northern Europe, and a pronounced downstream trough over eastern Europe.

An inspection of the associated $z_{int}$ composites for these same months, shown in Figs. 4.5(a) and 4.5(d), yields a different perspective than would be gained from looking at conventional anomaly maps of $z_6$ shown in Figs. 4.5b and 4.5(c). Composites for contrasting extremes of $z_{int}$ are remarkably similar, apart from the reversal in sign. Both are dominated by a single strong center of action over the reference grid point, with a weaker downstream center of opposing polarity over Scandinavia. The amplitudes, spatial scales, and orientations of the primary centers of action in the two composites are quite comparable, despite the nonlinear appearance of the composites of the $z_6$ field in the middle panels.

The patterns shown in Fig. 4.5 are largely insensitive to the choice of number of events used in the composites. Including 25 events in the composites yields similar structures that are only slightly weaker in amplitude (Fig. 4.6). The patterns are also robust with respect to the various choices of filtered data. Basing the composites on extreme events in $z_{int}$ rather than $Z_6$ does not significantly change the dates included in the composite, nor does compositing based on the full, unfiltered $Z$ field that includes baroclinic waves (not shown).

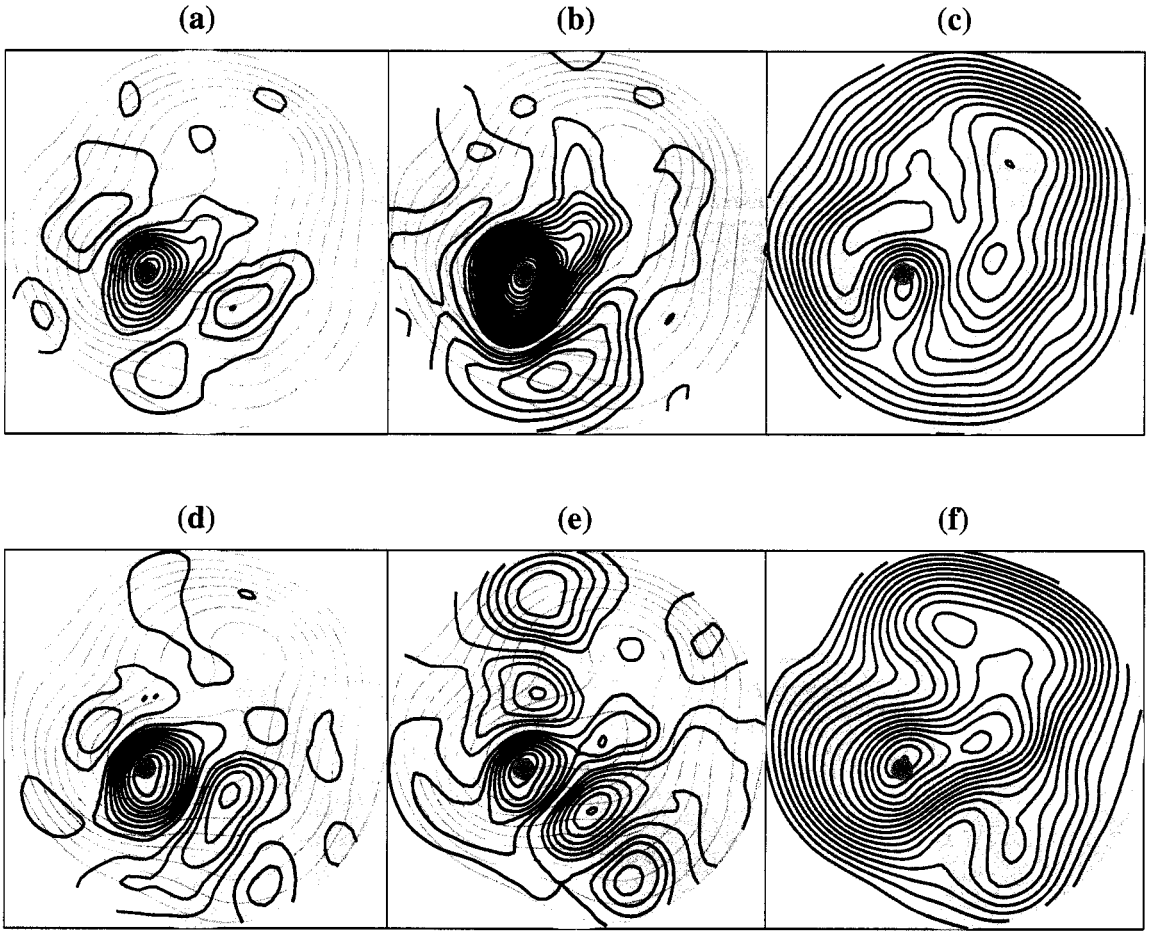


Figure 4.5: Panels (a)-(c) show the mean of the $z_{int}$, $z_6$, and full $Z_6$ fields for the days with the 10 highest values of $z_{int}$ at $(70N, 60W)$ during the 20 most negative months of the monthly NAO index. Panels (d) - (f) are as in (a) - (c) but for the lowest 10 $z_{int}$ for those same months. The thin, light gray contours indicate the winter climatological 500 HPa height field. Contour interval is 50 m for the $Z_6$ field, 25 m for $z_6$ and $z_{int}$.

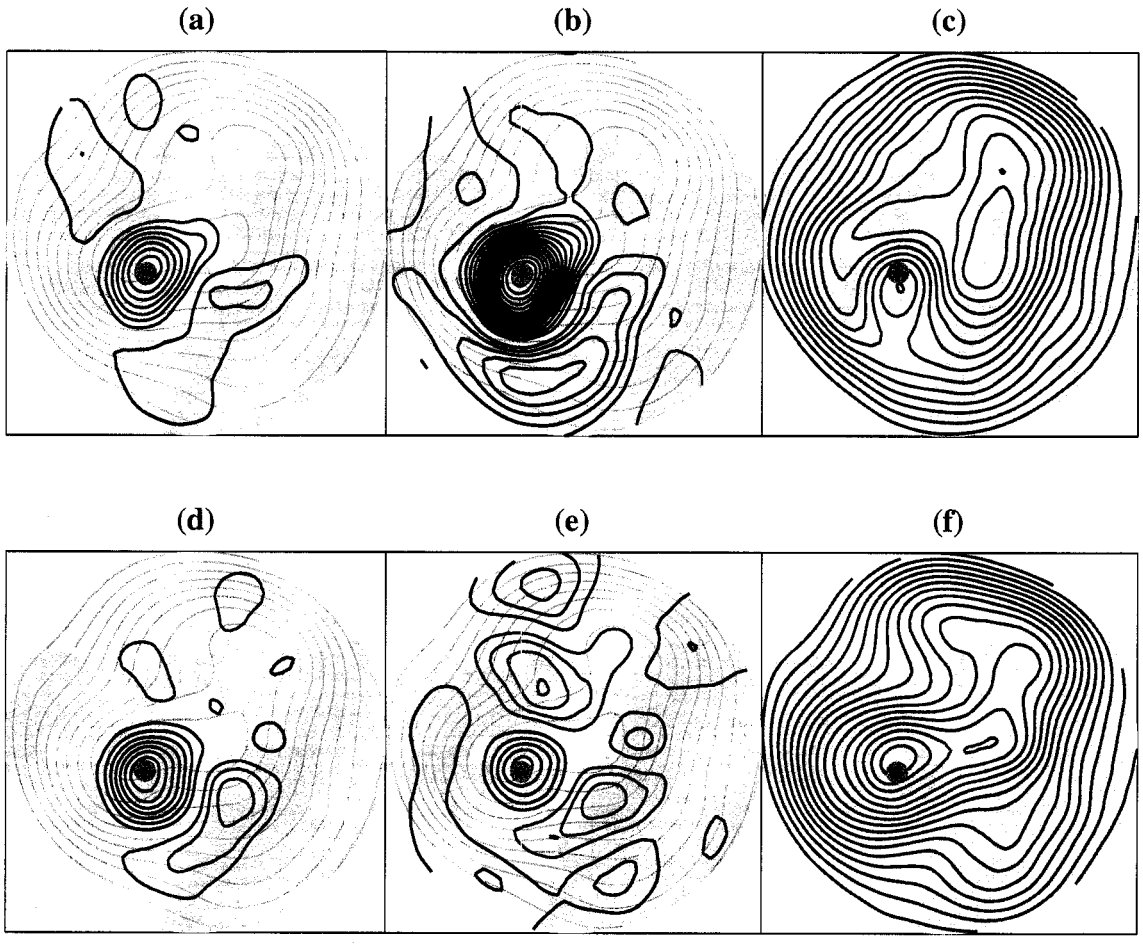


Figure 4.6: As in Fig. 4.5, but including 25 events in each composite.

### *4.4 Composite maps for extreme values of Z over Scandinavia*

Repeating the analysis in section 4.3 for our Scandinavian center of variance $(65N, 20E)$ yields a similar set of patterns that have more direct consequences in terms of extreme weather over Europe. In view of the proximity of the Scandinavian grid point to the node of the NAO, these composites have been drawn from all months of data rather than strictly from $NAO^-$ months. Fig. 4.7(a) and (c) show the $z_{int}$ composites for the positive and negative $z_{int}$ cases. As in the previous section, these contrasting maps exhibit a high degree of similarity apart from the reversal in sign. Each of them features a strong center of action over the reference grid point, and a pair of centers of opposing polarity; one upstream over Baffin Bay and one downstream over Siberia. The high $Z_6$ composite shows the anticyclone over Scandinavia to be part of a modon-like structure, with a splitting of the westerlies and northwesterly flow into southern Europe. This flow pattern is associated with anomalous warmth over Scandinavia and cold air outbreaks over southern Europe. The contrasting $Z_6$ composite for low $Z_{int}$ shown in Fig. 4.7(d) features strong ridging over Greenland and a deep downstream trough over Scandinavia. As is the case for the Baffin Bay gridpoint, the $z_{int}$ maps for contrasting polarities are similar in many respects, but in this case the primary center is more zonally elongated when it appears with positive polarity, and the upstream center over Baffin Bay is more pronounced.

Results from the Baffin Bay and Scandinavia composites are also compared with the same analysis for the Atlantic col grid point referenced in the previous section. In Fig. 4.4 it was shown that blocking at this location is unrelated to fluctuations in the NAO, as evidenced by the large positive height anomalies that occur during both polarities of the NAO. Hence, for compositing at this location, we chose the highest and lowest $Z_6$ heights during all months, rather than the $NAO^-$ months. As can be seen in Figure 4.8b, the high $Z_6$ composite exhibits a strong "omega block" signature over the north Atlantic in the $Z_6$ field. The low height composite (Fig. 4.8d) exhibits a trough over the col grid point, with an upstream ridge over the Labrador Sea. The $z_{int}$ anomalies for both high and low composites have weaker primary centers of action than do either the Scandinavia or Baffin Bay points, and weaker secondary centers. The primary centers for contrasting polarities

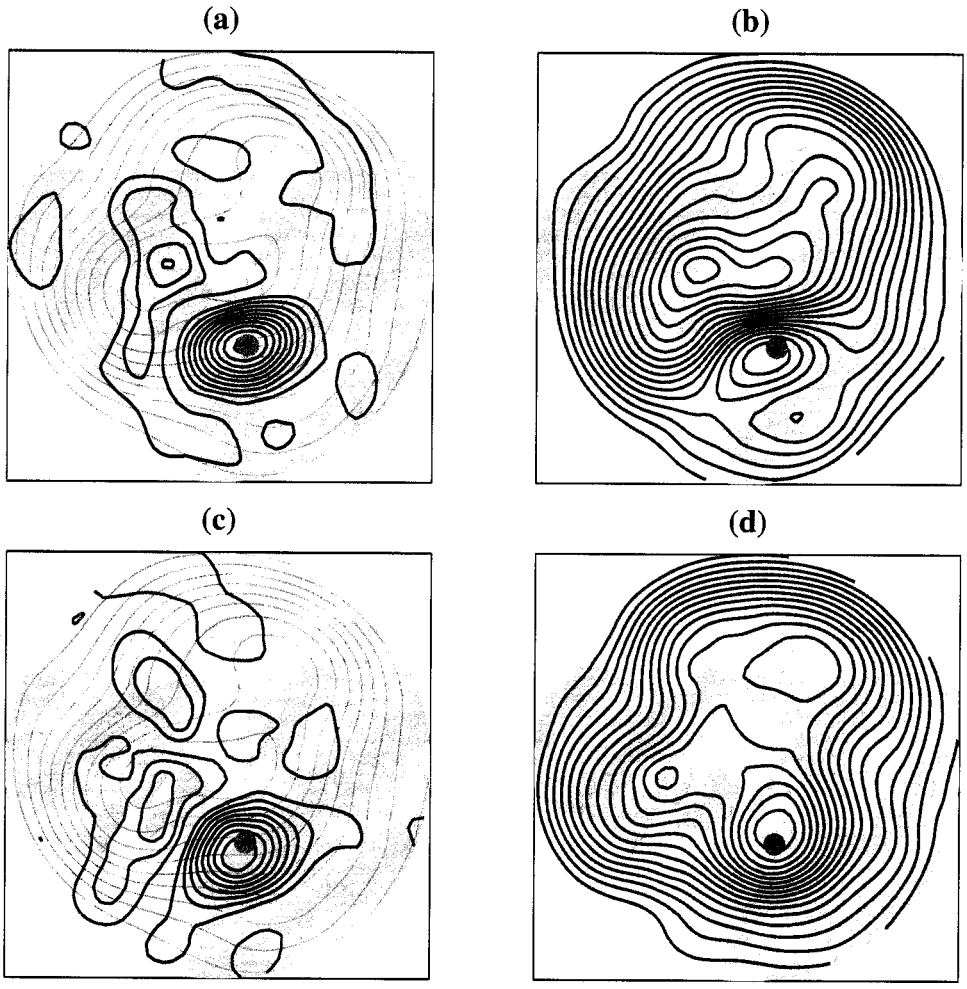


Figure 4.7: Panels (a), (b), (c) and (d) are after Fig. 4.5, panels (a), (c), (d), and (e) respectively, for the Scandinavian point $(65N, 20E)$. The composites in this case are drawn from all months of data, rather than months of negative polarity NAO.

are similar in amplitude and horizontal scale, but the positive center is zonally elongated, whereas the negative center is more isotropic.

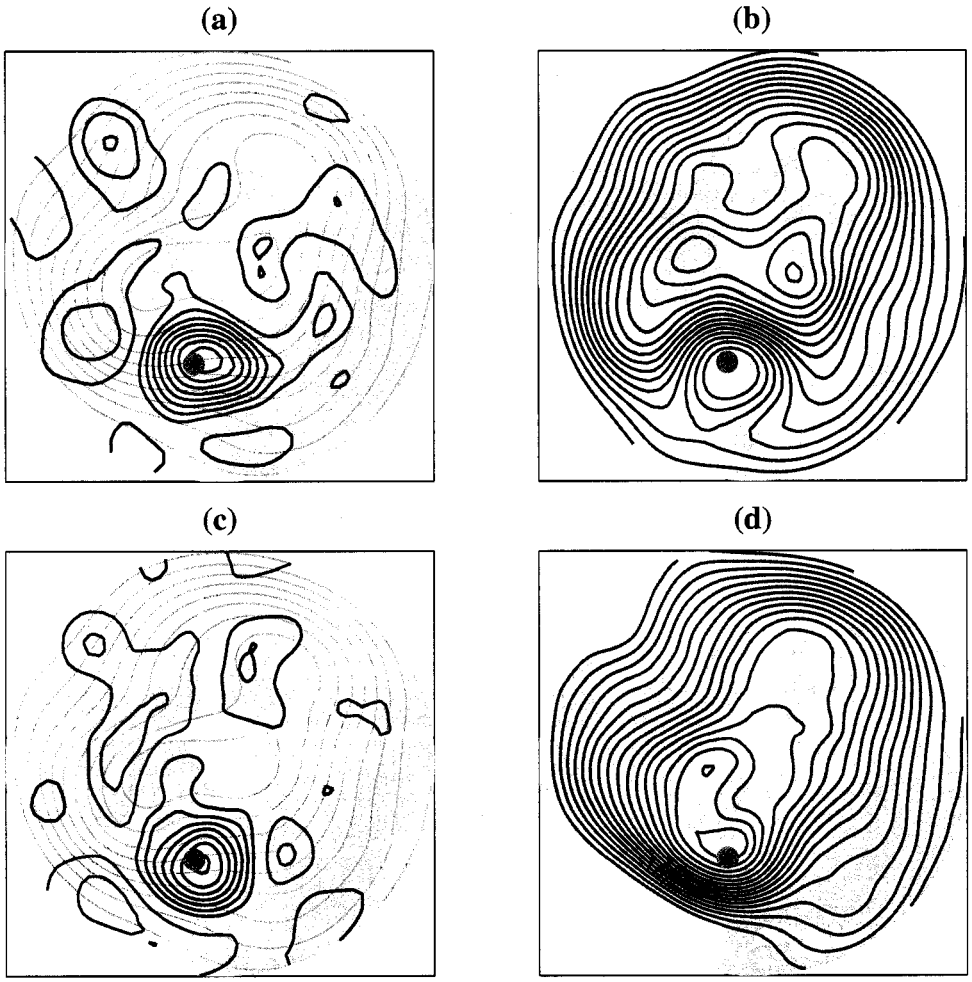


Figure 4.8: As in Fig. 4.7 but for the Atlantic 'col' location $(60N, 15W)$.

### *4.5 Summary*

In this chapter, we have shown that the NAO$^-$ is associated with enhanced low and intermediate frequency variability over the Atlantic sector. The strong positive skewness of the 500 hPa height field over Baffin Bay can be explained as being due to enhanced variability in $z_{int}$ during NAO$^-$ superposed on anomalously high monthly-mean heights characteristic

of $NAO^-$ at this location. During months of $NAO^-$, the variance in $z_{int}$ is on the order of 2-3 times as large over these regions as it is during months of $NAO^+$. This enhanced variance during $NAO^-$ is associated with an increased frequency of occurrence of contrasting patterns of height anomalies with centers of action over Greenland and Scandinavia. Blocking highs over Greenland tend to occur in association with deep troughs or cutoff lows over Scandinavia and vice versa, though the simultaneous temporal correlations between 500 hPa heights over these gridpoints are modest ($r = -0.23$). This relationship is consistent with the most prominent pattern of variability in Atlantic ${z_{int}}^2$ (Fig. 2.5) discussed in Chapter 2. Although the spatial patterns in the total 500 hPa field appear to be quite nonlinear, with distinct wave-breaking signatures for the anticyclones in particular, the structure of the patterns for the Baffin Bay grid point in the $z_{int}$ field looks much more linear, as evidenced by the similarity of the composites for positive and negative anomalies, apart from the reversal of sign. The Scandinavian and Atlantic Col points exhibit a slightly lower degree of symmetry between high and low composites.

Results in this chapter are consistent with the basic premise of Lejenäs and Madden (1992), that localized, developing ridges may be further augmented by the superposition of height anomalies associated with the slowly varying planetary-scale modes, and that this could play a role in generating blocking behavior. In their work, a traveling Rossby wavenumber 1 provided the slow variations, whereas we've shown here that fluctuations in the NAO could act in a similar manner to amplify developing ridges near Greenland. The symmetry between Baffin Bay and Scandinavia exhibited in the $z_{int}$ composites is also broadly consistent with the notion of barotropic normal modes associated with the development of blocks as postulated by Frederiksen (1989), and suggests that these patterns could arise from barotropic instability of the basic state. This idea has been examined in a simple barotropic model, and will be discussed further Chapter 6. The results presented here also help explain the high frequency of occurrence of extreme weather events in association with the low index polarity of the NAO, particularly over Europe.

# Chapter 5

# EVOLUTION OF INTERMEDIATE FREQUENCY ANOMALIES

## *5.1 Introduction.*

Up to this point, we have considered only the signature of intermediate scale anomalies when they are at their maximum amplitude. Previous chapters have documented the appearance of these anomalies using EOF, MCA, and regression analysis. We have also shown evidence of symmetry between positive and negative height composite anomalies over Baffin Bay during low index periods of the NAO. It remains to be determined whether the symmetry prevails during the growth and decay phases as well. This chapter seeks to extend our analyses of the peak amplitude events by investigating the growth and decay of the largest intermediate scale disturbances.

Previous studies of blocking anticyclones and other long-lived disturbances, have emphasized a tendency for the disturbances to retrograde as they mature, and to exhibit characteristics of downstream development. Blackmon (1976) showed that disturbances with periods longer than 10 days tended either to be stationary or to retrograde. Mullen (1986) attributed the direction of propagation of blocking anticyclones to an imbalance of forcings, with vorticity perturbations from upstream high-frequency transients seeking to draw the anticyclone upstream and the mean flow advecting it generally eastwards. Kushnir (1987) studied long-lived, retrograding disturbances over the North Pacific using complex EOF analysis, a technique well-suited for extracting traveling modes of variability. This analysis showed the main pattern of intermediate timescale variability over the Pacific to be a large-scale dipole over the North Pacific, straddling the Pacific jet exit region. This pattern was shown to be distinct from the PNA pattern, and the positive center of action located over central Alaska was shown to exhibit westward propagation. Branstator (1987) studied a particularly long-lived example of this phenomenon that evolved over a four month period in the winter of 1979/80. Both of these studies found differences between the travel-

ing mode and the theoretical free Rossby wave of zonal wavenumber one. Blackmon et al. (1984b) used lag-correlation statistics to document the evolution of intermediate timescale anomalies, and noted a tendency for upstream correlations to be strongest for negative lags and downstream correlations to be strongest for positive lags. They attributed this result to downstream development related to Rossby wave-train dispersion.

In this chapter, we investigate the evolution of the largest positive and negative intermediate timescale anomalies for the four locations that we have considered in the northern hemisphere. We begin with an overview of the evolution at these points as revealed by lag-correlation analysis. This analysis is then augmented by an extension of the compositing analyses carried out in Chapter 4, wherein we compare the positive and negative $z_{int}$ anomalies throughout their life cycles in terms of amplitude, duration, and direction of propagation.

## *5.2 Lagged Correlations*

The most general characteristics of the evolution of large, intermediate timescale anomalies for the four locations may be elicited through lag-correlation analysis. This technique takes advantage of the maximum number of degrees of freedom available in the chosen data sets, but it is unable to discern differences of evolution between positive and negative events. Here, we perform the analysis on the $Z_6$ (Fig. 5.1) and $z_{int}$ (Fig. 5.2) data sets. It is to be expected that the $z_{int}$ correlation maps should primarily show patterns characteristic of downstream development and westward propagation, similar to that documented in Blackmon et al. (1984b). The $Z_6$ field encompasses both the intermediate timescale variability as well as the variability associated with the longer-lived planetary-scale modes, and its patterns may therefore reflect dynamics on both timescales. Contrasting the two sets of lag correlations yields insight into the relative importance of dynamics operating on the two timescales at each location.

The proximity of the Baffin Bay location to the Arctic center of action of the NAO results in $Z_6$ lag correlations that are dominated at all lags by a pattern that strongly resembles the NAO. The local lag correlations at Baffin Bay are high ($> 0.55$) throughout the period. $Z_6$ at the Baffin Bay grid point is negatively correlated with a broad midlatitude

region extending from the eastern United States to western Europe for all lags shown, but the strongest center of action within that region shifts eastwards from the central Atlantic to over western Europe by day +3. In addition, a positively correlated center develops over the Middle East at increasingly positive lags, indicative of southeastward Rossby wave dispersion. In the $z_{int}$ field, the event is shorter lived, the development of the downstream center over Western Europe is more strongly emphasized, and there is evidence of westward propagation of the primary center of action from lag +1 to +3.

The similarity between the evolution of the Scandinavian $Z_6$ and $z_{int}$ correlations indicates the dominance of the intermediate timescale over this location. For a lag value of −3 days, both fields show an upstream, negatively correlated center over the southern tip of Greenland that increases in amplitude through lag −1. As the correlation at the upstream center weaken for lags 0 through +3, a negative center develops over western Russia, consistent with established ideas of downstream development.

Lag correlations of $Z_6$ for the Atlantic col point combine elements of a stationary teleconnection pattern and downstream development. All lags are dominated by a largely stationary meridional dipole between the col and the midlatitude Atlantic ocean. At positive lags, a secondary, downstream negative center over eastern Europe is shown to develop. In the $z_{int}$ field, this evolution is apparent as a weak upstream, negative center that has the appearance of propagating downstream around the perimeter of the col from lag −3 to +3. The negative center has split into distinct centers of action over Morocco and eastern Europe by a lag of +3.

The $Z_6$ and $z_{int}$ lag-correlation patterns at the Anchorage point have only slight differences from each other, indicating the dominance of intermediate timescale variability at this location. For a lag of −5, both show an upstream, negatively correlated center over eastern Siberia and a positively correlated center displaced slightly eastwards of the Anchorage point. The upstream center weakens with more positive lags, and centers with negative correlations develop over the tropical Pacific as well as downstream over central Canada. For lags of −1 through −5, the tropical Pacific center weakens while the downstream downstream center intensifies. At the most positive lags, a second, positively correlated, downstream center has developed off of the southern tip of Florida, and the other two centers have

retrograded slightly.

## 5.3 *Lagged Composites*

The methodology followed for the compositing analysis described in this section is a straightforward extension of the technique used in the previous chapter. At each location, the 10 days with the most extreme positive and 10 most negative $z_{int}$ anomalies are selected, with the requirement that all selected dates be at least 10 days apart. Depending on the specifics of the location, the largest anomalies may be selected from a subset of low index polarity months of the PNA or NAO. These peak days serve as $t = 0$ for the purposes of the time evolution of the events. Daily composites based on the days preceding and following these peak days are then created. To refer to the timing of an individual composite relative to the maximum anomaly at $t = 0$, and to designate whether it is based on a positive or negative anomaly, the nomenclature $field_{(lag,sign)}$ will be used. For example, the most extreme positive anomalies in $z_{int}$ at $t = 0$ as shown in Fig. 4.5(a) would be referred to as $z_{int(0,+)}$. Negative lag values precede the maximum anomaly in time, positive lags follow it.

Potential drawbacks to compositing analysis are the potential for sensitivity to sample size, as well as for the composite patterns to combine events demonstrating distinctly different evolutions into a single, averaged pattern that does not occur in nature. The results presented here for composites of 10 events are relatively insensitive to sample size as documented in Appendix I, which shows sets of composites with greater numbers of events included for each location.

### *5.3.1 Baffin Bay center*

Results of the compositing analysis for Baffin Bay positive and negative anomalies drawn from the 20 most negative index NAO months are shown in Fig. 5.3. The origins of the positive $z_{int}$ events are discernible 5 days before peak amplitude as a dipole with a negative anomaly over Baffin Bay and a meridionally elongated anomaly centered just west of the United Kingdom. Both centers exhibit westward propagation, with the upstream negative anomaly weakening as the positive anomaly amplifies and becomes more isotropic. As the positive anomaly reaches its peak amplitude over Baffin Bay at $t = 0$, a pair of downstream

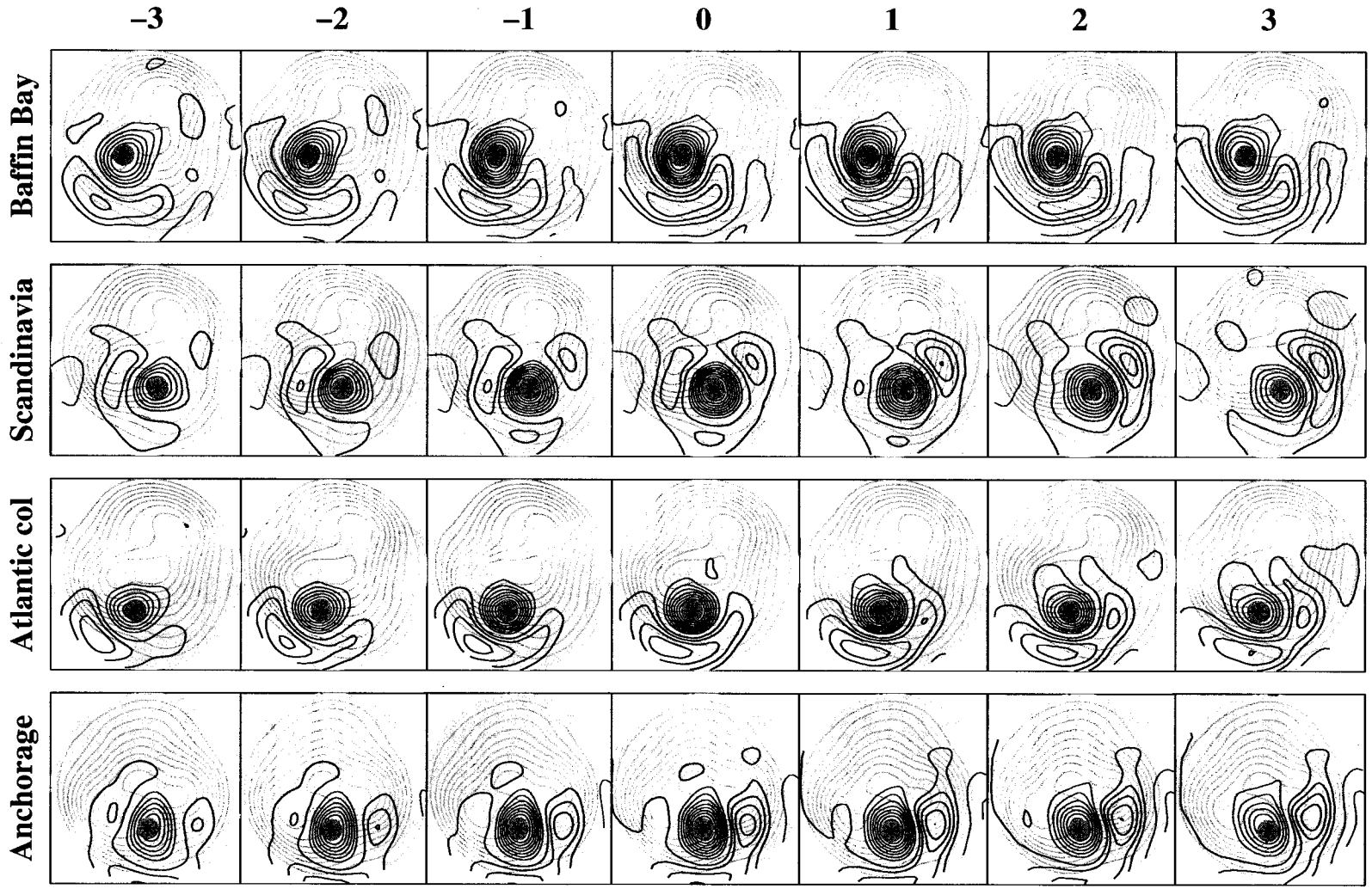


Figure 5.1: One point lag correlations for $Z_6$ for the Baffin Bay, Scandinavia, Atlantic col, and Anchorage points. Contour interval is .1 .

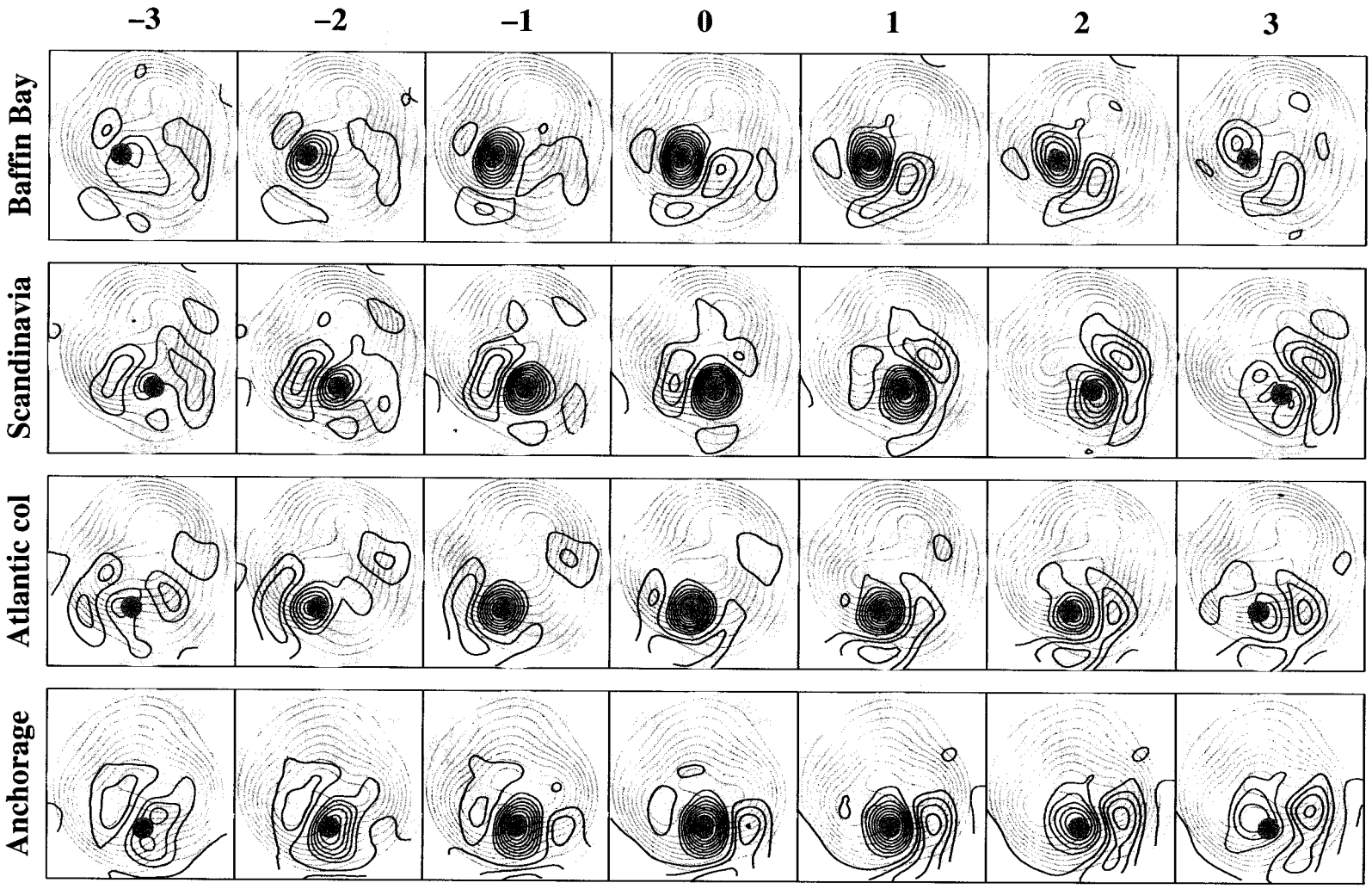


Figure 5.2: As in 5.1, but for the $z_{int}$ data set.

negative anomalies become evident: one centered over Scandinavia, and the other just off of the western coast of Spain. At $t = +1$, the downstream negative centers have strengthened slightly, and the centers are closer together. By $t = +3$, the positive center over Baffin Bay is greatly diminished, and has propagated over the Canadian archipelago, while the negative center downstream of it has maintained much of its amplitude.

The evolution of the negative composites over Baffin Bay for $NAO^-$ months is similar to that of the positive anomalies. The weak, westward propagating dipole between Baffin Bay and the midlatitude Atlantic ocean that is evident from $t = -5$ through $t = -3$ resembles the pattern of anomalies at the same lags for the positive events, except for a reversal of sign and lesser amplitude. The negative Baffin Bay anomalies attain similar r.m.s. amplitude to those in the positive composite at their peak, and therefore develop much more rapidly between $t = -3$ and $t = -1$. As has been previously discussed, the anomaly pattern at $t = 0$ is very similar to that of the positive composites with reversed sign. The downstream positive anomaly is slightly stronger at $t = +1$ than at $t = 0$, suggesting the occurrence of downstream development. From $t = +3$ to $t = +5$, both the negative and positive anomalies exhibit westward propagation, with the downstream positive anomaly maintaining much of its amplitude through $t = +5$.

To determine the dependence of the evolution of these patterns on NAO polarity, the compositing analysis was repeated for all months, rather than just low polarity NAO (Fig. 5.4). In other words, we performed conventional compositing analysis based on positive and negative extreme values of $z_{int}$. As is evident from the scatter plot of $z_{int}$ and the NAO index shown in Fig. 4.3, almost all of the highest $z_{int}$ anomalies occur during months of low NAO index, so the events composited are largely the same as in the previous analysis. Thus the evolution of the highest $z_{int}$ anomalies for all months is nearly identical to that of anomalies constrained to occur during times of low-index polarity NAO. In contrast, the most negative $z_{int}$ events occur during both polarities of the NAO, and the negative $z_{int}$ composites for all months show a slightly different evolution than those sampled from $NAO^-$ months. The upstream positive anomaly present during the early development of the Baffin Bay anomaly is slightly more prominent, and the downstream positive anomaly that develops after the Baffin Bay anomaly has peaked is weaker.

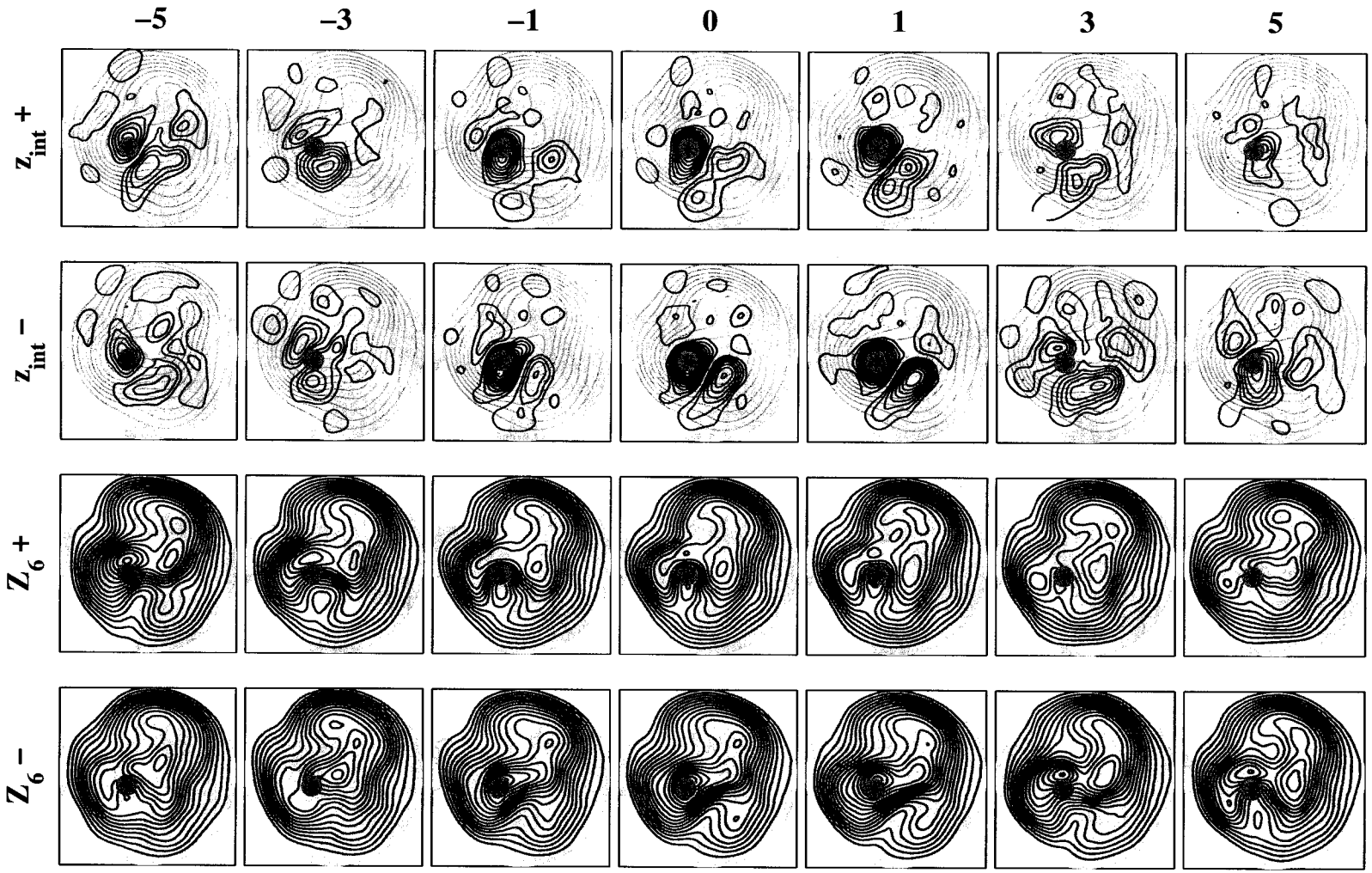


Figure 5.3: Evolution of $z_{int}$ anomalies for Baffin Bay for NAO$^-$ months. The top row shows the evolution of the highest $z_{int}$ anomalies for lags of -5,-3,-1,0,1,3, and 5 days superimposed on the climatological wintertime 500 hPa height field. The second row shows the corresponding sequence for the most negative $z_{int}$ anomalies. The third and fourth rows show composites for the full $Z_6$ field for same days as in the high and low $z_{int}$ evolution respectively.

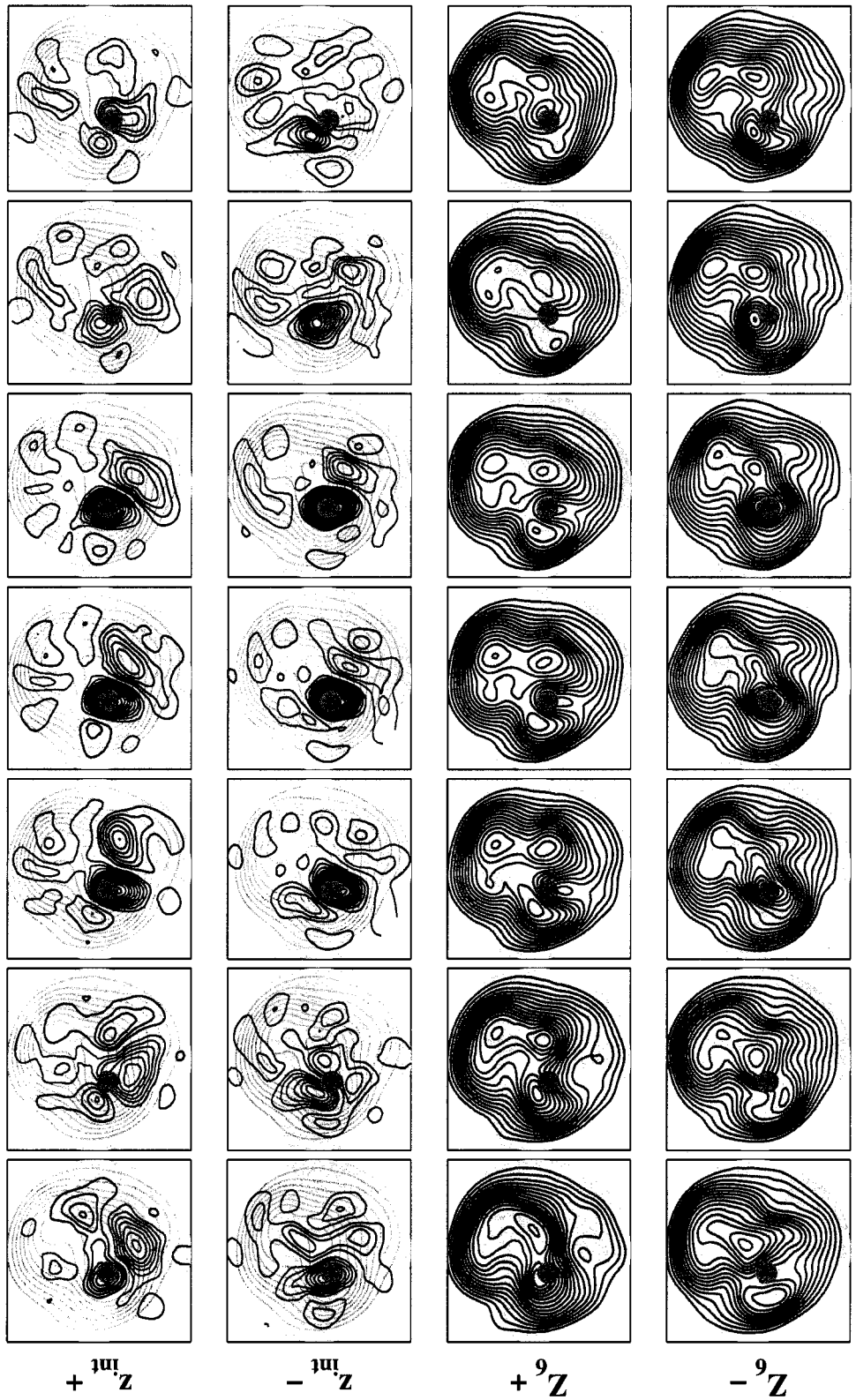


Figure 5.4: As in Figure 5.3 but for all months.

### *5.3.2 Scandinavian center*

The evolution of the Scandinavian center for all months is shown in Fig. 5.5. The positive events develop largely in place, with a weak positive anomaly developing over Scandinavia in the presence of an upstream, negative anomaly of much greater amplitude centered over Baffin Bay. The high amplitude and location of these anomalies leads to a modon-like configuration visible in the full $Z_6$ field for this time period. The Baffin Bay anomaly weakens as the Scandinavian center increases in amplitude from $t = -3$ through $t = 0$. The positive anomaly is fairly short-lived; it attains significant amplitude primarily between days $-1$ and $+1$, and subsequently weakens in place rapidly.

The most negative anomalies over Scandinavia are also fairly short-lived, largely stationary, and somewhat weaker than their positive counterparts. At $t = -1$, they are shown to develop in place over Scandinavia at the same time as an upstream, meridionally elongated positive anomaly over Greenland. The peak amplitude over Scandinavia is $\sim 75\%$ the r.m.s. amplitude of the positive event peak amplitude. The negative anomaly is greatly weakened by $t = +3$, while the upstream positive anomaly is no longer evident for this lag. There is a suggestion of weak westward propagation during the later stages of the event.

### *5.3.3 Atlantic Col*

By construction, blocking events at the Atlantic col point have little relationship to NAO polarity. The composites for these events shown in Fig. 5.6, are therefore selected from all months rather than from the $\mathrm{NAO}^-$ subset. The early set up of the positive composites comes from a weak positive anomaly slightly upstream of the "col" location. From $t = -3$ to $t = -1$, the positive anomaly more than doubles in amplitude, and an upstream, meridionally-elongated, negative anomaly centered over Newfoundland develops. As the positive center of action strengthens from $t = -1$ to $t = 0$, the upstream anomaly diminishes, and a new negative anomaly downstream from the "col" develops, suggesting a slight degree of downstream development. The positive anomaly decays in place, and is greatly weakened by 3 days after peak amplitude.

The growth and decay phases of the negative $z_{int}$ events follow a relatively similar

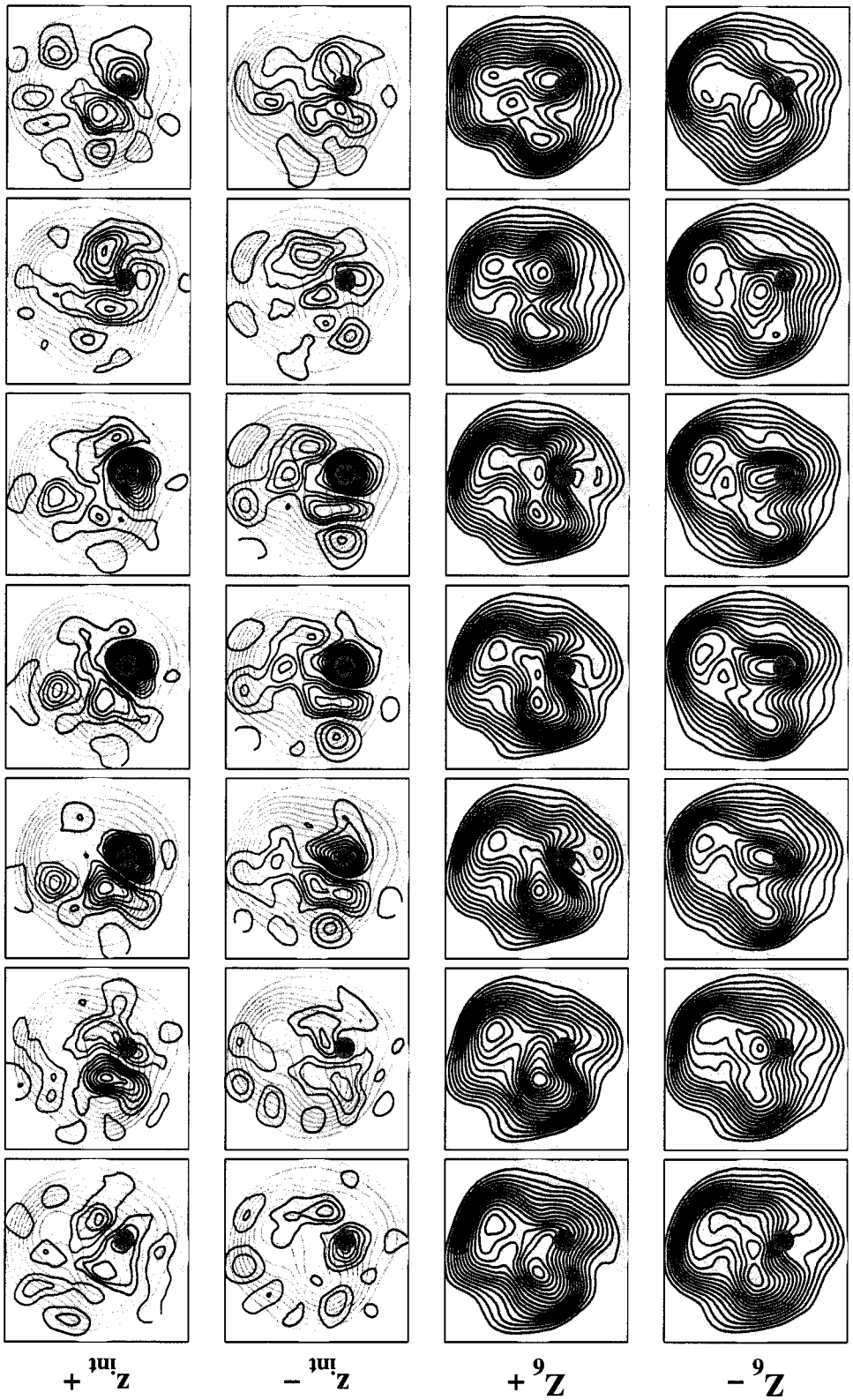


Figure 5.5: As in Figure 5.4 but for the Scandinavian point.

progression. The negative anomalies develop largely in place between $t = -1$ and $t = +1$ in conjunction with an upstream anomaly of opposing sign. The upstream anomaly begins to decay slightly before the "col" anomaly. Both are largely gone by three days after the peak, while a downstream anomaly of opposing sign has developed and moved over the "col" by $t = +5$.

### *5.3.4 Anchorage*

The grid point over Anchorage has been shown in previous sections to have enhanced high and intermediate timescale variability during the negative phase of the PNA. Intermediate timescale anomalies over this location have also been shown to be related to the traveling mode documented by Kushnir (1987) and Branstator (1987). It is a natural extension of our work in the Atlantic sector to examine the evolution of $z_{int}$ anomalies in the same manner as for the Atlantic points, but composited with respect to low-index polarity months of the PNA.

The high $z_{int}$ anomalies over Anchorage during PNA$^-$ (Fig. 5.7) are characterized by isolated positive anomalies that develop and decay rapidly in place, having significant amplitude only between days -1 and +1. The anomalies exhibit only a slight degree of westward propagation. The low $z_{int}$ composites also show anomalies that develop and decay rapidly, with little signal outside of a day before or after the peak amplitude.

That these results don't match the expectations of long-lived, westward-propagating anomalies over this location may be understood through a scatter plot of $z_{int}$ over Anchorage versus the monthly PNA index (Fig 5.8). Unlike the relationship between the NAO and $z_{int}$ over Baffin Bay, shown in Fig. 4.3, this plot indicates that, although the variability in $Z_6$ and $z_{int}$ over Anchorage is enhanced during the negative polarity of the PNA, it is enhanced to a lesser degree during the most extreme negative polarity months of the PNA. By restricting our $z_{int}$ composites to the most extremely negative polarity months of the PNA, we have effectively eliminated some of the largest amplitude events.

Removing the PNA$^-$ restriction and compositing $z_{int}$ anomalies sampled from all months increases the degrees of freedom of the composites and ensures that the largest anomalies are

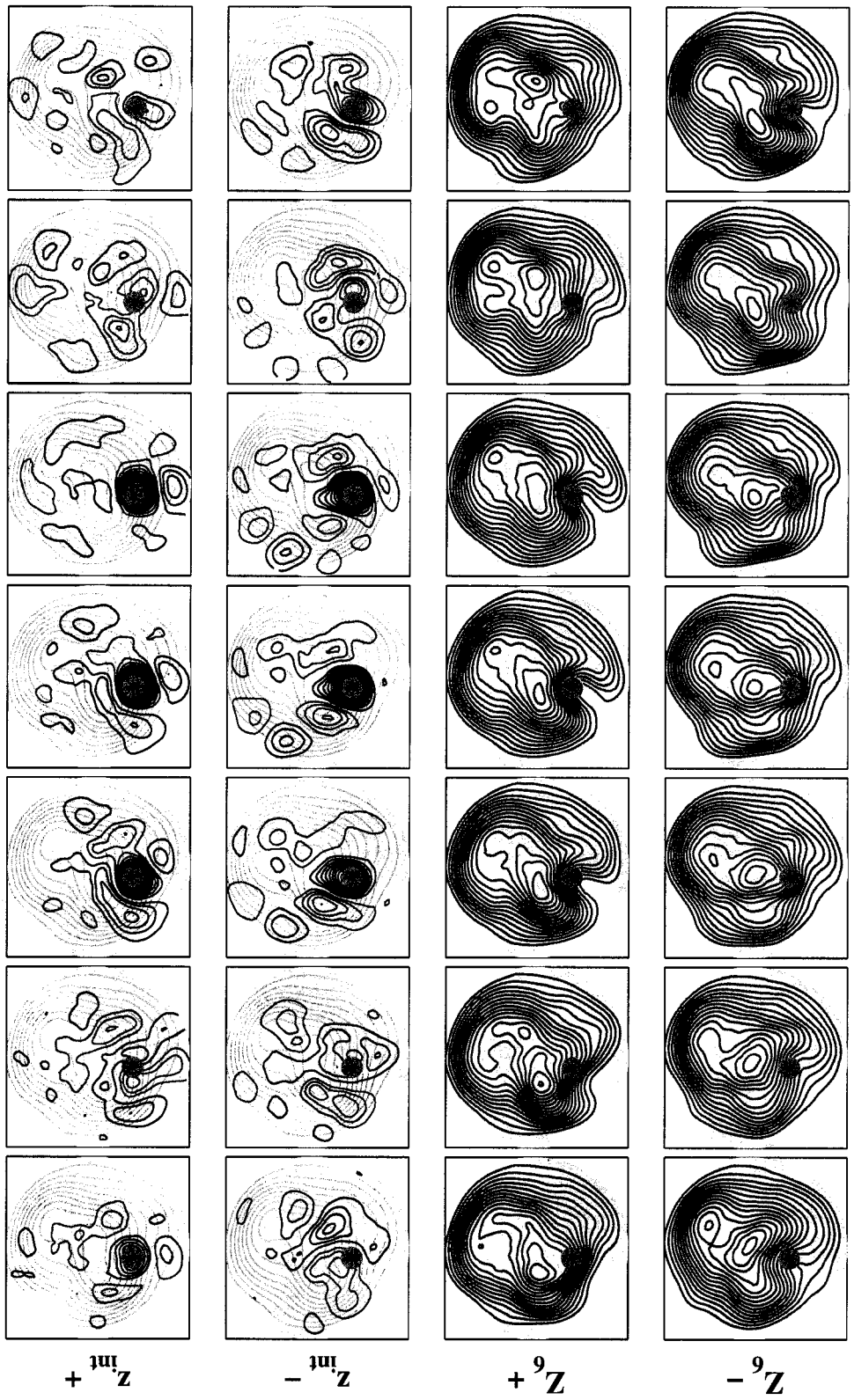


Figure 5.6: As in Figure 5.4 but for the Atlantic col point.

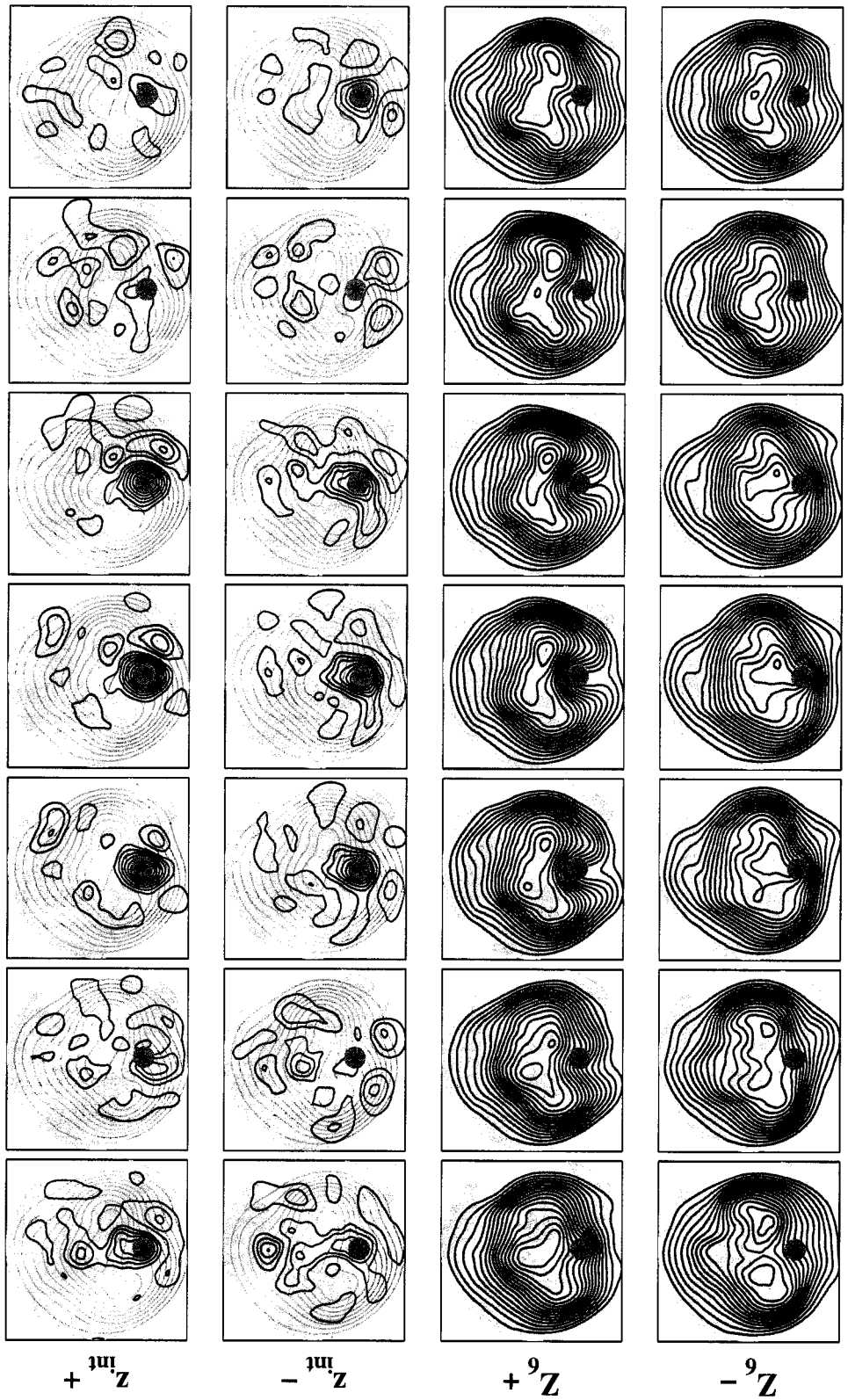


Figure 5.7: As in figure 5.3 but for Anchorage in negative PNA months.

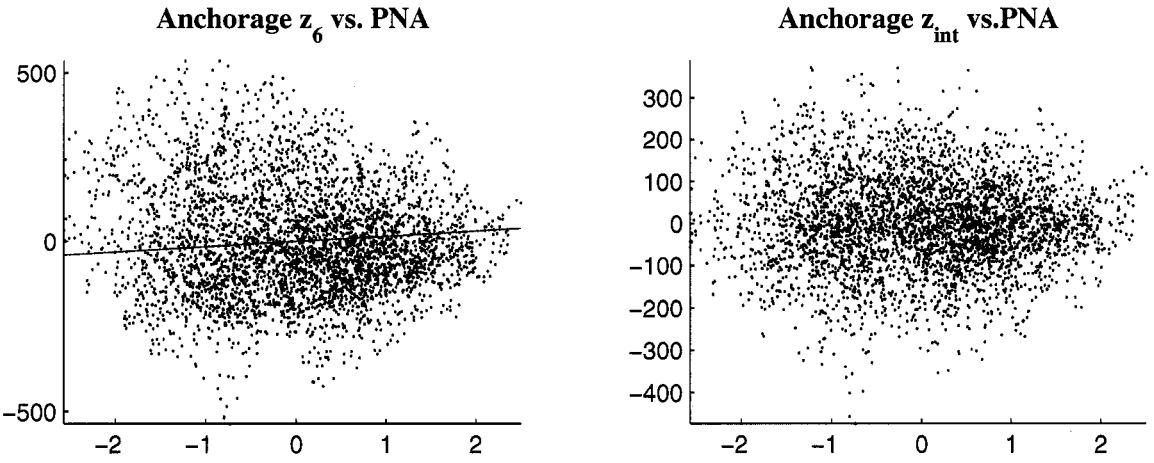


Figure 5.8: As in Figure 4.3 but for the Anchorage location and the PNA index.

sampled. The positive composites, shown in Fig. 5.9, originate as part of a broad, positive anomaly evident at day $-3$. The positive anomaly more than doubles in amplitude to $\sim 250m$ by $t = -1$, and exhibits a slight meridional tilt, extending from the central Pacific to the Northwest Territories of Canada. The day after its peak amplitude, the positive anomaly is slightly weakened and has become more isotropic, and a downstream negative anomaly over the western United States has gained in amplitude. By day +3, the positive anomaly has propagated westwards and become meridionally stretched with an upstream meridional tilt. Both the positive and negative anomalies have propagated westwards by $t = +5$, and the negative downstream center has continued to gain in amplitude.

The pattern of westward propagating anomalies and downstream development are exceptionally clear in the negative $z_{int}$ composites. The $t = -5$ anomaly field features a positive anomaly over the northern Pacific approximately 150 $m$ in amplitude. At $t = -3$, the positive anomaly is centered over the Bering Sea and has become zonally elongated to cover much of eastern Siberia, while a negative anomaly has developed east of Anchorage. Lags $-1$ through 0 show the continued weakening of the upstream positive anomaly, the growth and continued westward propagation of the negative anomaly over Anchorage, and the development of another downstream positive anomaly centered over central Canada. From lags 1 through 3, the Canadian positive anomaly continues to grow in amplitude

as the Anchorage anomaly weakens, and the entire pattern is shown to retrograde. The evolution for the negative composites at this location is notably similar to its positive counterpart, aside from a reversal of sign. The consistency of evolution about $t = 0$ between the two is such that early stages of the negative composites bear a striking resemblance to the mature stages of the positive composites, and vice versa. This is broadly consistent with the existence of traveling mode for this region operating on this timescale.

### *5.4 The Role of Transients in Composite Anomalies*

As has been discussed in previous chapters, there is a large body of literature that highlights the role of high-frequency, baroclinic disturbances in developing and maintaining the intermediate-scale anomalies. The compositing technique we've employed in the previous section would appear to be a useful tool for eliciting these relationships.

The evolution of $Z_6$ field for the single strongest positive event over Baffin Bay is shown together with the anomalies from the the high-frequency field ($z_{HP}$) in Fig. 5.10. As the ridge builds over the Atlantic, an eastward propagating wave-train of high frequency disturbances is shown propagating polewards of the ridge along the $Z_6$ contours. These transients behave in a manner consistent with that discussed by Nakamura and Wallace (1993), deforming meridionally as they approach the blocking ridge. The highest amplitude in $Z_6$ field at $t = 0$ is coincident with the arrival of an positive anomaly in the high-frequency field.

Other individual events (not shown) exhibit a broadly similar behavior, but subtle differences in the evolution of the events cause composites of the high-frequency field to exhibit a high-degree of cancellation, and a very weak signal in the composite field (5.11). The features of individual events in the $z_{int}$ field are large enough in scale that differences between the individual events composited do not greatly impact the overall composites, but this is not so for the smaller-scale transients. To explore this in greater depth would likely require a methodology similar to that of Nakamura and Wallace (1993), in which the authors specifically compensated for variations in the position of the high-frequency transients in order to minimize cancellation in compositing. Such an analysis is beyond the scope of the present study.

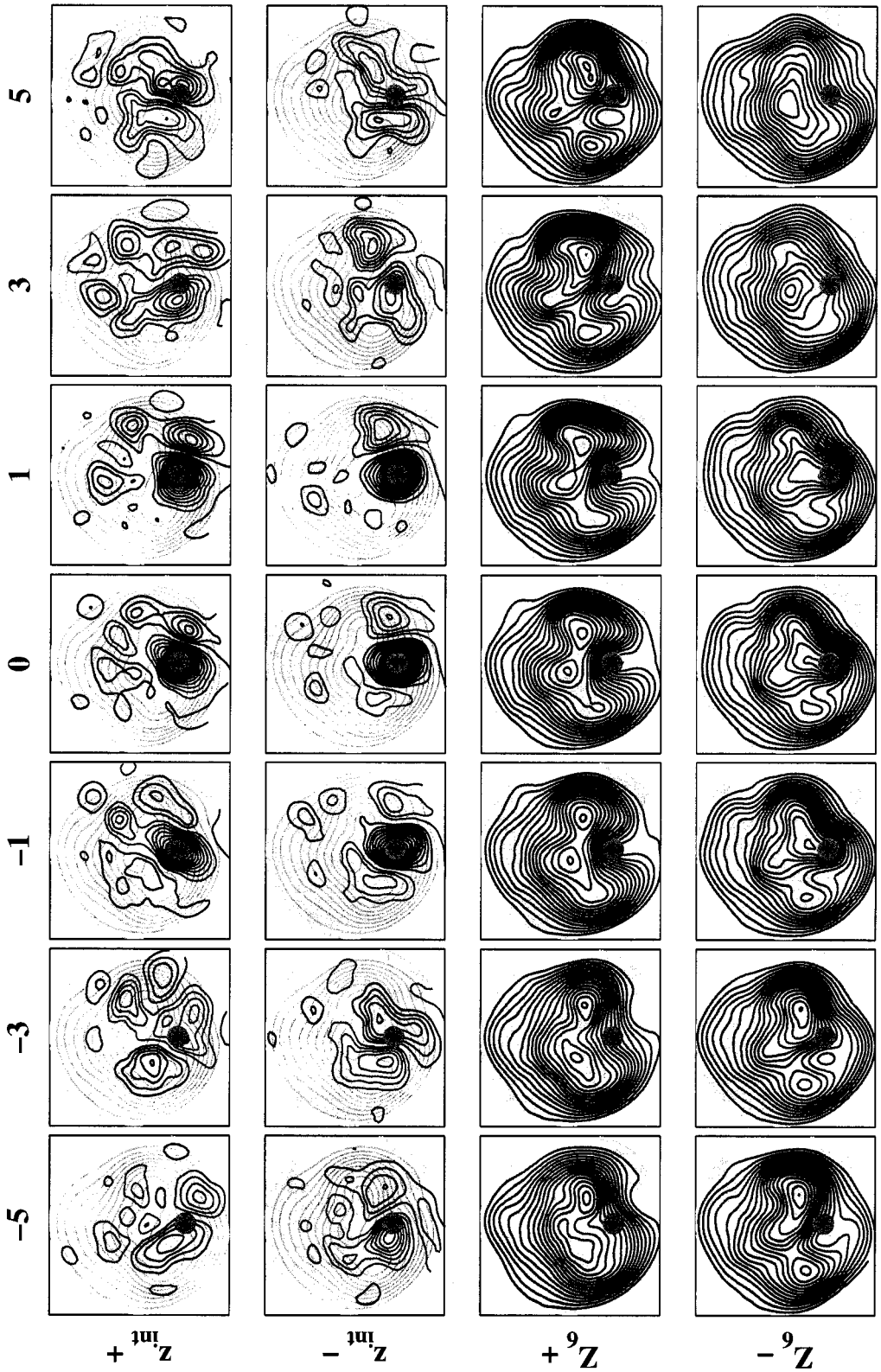


Figure 5.9: As in figure 5.3 but for Anchorage all months.

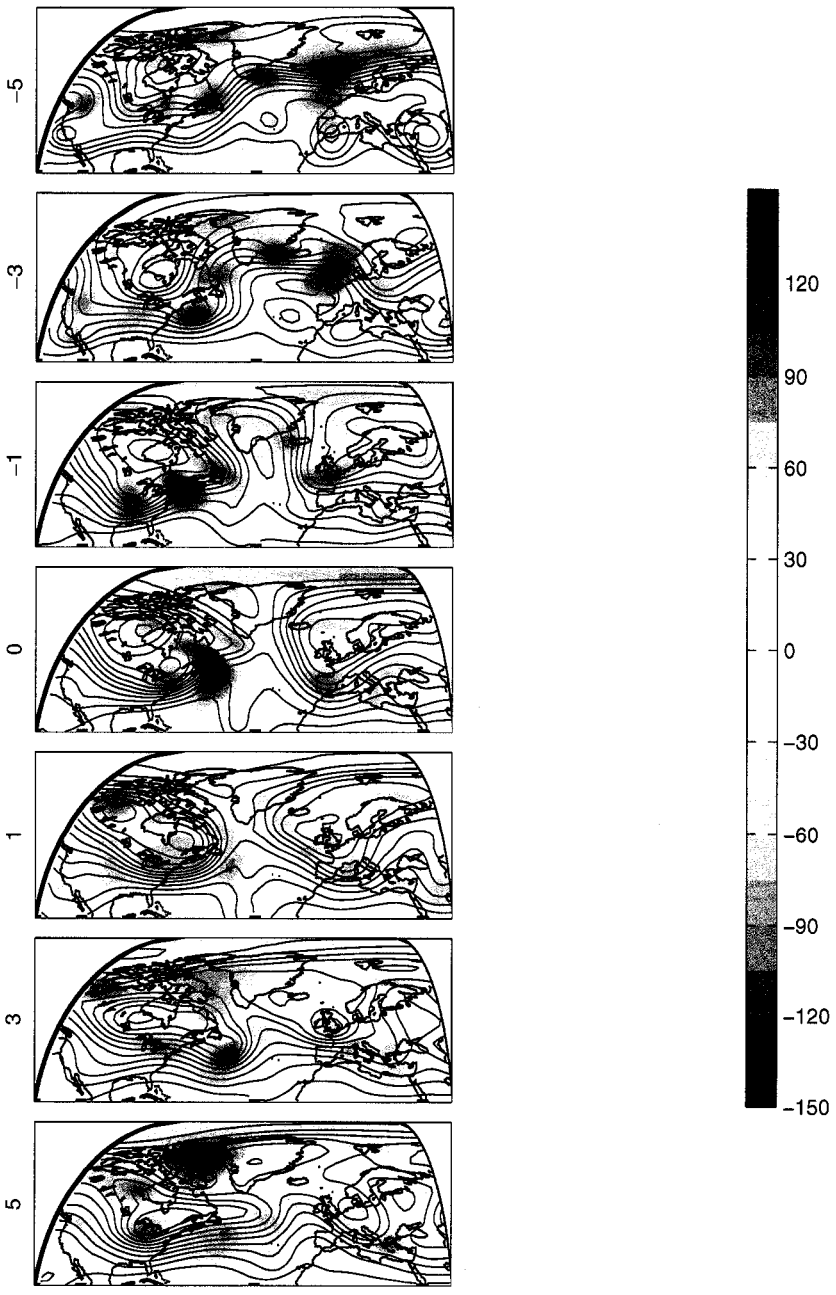


Figure 5.10: The evolution of the short timescale anomalies from the $z_{HP}$ field for the highest amplitude $z_{int}$ event over Baffin Bay. The $z_{HP}$ is shown in color. The $Z_6$ field for the same time period is contoured at intervals of 50 m. The lag is indicated to the left of each panel.

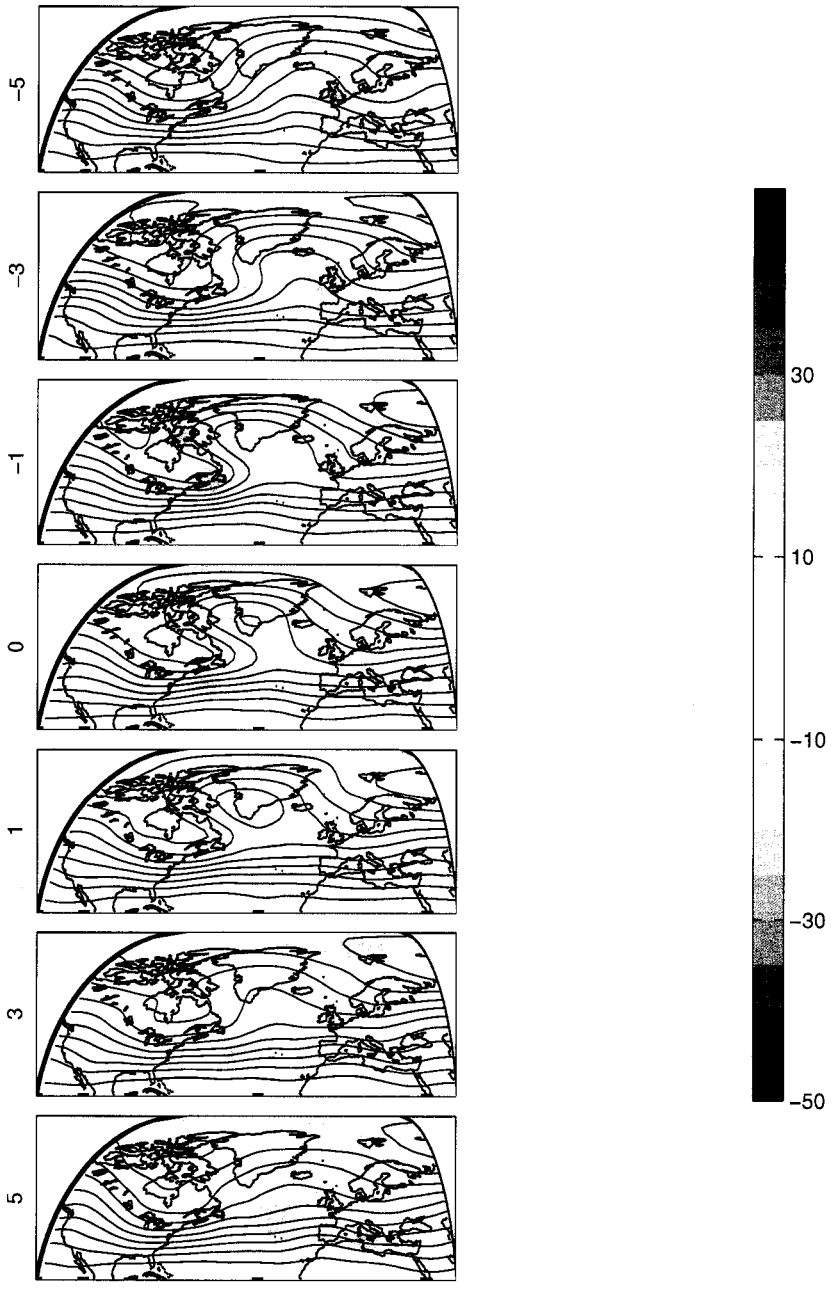


Figure 5.11: As in Fig. 5.10, but for composites of the 10 highest amplitude positive events over Baffin Bay.

## 5.5 *Discussion*

In this chapter we have investigated the evolution of the most prominent intermediate-timescale events for four locations relevant to our study. Lagged correlation analysis of $z_{int}$ has shown each of the locations to exhibit downstream development. The Baffin Bay and Anchorage points displayed a tendency to retrograde throughout their evolution, but retrogression was less evident for the other gridpoints. The $Z_6$ correlations may be interpreted as displaying the intermediate scale behavior superposed on more geographically fixed, longer-lived teleconnection patterns. The proximity of Baffin Bay to a center of action of the NAO causes its $Z_6$ lagged correlations to be dominated by the NAO signal. The Scandinavian center is closer to the node of the NAO, and $Z_6$ lagged correlations there primarily reflect the downstream development characteristics of the intermediate timescales.

The compositing analysis has demonstrated a broad range of behaviors of $z_{int}$ composites for the locations chosen. Positive events over Baffin Bay during NAO$^-$ months were shown to have identifiable, upstream origins 5 days before their peak amplitude. Negative anomalies there exhibited a similar pattern of evolution, but developed much more rapidly near $t = 0$. Both were shown to decay approximately three days after their peak. Positive and negative composites over Scandinavia and the Atlantic col were shown to develop and decay over a shorter time span, attaining significant amplitude only between lags $-1$ and $+1$. Composites of both signs over Anchorage were shown to have the longest lifetime after the peak; the composite anomaly had largely decayed by $t = +3$, the downstream anomalies that developed from it still had large amplitudes at $t = +5$.

In general, the direction of propagation of the anomalies varied in accordance with their lifetime. Short-lived anomalies such as those over Scandinavia and the Atlantic col largely developed and decayed in place. Both positive and negative events over Baffin Bay displayed westward propagation, though this tendency was slightly stronger in the positive composites. Composite anomalies of both signs over Anchorage retrograded throughout their evolution.

It is noteworthy that the compositing results for both Baffin Bay and for Anchorage exhibit a higher degree of consistency and longevity than do those for the other locations. Both Baffin Bay and Anchorage have emerged repeatedly in this work as the strongest cen-

ters of intermediate scale variability within their respective sectors. Each of these locations have also been shown to be relevant for traveling modes operating on this timescale, and our analysis in this chapter is consistent with these ideas. In the Atlantic sector, the NAO appears to play a strong role in organizing these events. Results for the Anchorage point, however, indicate that the PNA may play less of a role in organizing intermediate timescale events there.

# Chapter 6

# SUMMARY AND DISCUSSION

This dissertation has elucidated the role that fluctuations on low-frequency timescales play in determining the patterns and amplitudes of the dominant structures of variability on intermediate timescales. The low-frequency fluctuations of primary importance have been objectively determined through MCA to be the NAO and the PNA in the Atlantic and Pacific basins respectively. The negative polarity of these modes, corresponding to an anomalously weak and diffuse jet in their respective basins, is associated primarily with an enhancement of intermediate timescale variability. In the Atlantic, the enhancement during $NAO^-$ periods has been shown to occur in a dumbbell-shaped region connecting centers of action over Baffin Bay and Scandinavia. In the Pacific, periods of low index PNA are associated with increased intermediate timescale variance for a region centered over the Gulf of Alaska.

The shift in mean heights due to fluctuations of the NAO and PNA, in conjunction with the enhancement of intermediate timescale variance, has been shown to generate regions of skewness in the full geopotential height field. We have demonstrated that the skewness, previously documented as an indicator of blocking activity, is not a result of skewness occurring solely on intermediate or long timescales, but is instead primarily attributable to a cross-frequency term involving low-frequency variations and intermediate-scale variance. The importance of this term in generating skewness over Baffin Bay was demonstrated as follows: During $NAO^-$ conditions, Baffin Bay exhibits enhanced intermediate timescale variance and a positively shifted mean geopotential height, and the reverse is true for the $NAO^+$ background state. In this manner, the superposition of two normal distributions with these characteristics yields a skewed overall distribution.

The centers of enhanced variance during negative polarities of the NAO were also demonstrated to be centers of action of the leading pattern of variability on the intermediate

timescale. The first EOF of $z_{int}$ for the Atlantic sector was shown to be a zonally-oriented dipole between Greenland and Scandinavia. Contrasting the leading patterns of variability by polarity of the NAO demonstrated that the structure of the EOF of the total field primarily reflects the structure of variability in $NAO^-$ months. In one polarity of the mode, anomalously high heights over Greenland occur with low height anomalies over Scandinavia, corresponding to a pattern of Greenland blocking. As has been discussed, the nonlinear appearance of this state, and its apparent preferential occurrence during months of low-index polarity NAO, has caused this configuration of anomalies to receive considerable attention in the literature. The associated PC time series, however, indicates that the opposite polarity of this pattern occurs with equal amplitude and frequency. This result was corroborated by composite analysis of extreme positive and negative events in the $z_{int}$ field over Baffin Bay. Composites for this location exhibited strong symmetry, aside from a reversal of sign, as well as a strong resemblance to the two polarities of the Atlantic intermediate-timescale EOF pattern. The symmetry is quite apparent in the $z_{int}$ field, but would not have been noticed upon inspection of a more typical map of total anomalies.

The symmetry between the positive and negative composite events over the Baffin Bay and Anchorage gridpoints was shown to extend throughout their evolution. The primary centers of action at these two locations exhibit westward propagation and downstream development of new centers, consistent with Rossby wave dynamics. The evolution of the Anchorage composites is qualitatively consistent with the Pacific traveling mode documented by Kushnir (1987). Over Baffin Bay, the evolution of the composites was shown to resemble elements of the westward propagating, hemispheric-scale pattern discussed by Branstator (1987). Branstator's pattern implies a lagged correlation relationship between Anchorage and Baffin Bay, however, and initial testing has revealed no significant $z_{int}$ correlation between these two grid points for any lag.

The most important implication of this work is that the intermediate timescale of variability appears to be be governed, to first order, by linear Rossby wave dynamics. On intermediate timescales, high amplitude anomalies of each sign have been shown to occur with equal strength and regularity. This implies that the emphasis that has been placed on the nonlinear appearance of blocking events over Greenland and the northeast Pacific

effectively focuses on a single polarity of a bipolar pattern. Our results indicate that nonlinear dynamics are not required to explain the extreme signature of the blocking events; they may be more appropriately viewed as a linear superposition of intermediate timescale Rossby waves on slow variations associated with the PNA or NAO. The generation of Rossby waves appears to be favored during the relatively weak jet states corresponding to the low index polarity of the modes. The linear interpretation suggested by the present study is in sharp contrast to the nonlinear interpretation offered by Woollings et al. (2007) that the $NAO^-$ state solely reflects the incidence of wave-breaking events on the tropopause.

The evidence for the linear interpretation offered here is strongly supported by the analysis presented in this thesis, but additional work is required to more completely describe the behaviors shown. The present study has focused exclusively on anomalies in the 500 hPa field, and it is desirable to extend our analysis to other levels to obtain a more complete description of the vertical structure of the intermediate-timescale anomalies. Work is currently underway to repeat selected analyses from this study for a selection of fields ranging from sea-level pressure to a level near the maximum of the midlatitude jet (250 hPa). In addition, it is of interest to determine whether increasing the number of degrees of freedom of the data set by extending the winter season to include November and March significantly impacts the results shown here.

This study raises a number of interesting dynamical questions about variability on intermediate timescales. Why the Rossby waves demonstrated here should favor the particular centers over Baffin Bay, Scandinavia, and Anchorage, as as well as why their generation is favored in the low index polarities of the PNA and NAO, remain to be determined. One hypothesis is that the background state corresponding to $NAO^-$ and $PNA^-$ state is conducive to barotropic energy conversion in regions relevant to our study. A general assessment of the background state corresponding to $NAO^-$ conditions, for example, indicates that geopotential height anomalies over Baffin Bay with structure similar to those composited would favor the barotropic conversion of energy from the background state.

It has also been suggested the $NAO^-$ state might favor a different set of normal modes than the winter mean state, potentially favoring one involving the Baffin Bay and Scandinavian centers. Initial attempts to test this hypothesis were carried out using the barotropic

model employed in Simmons et al. (1983). In their work, they analyzed the normal modes for a base state linearized about a wintertime climatological height field. We followed a similar methodology, but utilized a perturbed base state corresponding to $NAO^-$ conditions. Initial results with this model did not yield any modes with obvious correspondence to the Baffin Bay and Scandinavian centers to be among the fastest-growing normal modes of the system. A slight enhancement of stationary-wave solutions in the vicinity of Baffin Bay was found, but its significance and relevance to the results shown in this study are unclear.

The role of the intermediate timescale in the dynamics of the NAO remains to be clarified, and it is noteworthy that there is a set of seemingly contradictory theories in the current literature. Work by Lorenz and Hartmann (2003) indicates that the intermediate timescale variations serve to damp the feedback between the high and low-frequency anomalies that give the annular modes their long characteristic timescales. The work of Woollings et al. (2007) indicates that dynamics on intermediate timescales is of singular importance. The results of the present study would imply that both intermediate and long-timescale variability are important. It is expected that a comprehensive reconciliation of these three viewpoints will provide a wealth of interesting challenges and dynamical insights in the coming years.

# BIBLIOGRAPHY

Alexandersson, H., K. Iden and H. Tuomenvirta, 1998: Long-term variations of the storm climate over NW Europe. *The Global Ocean Atmosphere System*, **6**, 97–120.

Austin, J. F., 1980: The blocking of middle-latitude westerly winds by planetary waves. *Quart. J. Roy. Meteor. Soc.*, **106**, 327–350.

Barriopedro, D., R. Garcia-Herrera, A. R. Lupo and E. Hernandez, 2006: A Climatology of Northern Hemisphere Blocking. *J. Climate*, **19**, 1042–1063.

Blackmon, M., 1976: A Climatological Spectral Study of the 500 mb Geopotential Height of the Northern Hemisphere. *J. Atmos. Sci.*, **33**, 1607–1623.

Blackmon, M., J. Wallace, N. Lau and S. Mullen, 1977: An Observational Study of the Northern Hemisphere. *J. Atmos. Sci.*, **34**, 1040–1053.

Blackmon, M. L., Y.-H. Lee and J. Wallace, 1984a: Horizontal structure of 500 mb height fluctuations with long, intermediate and short time scales. *J. Atmos. Sci.*, **41**, 961–979.

Blackmon, M. L., Y.-H. Lee, J. Wallace and H.-H. Hsu, 1984b: Time variation of 500 mb height fluctuations with long, intermediate and short time scales as deduced from lag-correlation statistics. *J. Atmos. Sci.*, **41**, 981–991.

Branstator, G., 1987: A Striking Example of the Atmosphere's Leading Traveling Pattern. *JAS*, **62**, 2310–2323.

Chang, E. K. M., S. Lee and K. L. Swanson, 2002: Storm Track Dynamics. *J. Climate*, **15**, 2163–2183.

Elliott, R. and T. B. Smith, 1949: A study of the effects of large blocking highs on the general circulation in the Northern-Hemisphere westerlies. *J. Meteor.*, **6**, 67–85.

Frederiksen, J. S., 1989: The role of instability during the onset of blocking and cyclogenesis in Northern Hemisphere synoptic flows. *J. Atmos. Sci.*, **46**, 1076–1092.

Frederiksen, J. S., 1998: Precursors to Blocking Anomalies: The Tangent Linear and Inverse Problems. *J. Atmos. Sci.*, **55**, 2419–2436.

Frederiksen, J. S. and R. Bell, 1990: North Atlantic Blocking during January 1979: Linear theory. *Quart. J. Roy. Meteor. Soc.*, **116**, 1289–1313.

Haines, K., 1989: Baroclinic Modons as Prototypes for Atmospheric Blocking. *JAS*, **46**, 3202–3218.

Hartmann, D. L. and S. J. Ghan, 1980: A Statistical Study of the Dynamics of Blocking. *MWR*, **108**, 1144–1159.

Haupt, S. E., J. C. McWilliams and J. J. Tribbia, 1993: Modons in Shear Flow. *JAS*, **50**, 1181–1198.

Hurrell, J., 1995: Decadal trends in the North Atlantic Oscillation: Regional temperatures and precipitation. *Science*, **269**, 676–679.

Hurrell, J., Y. Kushnir, G. Ottersen and M. Visbeck, 2003: *An overview of the North Atlantic Oscillation.* Vol. 134, Chap. 1, pp. 1–35. American Geophysical Monograph.

Hurrell, J. and H. van Loon, 2003: Decadal variations in climate associated with the North Atlantic Oscillation. *Climatic Change*, **36**, 301–326.

Kimoto, M. and M. Ghil, 1993: Multiple flow regimes in the Northern Hemisphere winter. Part I: Methodology and hemispheric regimes. *J. Atmos. Sci.*, **50(16)**, 2625–2643.

Kushnir, Y., 1987: Retrograding wintertime low-frequency disturbances over the North Pacific Ocean. *JAS*, **62**, 2727–2742.

Lau, N.-C., 1988: Variability of the Observed Midlatitude Storm Tracks in Relation to Low-Frequency Changes in the Circulation Pattern. *J. Atmos. Sci.*, **45**, 2718–2743.

Lejenäs, H. and R. A. Madden, 1992: Traveling Planetary-Scale Waves and Blocking. *Mon. Wea. Rev.*, **120**, 2821–2830.

Lejenäs, H. and H. Økland, 1983: Characteristics of Northern Hemisphere blocking as determined from a long series of observational data. *Tellus*, **35A**, 350–362.

Lorenz, D. and D. Hartmann, 2001: EddyZonal Flow Feedback in the Southern Hemisphere. *J. Atmos. Sci.*, **58(21)**, 3312–3327.

Lorenz, D. and D. Hartmann, 2003: EddyZonal Flow Feedback in the Northern Hemisphere Winter. *J. Climate*, **16(8)**, 1212–1227.

Luo, D., 2005: Why is the North Atlantic block more frequent and long-lived during the negative NAO phase? *Geophys. Res. Lett.*, **32**.

Mullen, S., 1986: The local balances of vorticity and heat for blocking anticyclones in a spectral geneal circulation model. *JAS*, **43**, 1406–1441.

Mullen, S., 1987: Synoptic Behavior of Baroclinic Eddies during the Blocking Onset. *JAS*, **44**, 3–22.

Nakamura, H. and J. M. Wallace, 1993: Synoptic Behavior of Baroclinic Eddies during the Blocking Onset. *MWR*, **121**, 1892–1903.

Namias, J., 1947: Characteristics of the general circulation over the Northern Hemisphere during the abnormal winter 19461947. *Mon. Wea. Rev.*, **75**, 145–152.

Palmer, T., 1988: Medium and extended range predictability and stability of the Pacific/North American mode. *Quart. J. Roy. Meteor. Soc.*, **114**, 697–713.

Pelly, J. and B. Hoskins, 2003: A new perspective on blocking. *J. Atmos. Sci.*, **60**, 743–755.

Pierrehumbert, R. and P. Malguzzi, 1984: Forced coherent structres and local multiple equilibria in a barotropic atmosphere. *J. Atmos. Sci.*, **41**, 246–257.

Quadrelli, R. and J. M. Wallace, 2004a: A simplified linear framework for interpreting patterns of Northern Hemisphere wintertime climate variability. *J. Climate*, **17**, 3728–3744.

Quadrelli, R. and J. M. Wallace, 2004b: Varied Expressions of the Hemispheric Circulation Observed in Association with Contrasting Polarities of Prescribed Patterns of Variability. *J. Climate*, **17**, 4245–4253.

Renwick, J. A. and J. M. Wallace, 1996: Relationships between North Pacific wintertime blocking, El Niño, and the PNA pattern. *Mon. Wea. Rev.*, **124**, 2071–2076.

Rex, D., 1950a: Blocking action in the middle troposphere and its effect upon regional climate. *Tellus*, **2**, 196–211.

Rex, D., 1950b: Blocking action in the middle troposphere and its effect upon regional climate II: The climatology of blocking action. *Tellus*, **2**, 275–301.

Rogers, J. C., 1990: Patterns of low-frequency monthly sea level pressure variability and asociated wave cyclone frequencies. *J. Climate*, **3**, 1364–1379.

Rogers, J. C., 1997: North Atlantic storm track variability and its association to the North Atlantic Oscillation and climate variability ofNorther Europe. *J. Climate*, **10**, 1635–1645.

Serreze, M., F. Carse, R. Barry and J. Rogers, 1997: Icelandic low activity: climatological features, linkages with the NAO, and relationships with recent changes in the Northern Hemisphere circulation. *J. Climate*, **10**, 453–464.

Shabbar, A., J. Huang and K. Higuchi, 2001: The relationship between the wintertime North Atlantic Oscillation and blocking episodes in the North Atlantic. *Int. J. Clim*, **21**, 355–369.

Shutts, G., 1986: A case study of eddy forcing during an Atlantic blocking episode. *Advances in Geophysics*, **No. 29**, 135–162.

Simmons, A., J. M. Wallace and G. Branstator, 1983: Barotropic Wave Propagation and Instability and Atmospheric Teleconnection Patterns. *J. Atmos. Sci.*, **40**, 1363–1392.

Swenson, M., 1986: Equivalent Modons in Simple Shear. *JAS*, **43**, 3177–3185.

Takaya, K. and H. Nakamura, 2005: Geographical Dependence of Upper-Level Blocking formation Associated with Intraseasonal Amplification of the Siberian High. *JAS*, **62**, 4441–4449.

Thompson, D. J. W. and J. M. Wallace, 1988: The Arctic Oscillation signature in the wintertime geopotential height and temperature fields. *Geophys. Res. Lett.*, **25**, 1297–1300.

Thompson, D. J. W. and J. M. Wallace, 2000: Annular Modes in the Extratropical Circulation. Part I: Month-to-Month Variability. *J. Climate*, **13**, 1000–1016.

Tibaldi, S. and F. Molteni, 1990: On the operational predictability of blocking. *Tellus*, **42A**, 343–365.

Trenberth, K., 1986: An assessment of the impact of transient eddies on the zonal flow during a blocking episode using localized Eliassen-Palm flux diagnostics. *J. Atmos. Sci.*, **43**, 2070–2087.

Uppala, S. and coauthors, 2005: The ERA-40 re-analysis. *QJRMS*, **131**, 2961–3012.

van Loon, H. and J. C. Rogers, 1978: The Seesaw in Winter Tempeartures between Greenland and Northern Europe. Part I: General Description. *Mon. Wea. Rev.*, **106**, 296–310.

Vautard, R., 1990: Multiple weather regimes over the North Atlantic: Analysis of precursors and successors. *Mon. Wea. Rev.*, **118**, 2056–2081.

Wallace, J. and D. Gutzler, 1981: Teleconnections in the Geopotential Height Field during the Northern Hemisphere Winter. *Mon. Wea. Rev.*, **109**, 784–812.

White, G. H., 1980: Skewness, Kurtosis and Extreme Values of Northern Hemisphere Geopotential Height. *Mon. Wea. Rev.*, **108**, 1446–1455.

Woollings, T., B. Hoskins, M. Blackburn and P. Berrisford, 2007: A New Rossby Wave-breaking Intepretation of the North Atlantic Oscillation . *J. Atmos. Sci.*, accepted.

# Appendix A

# SUPPLEMENTARY FIGURES

This appendix provides a set of supplementary figures to those shown in the compositing analysis of Chapter 5. In the earlier chapter, the compositing analysis was performed using only the 10 greatest anomalies of either polarity for each point. Such an analysis can be sensitive to the number of events included in the composites. To show that the behaviors demonstrated by the smaller numbers of events are largely insensitive to the number of events composited, this appendix includes a similar set of figures, including greater numbers of events in the composites.

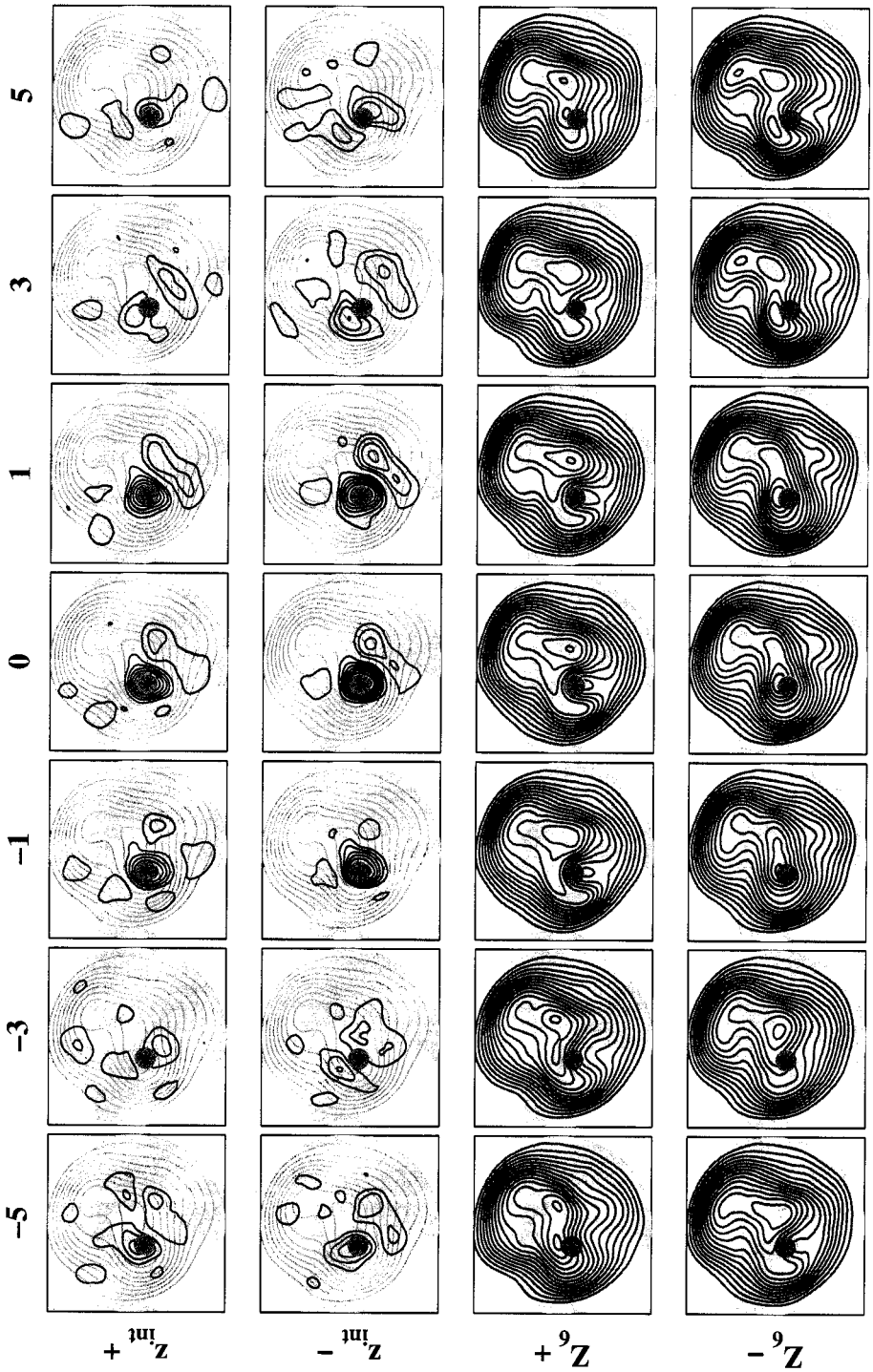


Figure A.1: As in Figure 5.3 but for the 30 highest amplitude events.

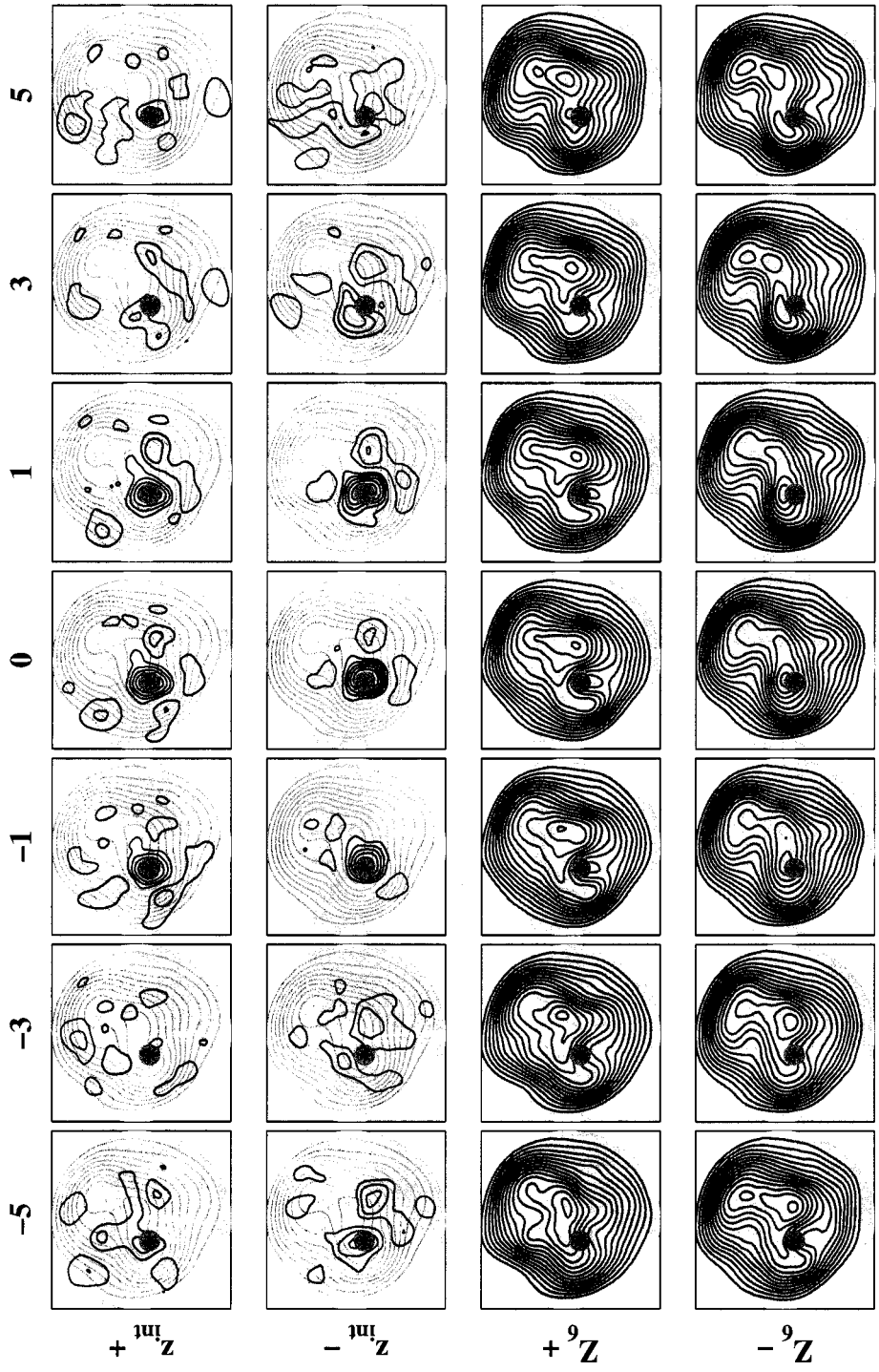


Figure A.2: As in Figure 5.3 but for the events ranked 10th through 30th in amplitude.

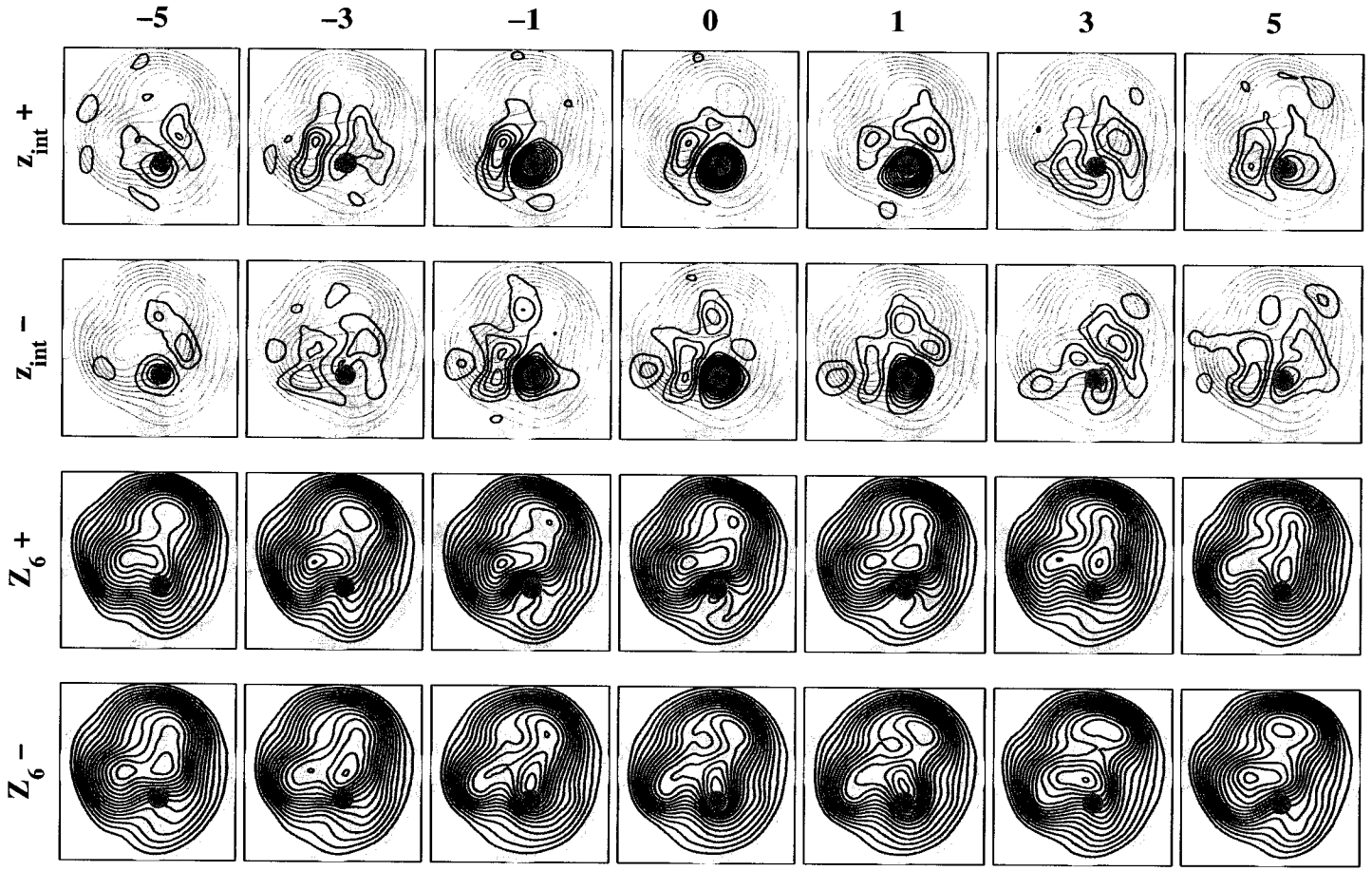


Figure A.3: As in Figure 5.3 but for the 30 highest amplitude events over the Scandinavia grid point drawn from all months.

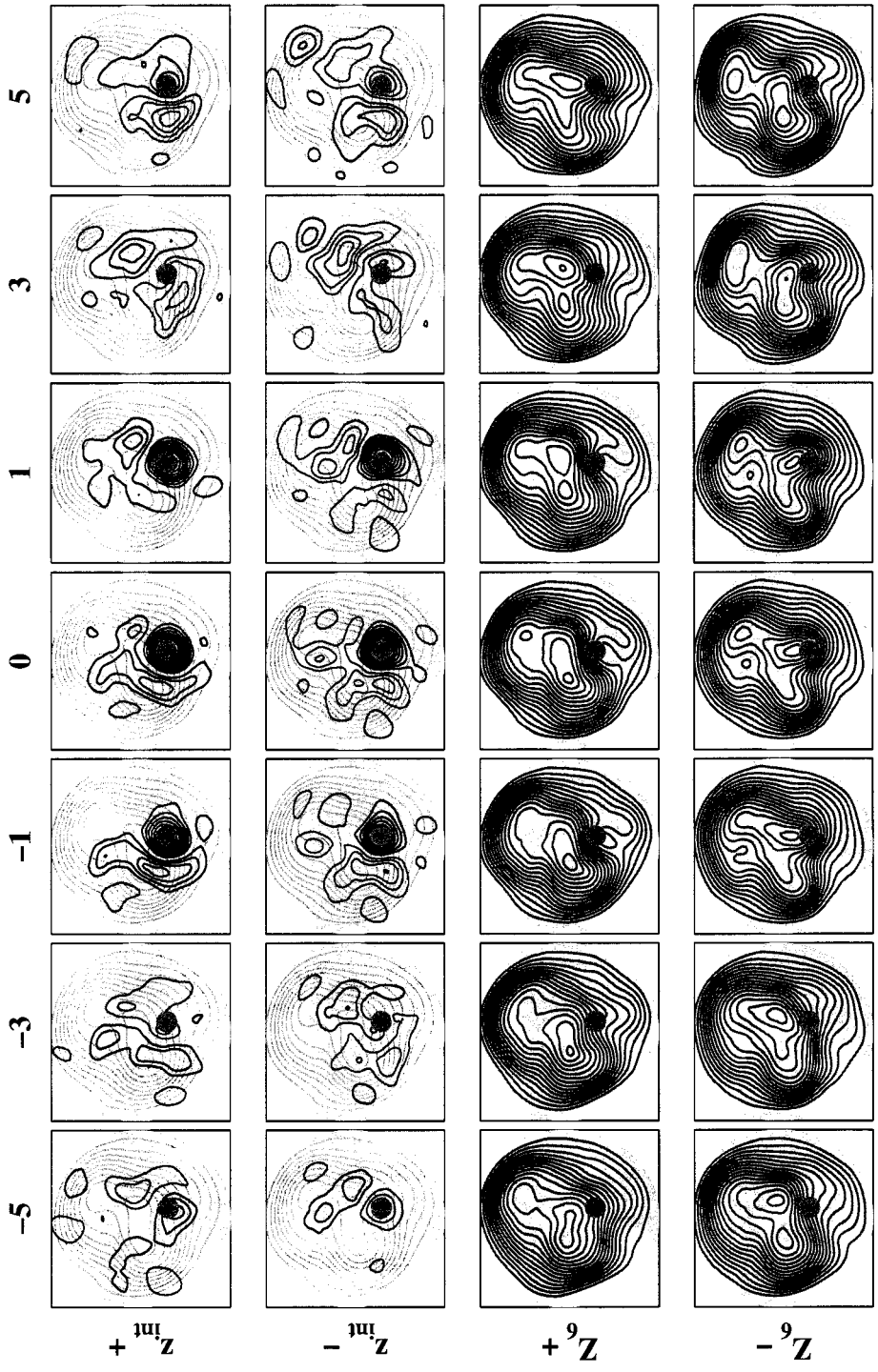


Figure A.4: As in Figure A.3 but for the events ranked 10th through 30th in amplitude.

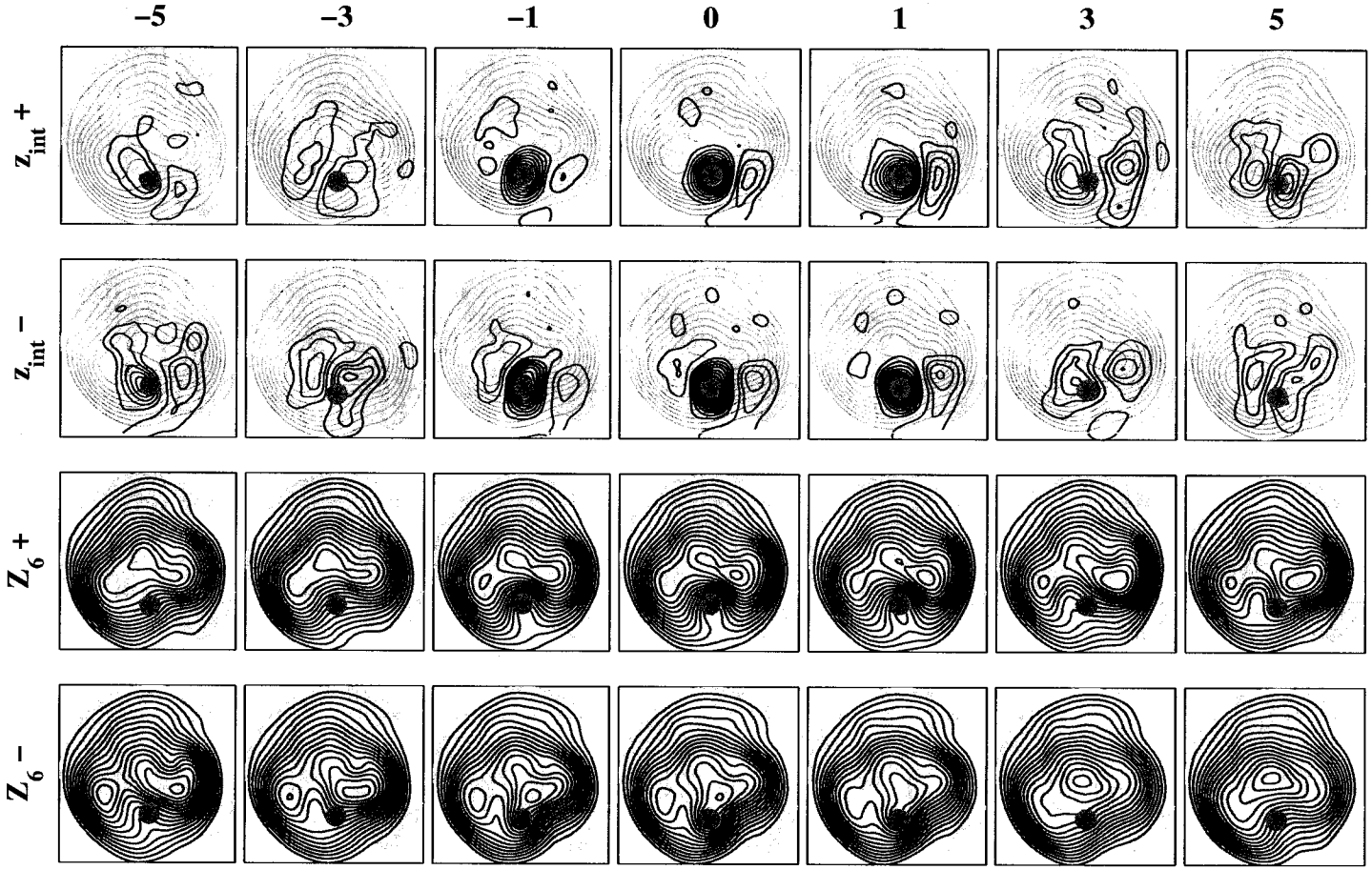


Figure A.5: As in Figure 5.3 but for the 30 highest amplitude events over the Anchorage grid point drawn from all months.

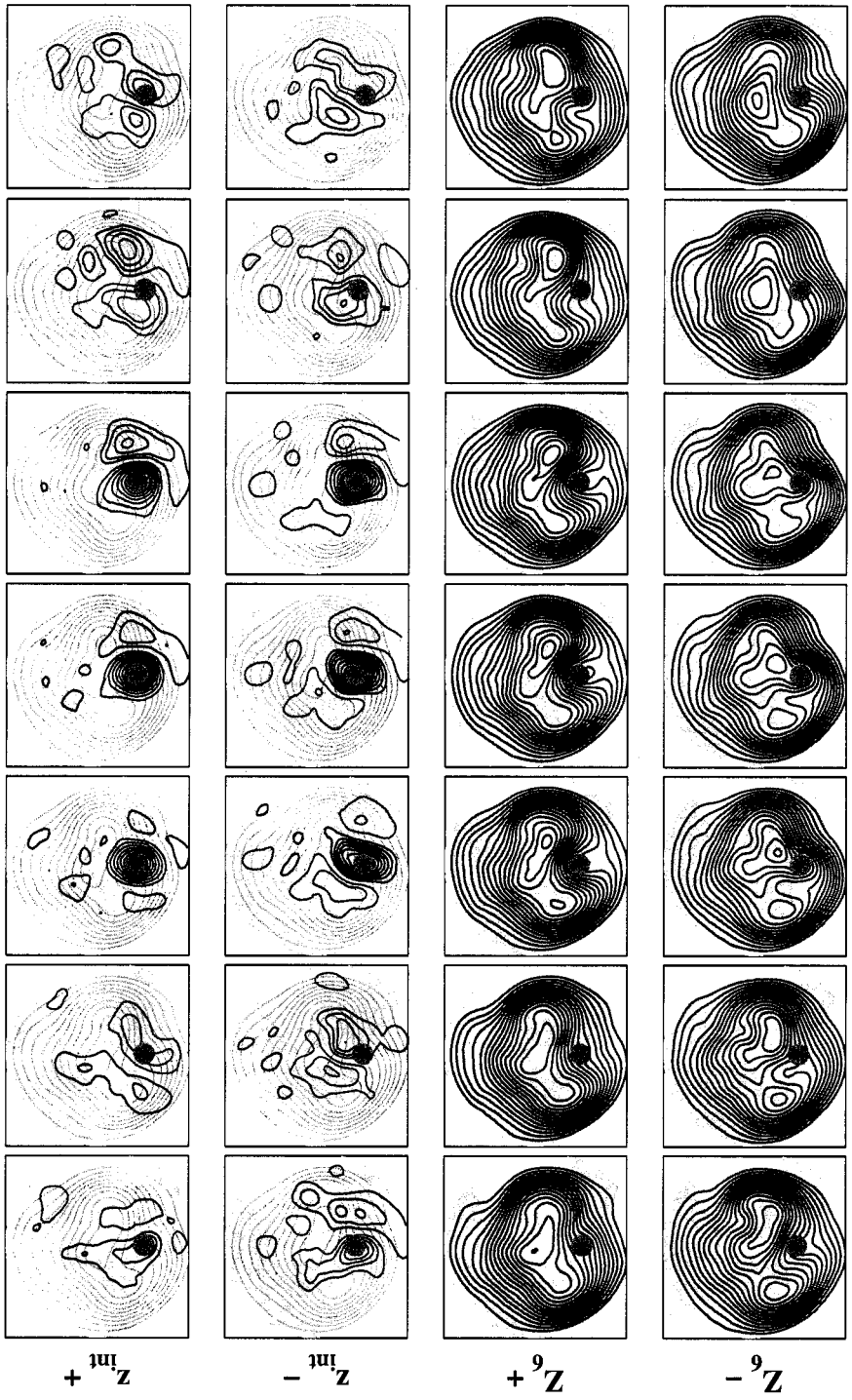


Figure A.6: As in Figure A.5 but for the events ranked 10th through 30th in amplitude.

# VITA

Kevin Rennert was born on Feb. 6th, 1976, in Findlay, Ohio, to Robert and Catherine Rennert. He spent many of his formative years in the village of Gambier, Ohio, and treated the campus of Kenyon College as his home. He attended Grinnell College in Grinnell, Iowa from 1993-1997 and earned a B.A. with honors in Physics. His interest in modes of climate variability and climate change was stimulated when his relocation to Palo Alto, California coincided with the extreme El Niño event of 1997-98. He was employed at the Stanford Linear Accelerator Center as an accelerator operator and software engineer until he began his doctoral studies at the University of Washington in August of 2000.